UNIVERSITE MOHAMED KHIDER - BISKRA
FACULTE DES SCIENCES ET SCIENCES DE L'INGENIEUR
DEPARTEMENT DE GENIE CIVIL

N° d'ordre: ....
Série: ....

THESE DE DOCTORAT D'ETAT

Spécialité : **GENIE CIVIL**
Option : **STRUCTURE**

Présentée par

Djamel HAMADI

ANALYSIS OF STRUCTURES BY NON- CONFORMING FINITE ELEMENTS

"ANALYSE DES STRUCTURES PAR ELEMENTS FINIS NON CONFORMES"

Soutenue le: 20/12/2006

Devant le jury composé de :

Prof. BOUMEKIK Ahmed	**Prof.**	**Université de Constantine**	**Président**
Prof. BELARBI M. Tahar	**Prof.**	**Université de Biskra**	**Rapporteur**
Prof. hab. MELLAS Mekki	**M.C.**	**Université de Biskra**	**Examinateur**
Dr. NOUAOURIA M. Salah	**M.C.**	**Université de Guelma**	**Examinateur**
Dr. CHEBILI Rachid	**M.C.**	**Université de Biskra**	**Examinateur**

AKNOWLEDGEMENT

This work has been realised at the civil engineering department, Biskra University.

The author wishes to express his deepest appreciation to his supervisor, Professor Belarbi Mohamed Tahar, for his invaluable guidance, support and encouragement throughout the period of this research.

He also wishes to thank deeply the jury members:
The president BOUMEKIK Ahmed, Professor at Constantine University
The examiners:

NOUAOURIA Mohamed Salah, Lecturer at GUELMA University
CHEBILI Rachid, Lecturer at BISKRA University
MELLAS Mekki, Lecturer at BISKRA University

He also wishes to thank:
-Professor CHARIF Abdelhamid for his support and encouragement
-Professor GUENFOUD Mohamed for his support and encouragement
-Professor SLATNIA Belgacem, chancellor of the University
-Professor BOUTARFAIA Ahmed, Vice-chancellor of the University
-The dean of the Faculty and the head of the civil engineering department as well
-The staff members of the civil engineering department

CONTENTS

CHAPTER 1

GENERAL INTRODUCTION

CHAPTRE 2

A NEW STRAIN BASED MIXED SECTOR ELEMENT

CHAPTER 3

A NEW INTEGRATION SOLUTION ROUTINE FOR QUADRILATERAL AND TRIANGULAR SHAPES

CHAPTRE 4

A NEW QUADRILATERAL FINITE ELEMENT FOR GENERAL PLANE ELASTICITY PROBLEMS

CHAPTRE 5

FORMULATION OF A NEW FLAT SHELL ELEMENT

CHAPTRE 6

AN EFFICIENT PARALLELEPIPED FINITE ELEMENT BASED ON THE STRAIN APPROACH "SBP8C"

Captions of figures

CHAPTER 4

CHAPTER 5

CHAPTER 6

Captions of tables

CHAPTER 2

CHAPTER 3

CHAPTER 4

CHAPTER 5

CHAPTER 6

ABSTRACT

The general purpose of this thesis is to develop new finite elements based on the strain approach. In order to ameliorate the accuracy of the results, the static condensation technique has been used. Most of the finite elements developed by Sabir are characterized by a regular form and appropriate coordinates with the form of the element. To overcome this geometrical inconvenience; a new analytical integration is developed to evaluate the element stiffness matrix for the finite elements with distorted shapes. This will help to know how the elements will behave when they have irregular form, and to extend their applications domain for the curved structures no matter what the geometrical shape of the element might be.

In the first chapters, the work deals with the development of two different membrane finite elements. The first element is a sector element baptised **SBMS-BH** (Strain Based Mixed Sector Belarbi and Hamadi) has four nodes and two degrees of freedom per node (2 d.o.f/node) U and V. This element helps greatly to solve plane elasticity problems with circular shape and with a minimum number of elements. The second one is a new quadrilateral element that satisfies the equilibrium equations called **Q4SBE1**. Both elements have two degrees of freedom (d.o.f) at each corner node in addition to the internal node. Through the introduction of additional internal node, the efficiency of these elements is established and the convergence of the results to a satisfactory degree of accuracy was shown to be faster when compared with other elements.

The forth chapter deals with the formulation of a new flat shell element **(ACM_Q4SBE1),** where the membrane element **Q4SBE1** is superposed with the standard plate bending element **ACM** . Several case-tests of the shell considered as a device of element validation were examined and good results were obtained.

The last chapter of the work is concerned with the development of a new parallelepiped finite element, simple and effective baptized **SBP8C** (Strain Based Parallelepiped 8-nodes condensed), contributing to enrich the existing finite elements library. This last one is formulated, by the use of the static condensation. This element can be used for the analysis of three dimensional problems and also for the thin and thick plates bending. Some standard tests of element validation were also examined.

ملخـــص

تهدف هذه الأطروحة بصفة عامة إلى تطوير مجموعة جديدة من العناصر المحدودة اعتمادا على مبدأ التشوه. من أجل تحسين الدقة في النتائج، تم استعمال تقنية التكثيف الستاتيكي. بما إن أغلب العناصر المحدودة المطورة من طرف الباحث Sabir والتي تعتمد على مبدأ التشوه، تتميز بالشكل الهندسي المنتظم والإحداثيات الخاصة بشكل العنصر، فمن أجل تجاوز هذه السلبية الهندسية التي تحد من مجال استعمالها، تم تطوير علاقة تكامل تسمح بحساب مصفوفة الصلادة للعنصر حتى وإن كان شكله الهندسي غير منتظم. إن هذه العلاقة تسمح بمعرفة سلوك العنصر في حالة الشكل الكيفي، وفي الحالة الإيجابية، توسيع مجال استعماله في الإنشاءات مهما كان شكلها الهندسي غير منتظم.

في الفصول الأولى، تم تطوير عنصرين محدودين غشائيين ومختلفين. يتمثل الأول في عنصر قطاعي سمي **SBMS-BH** (Strain Based Mixed Sector Belarbi and Hamadi) يحتوي على أربع عقد بدرجتي حرية في كل عقدة **(2 d.o.f/node)**. يساهم هذا العنصر بفعالية في تحليل مسائل المرونة ذات الشكل الدائري وباستعمال عدد قليل من العناصر. أما العنصر الثاني فهو عنصر رباعي جديد يحقق معادلات التوازن سمـــي **Q4SBE1**. كل من العنصرين السابقين يحتوي على درجتي حرية في كل عقدة زاوية بالإضافة إلى العقدة الداخلية. من خلال إضافة العقدة الداخلية تم تحسين التقارب في النتائج مقارنة مع عناصر أخرى من خلال سلسلة من الاختبارات المرجعية.

سخر الفصل الرابع لتكوين عنصر قشري باعتماد فرضية الصفائح المستوية هندسيا، سمي هذا العنصر **(ACM_Q4SBE1)** مؤلف من تراكب العنصر الغشائي **Q4SBE1** وعنصر الانحناء **ACM**. من خلال عدة اختبارات مرجعية للعناصر القشرية، تم التأكد من الحصول على نتائج جيدة مقارنة مع عناصر أخرى.

أما الفصل الأخير فقد خصص لتطوير عنصر متوازي السطوح، بسيط وفعال، سمي **SBP8C** (Strain Based Parallelepiped 8-nodes condensed)، تم تطويره باستعمال تقنية التكثيف الستاتيكي. يساهم هذا العنصر بفعالية جيدة في تحليل المسائل الثلاثية الأبعاد وكذلك الصفائح الرقيقة والسميكة على حد سواء.

CHAPTER 1

GENERAL INTRODUCTION

CHAPTER 1

GENERAL INTRODUCTION

1.1. Introduction

The analysis and design of structures is a topic of interest in a variety of engineering disciplines. The civil engineer is concerned with the design of large span roofs, liquid storage facilities, silos and many other structures. The mechanical engineer is interested in the design of pressure vessels, including nuclear reactor containment and pipes. The aeronautical engineer is involved in the structural design of aircrafts, rockets and aerospace vehicles. All of these structures require the analysis and design in one form or another. In problems of structural mechanics the analyst seeks to determine the distribution of stresses throughout the structure to be designed. Also it is necessary to calculate the displacements of certain points of the structure to ensure that specified allowable values are not exceeded.

For the skeletal structures, the analysis can be carried out by first considering the behaviour of each individual part independently and then assembling these parts together in such away that equilibrium of forces and compatibility of displacements are satisfied at each junction. An example of such process is the analysis of a continuous beam by the slope deflection method. However when a structure consists of many members forming a multi-storey frames, is being analysed, this type of approach becomes very laborious and involves the solution of a large number of simultaneous equations. Hence efforts were concentrated on the development of analytical techniques based on a physical appreciation of the structural behaviour. In some cases this lead to the reduction of the amount of work required to complete an analysis and a direct solution of the many simultaneous equations was not necessary. With the advent of the electronic digital computers, however, engineers realised that the resolution of a large number of simultaneous equations, no longer posed problems. Thus a return to fundamental method of analysis is followed, and the resulting so-called matrix methods for analysing skeletal structures were established.

In the case of the continuum structures, such as slabs, shell structures, dam walls and deep beams, where the structural surface is continuous instead of being composed of a number of individual components. Such continua require more sophisticated numerical techniques such as the finite difference or the finite element methods of analysis, which are widely used in engineering problems. Both methods require the analyst to descretisize the structure being analysed.

When dealing with the continuum structures, the finite element method is a more suitable and powerful tool of analysis, we can vary the size, the shape, the thickness and the material property of an element to suit the overall property of the structure which makes it particularly suitable for complicated problems involving non-homogeneous material properties, such as composite structures.

1.2. Historical evolution of the finite element method

The finite element method has essentially been developed to provide approximate solutions for the analysis of continuum problems. As is often the case with original developments, it is rather difficult to quote an exact date on which the finite element was invented, but the roots of the method can be traced back to two separate groups, applied mathematicians and engineers. This method as known today was presented in 1956 hy Turner, Clough, Martin and Topp [TUR 56] and was first applied to the analysis of aircraft structural problems, which is considered as one of the key contribution to the development of the finite element method. Numerically it had been observed that the finite element method often leads to convergent results as the number of elements is increased. The earliest convergence studies of the finite element method were reported by Melosh [MEL 62] and later he published a paper, in which he developed a criterion to insure monotonic convergence [MEL 63]. Zienkiewicz and Cheung [ZIE 65] and Visser [VIS 65] in 1965 were the first to apply the method to general problems, such as the conduction heat transfer. Motivated by the specific formulation of elements for plane stress, a wide variety of elements were developed including bending elements, curved elements and the isoparametric concept was introduced [FEL 66, IRO 68]. Once these had been established for the purpose of linear static elastic analysis, attention turned to special phenomena such as dynamic response, buckling and material nonlinearity. These developments were followed by a period of rather intensive development of "general purpose" computer programs intended to place the capabilities of the method in the hands of the practitioner. Along with the development of high speed computers, the application of the finite element method also progressed at a very impressive rate. Thereafter within a decade, the potentialities of the method for the solution of different types of applied science and engineering problems were recognised, and many books have been written on the finite element method, the four editions of the books authored by Zienkiewicz [ZIE 88], received worldwide diffusion. During the same period a number of journals devoted most of their pages to the finite element method. On the development side many researchers continue to be occupied with formulation of the formulation of new elements, and further development of improved algorithms for special phenomena. At the same time a new approach of elements was developed at Cardiff, referred to as the strain based approach details of which will be given throughout this thesis. Within all this progress, today the finite element method is considered as one of the well established and convenient analysis tools by engineers and applied scientists. General purposes programs for the finite element analysis are now extensively dispersed in practice. The availability of such programs at a modest cost of acquisition accounts for the abundance of practical application of the method.

1.3. Different formulations (Models)

According to the choice of the interpolation field several models of the finite elements can be generated which are:

1.3.1. Displacement model

This model is the most popular and most developed, in which the finite elements are based on an interpolation of the displacements field. The displacements are determined in a single and detailed way in the structure, whereas the stresses are not continuous at the boundaries.

1.3.2. Stress model

In this model the element is formulated on the base of stress field approximation only.

1.3.3. Mixed model

This model is based on two independents interpolations of two or more various unknown fields, generally the displacements fields and stresses fields within the element. In general this model takes the unknowns parameters of theses fields as degrees of freedom.

1.3.4. Hybrid model

This model takes in consideration an assumed stress distribution within the element and assumed displacements along its edge.

1.4. Previous work on Strain Based Approach

Investigations by many researchers since 1970s on the suitability of the available finite elements, especially for curved structures, showed that to obtain satisfactory converged results, the assumed displacement elements required the curved structure to be divided into a large number of elements [ASH 71a]. At that time, the strain based approach was developed, not only for curved but also for flat elements. The approach is based on calculating the exact terms representing all the rigid body modes and the other components of the displacement functions are based on assumed independent strain functions insofar as it is allowed by the elasticity compatibility equations. This approach leads to the representation of the displacements by higher order polynomial terms without the need for the introduction of additional internal and unnecessary degrees of freedom; also good convergence can be obtained when the results are compared with the corresponding displacement elements i.e displacement elements having the same total number of degrees of freedom.

Earliest, numerical tests were carried out by Ashwell, Sabir and Roberts [ASH 71b], on simple circular arches with different aspect ratios, the results obtained show that better convergence can be obtained when assumed strain based elements are used instead of assumed displacement models.

Then, a new class of simple and efficient finite elements for arches of all proportions was developed, and the effectiveness of the strain based approach was demonstrated.

Moreover the opportunity was taken to develop high order elements requiring only the essential external degrees of freedom such as:

Cylindrical shell element was developed by Ashwell and Sabir [ASH 72]. The effectiveness of this element was tested by applying it to the analysis of the familiar pinched cylinder and barrel vault problems, and the results obtained were shown to converge rapidly for both displacements and stresses.

The work on the strain based was further extended by Sabir [SAB 75] to develop elements for arches deforming out of the plane as well as within. in order to investigate the performance of the strain shell element in predicting the high stresses at the neighbourhood of applied concentrated loads Sabir and Ashwell [SAB 78] carried out tests on thin shells and the loads applied were either radial or axial forces as well as moments about tangents to the circular cross section, and the results obtained corresponded closely with theoretical solutions Fosburg and flugge [FLU 66].

The development of elements based on the strain approach has continued, many elements were developed for general plane elasticity problems as well as shells by Sabir et al [SAB 85a, SAB 85b and SAB 86]. New classes of elements were developed by Sabir [SAB 83]; a basic rectangular element having the only essential nodal degrees of freedom and satisfying the requirements of strain free rigid body modes and compatibility within the element is first developed, this element is based on linear direct strains and constant shear strain. Other elements meeting the above basic considerations together with equilibrium within the element are also developed. The problem of the inclusion of the in-plane rotation as an additional degree of freedom has also been treated by using the strain approach and a simple and efficient rectangular element including the in-plane rotation is derived. This element was first applied to the simple problem of cantilevers and simply supported beams, where the results for deflections and stresses converged to the exact solution.

Furthermore, with the success of the application of the strain approach to the plane elasticity problems [SAB 85b], the extension of the work to the development of finite elements in polar coordinates has continued [SAB 85c, SAB 86]. Many elements for shells and three-dimensional elasticity have been developed by [DJO 95, SAB 96, SAB 97a, BEL 98a, 98b, 98c and 99, ASS 99].

Lately, Djoudi and Bahai have developed a new strain based cylindrical shell finite element using shallow shell formulation [DJO 2003, 2004a, 2004b]. This element is used for linear and non linear analysis of cylindrical panels. Belounar & Guenfoud developed a new rectangular finite element, which is the first plate bending element based on the strain based approach and the Reissner/Mindlin theory for plate bending [Bel 2004]. A new rectangular element is developed for the general plane elasticity by Belarbi & maalem [Bel 2005a]. On improved Sabir triangular element with drilling rotation is developed; this triangular element, with three nodes and three degrees of freedom, presents very good performance and may be used in various practical problems [Bel 2005b].

1.5. Advantage of the strain approach

Direct interpolation based on the strain approach provides a better precision on these values and on constraints and displacements (obtained by integration); compared to the classic formulation where deformations are obtained by derivation of the chosen displacement fields.

The main advantages of this approach [SAB 71] and [BEL 2000] are:

- Easily satisfaction of the main two convergence criteria bound directly to strains (constant strains and rigid body movement).
- Effortlessly decoupling of the various strain components (a field of uncoupled displacements generates coupled strains).
- Possibility of enriching the field of displacements by terms of high order without the introduction of intermediate nodes or of supplementary degrees of freedom (allowing so to treat the problem of locking).

1.6. Finite element method modeling and its applications to structures

1.6.1. Finite element method modelling

The finite element procedure reduce the continuum structure of any dimension to one of a finite number of unknowns by dividing the solution region into elements and by expressing the unknown field variable in terms of assumed approximating functions within each element. The approximating functions are defined in terms of the values of the field variables at specified points called nodes. The nodal values and the approximating functions for the elements completely define the behaviour of the field variable within the elements. For the finite element representation of a problem, the nodal values of the field variable become the new unknowns. Once these unknowns are found, the approximating functions define the field variable throughout the assemblage of elements. In the field of structural analysis, the most common approach, to finite element modeling of structure, is to consider that the displacements at the nodal points are the main unknown parameters of the problem.

1.6.2. Modelling the structure

The model should be chosen to represent the real structure as closely as possible with regard to the geometrical shape, loading and boundary conditions. The geometrical form of the structure is the major factor to be considered when deciding the shape of elements to be used (Fig.1.1). Another factor in the idealisation process is the size of the elements used. This, however, depends on many other factors, such as the efficiency of the elements and the importance of local features in the structure, e.g. stress concentrations. In many cases, only one type of elements is used for a given problem, but sometimes it is more convenient to adopt a mixed subdivision in which more than one type of elements is used, e.g. a beam element is connected to a shell element as a stiffener.

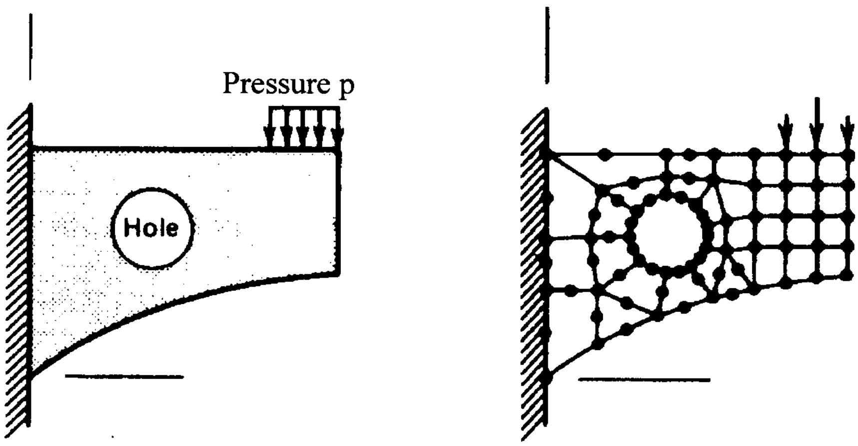

(a) (b)

Fig.1.1: (a) A plane structure of arbitrary shape
(b) A possible finite element model of the structure

1.6.3. Formulation of the element stiffness matrix

The evaluation of the stiffness matrix of the finite element is the most critical step in the whole procedure and in which the accuracy of the approximation is controlled. This step includes:

The number of nodes, the number of nodal degrees of freedom and the choice of the displacement functions used to represent the variation of the displacement within the element.

Each element may contain corner nodes, side nodes or even interior nodes. The degrees of freedom usually refer to the displacements and their first order partial derivatives at a node but very often may include second or even higher order partial derivatives.

By using the principle of virtual work or the principle of minimum potential energy, a stiffness matrix relating the nodal forces to the nodal displacement can be derived. Hence, the choice of suitable displacement functions is the major factor to be considered in evaluating element matrices.

With a good displacement pattern, convergence towards the correct value will be much faster than with a poor pattern, thus resulting in a saving in the computing time. In order to achieve the convergence towards the correct value, three rules govern the choice of displacement functions known as "convergence criteria":

* **Rigid Body Movement**: It must be possible for the element to move as a rigid body movement without at the same time causing any internal strains. For the displacement functions given in terms of simple polynomials, this requirement will only be satisfied when the elements become very small.

* **Constant Strains**: When the number of elements in a structures is very large (and their size very small), nearly constant strain conditions may exist in each element. Thus in the limit the displacement functions chosen must allow any state of constant strain to exist within an element.

* **Inter Element Compatibility:** The element subdivision must" fit" together both before and after deformation. Thus along a common edge between adjacent elements, the displacement must be described uniquely by the common nodes along that edge. A poor choice of displacement functions for any element type may however violate the requirement of continuity. In general, it is not always necessary that the element should be fully compatible across its boundaries (i.e. conforming). In f act, many elements exist which do not satisfy this requirement yet they yield accurate results [CLO 66].

The following steps summarise the general procedure for establishing the stiffness relations of plane finite elements, in matrix notation:

- The strains within an element are expressed in terms of the nodal displacements

$$\{\varepsilon\} = [B]\{\delta^e\}$$

- The stresses at any points in the element are expressed in terms of the strains at that point

$$\{\sigma\} = [D]\{\varepsilon\}$$

The external work done by the nodal forces:

$$\text{External work} \quad (W_{ext})_e = \frac{1}{2}\{\delta^e\}^T\{P^e\}$$

The internal work given by the strains energy of deformation within the element:

$$\text{Internal work} \quad (W_{in})_e = \frac{1}{2}\int_V \{\varepsilon\}^T\{\sigma\}d(vol)$$

Hence, substituting for $\{\sigma\} = [D][B]\{\delta^e\}$ and $\{\varepsilon\}^T = \{\delta^e\}^T[B]^T$ in the above two equations, and equating external and internal work we end up with:

$$\{P^e\} = \left\lfloor \int [B]^T[D][B]d(vol) \right\rfloor \{\delta^e\}$$

These are the stiffness relations

$$\{P^e\} = \lfloor k^e \rfloor \{\delta^e\}$$

Where: $\lfloor k^e \rfloor$ is the element stiffness matrix.

1.7. Scope of the work

To analyse a structure which has complex geometrical shape in real problem, by a limited number of finite elements with a regular shape is not sufficient at all. The purpose of this work is to overcome this geometrical inconvenience and to provide additional developments of new finite elements formulated essentially on strain based approach.

The application of the finite elements method and the results obtained in the analysis of structures has progressively improved with the development of elements based on the strain approach. Therefore to achieve this purpose, this thesis intend to the following contributions:

The second chapter is entirely devoted to the development of a new sector element based on the strain approach. This element has four nodes in addition to the central node. The performance of the developed sector element baptised **SBMS-BH** is tested by applying it to a thick cylinder under internal pressure.

The Third chapter attempts to develop a new analytical integration solution routine to evaluate the element stiffness matrix for the finite elements with irregular shapes. For reasons of importance and particularity of the developed elements based on strain rather than displacement approach (higher order shape functions expressed in terms of independent strains) with coupled variable kinematics; this complicates the use of the numerical integration, also, these elements are characterized by regular forms, which tend to decrease their utilization domain. To overcome this geometrical inconvenience, this chapter presents a new integration solution routine to extend their applications domain for the structures no matter what the geometrical shape might be.

The fourth chapter is entirely devoted to the development of a simple quadrilateral element having two degrees of freedom at each node and is formulated by using the concept of static condensation. It is based on the strain approach and satisfies the equilibrium equations. This element can be used to solve general plane elasticity problems. The results obtained are comparable with those given by the standard quadrilateral element Q4 and the robust element Q8.

The fifth and sixth chapters are dealing with the formulation of two finite elements. As it is well known, that calculations by finite elements of structures formed by plates and shells became a real tool with industrial vocation. It is very wide-spread in numerous sectors with high technology, civil or military (aprons of bridges, motor bodies, fuselages and wings planes…). Many engineers prefer to deal with the structures analysis by simple finite elements such as triangular elements with 3 nodes, quadrilateral with 4 nodes or solids with 8 nodes and with the same number of degrees of freedom per node:

The first element is a flat shell element **ACM_Q4SBE1,** is composed by assembling the two elements **Q4SBE1** and **ACM.** This element can be used for the analysis of shell structures.

The second element is a parallelepiped finite element baptized **SBP8C** (3 d.o.f/node; 9 nodes) based on the strain approach. It has the three essential external degrees of freedom at each corner node in addition to the centroidal node.

To test the performance of these elements, they have been applied to some reference validation examples and they are compared to the others elements.

CHAPTRE 2

A NEW STRAIN BASED MIXED SECTOR ELEMENT

CHAPTRE 2

A NEW STRAIN BASED MIXED SECTOR ELEMENT

2.1. Introduction

As described in the first chapter; in order to obtain satisfactory finite element results, the analysis of arbitrary shaped structures by displacements model, can be done by using finite elements with typical geometry. Argyris and Kelsey [ARG 60] have proposed the use of rectilinear elements such as triangles, rectangles and quadrilaterals for the analysis of complex structures. For structures with curved boundaries, it was revealed that, to obtain satisfactory converged results, the finite elements based on assumed independent polynomial functions, require the curved structures to be divided into a large number of elements. However in some particular cases where the boundaries are circular such as annular plates and at the neighbourhood of circular holes, it would appear more appropriate and economical to use sector element.

The success of the application of the strain based approach to the two dimensional plane elasticity problems impelled researchers to extend their work to the other structure types, arbitrary shaped structures and curved structures. The development of finite sector elements in polar coordinates can be achieved in three ways:

The first method " direct approach" is to derive strain based elements in polar coordinates, using a direct approach, i.e. by giving due consideration to the strain-displacement relationship in polar coordinate, assuming polynomial expressions for the strain and integrating the resulting equations to obtain the displacement functions. This method has been used by Sabir and Bouzerira [BOU 87].

The second method "Coordinate transformation" is to use the displacement fields obtained in Cartesian coordinates and converting the coordinates system to polar one. This method has been used by Sabir and Slahi [SAB 86].

The third method "Raju approach" is to use the displacement fields obtained in Cartesian coordinates and replacing x and y with r and θ (polar coordinates).

2.2. Previous developed Sector Elements

The following sector elements are developed using strain based approach:

2.2.1. Raju and Rao Element [RAJ 69]

One of the most commonly used finite elements for plane elasticity problems in Cartesian coordinates is the rectangular bilinear element where the displacement functions are given by

$$U = a_1 + a_2 x + a_3 y + a_4 x y \tag{2.1a}$$

$$V = a_5 + a_6 x + a_7 y + a_8 x y \tag{2.1b}$$

Raju *et al* developed a sector element based on the above functions by replacing x and y with r and θ ; hence the displacement field would be

$$Ur = a_1 + a_2 r + a_3 \theta + a_4 r \theta \tag{2.2a}$$

$$V_\theta = a_5 + a_6 r + a_7 \theta + a_8 r \theta \tag{2.2b}$$

2.2.2. Sabir and Salhi Element [SAB 86]

Sabir and Salhi used the second approach and developed a strain based sector element. It has two degrees of freedom at each corner node. The coordinates systems and displacements are as shown in Fig.2.1.

The displacement functions are given by the following equations:

$$\bar{U} = a_1 - a_3 y + a_4 x + a_5 xy + a_8 y/2 - a_7 y^2/2 \tag{2.3a}$$

$$\bar{V} = a_2 + a_3 x + a_6 y + a_7 xy + 0.5\, a_8 x - a_5 x^2/2 \tag{2.3b}$$

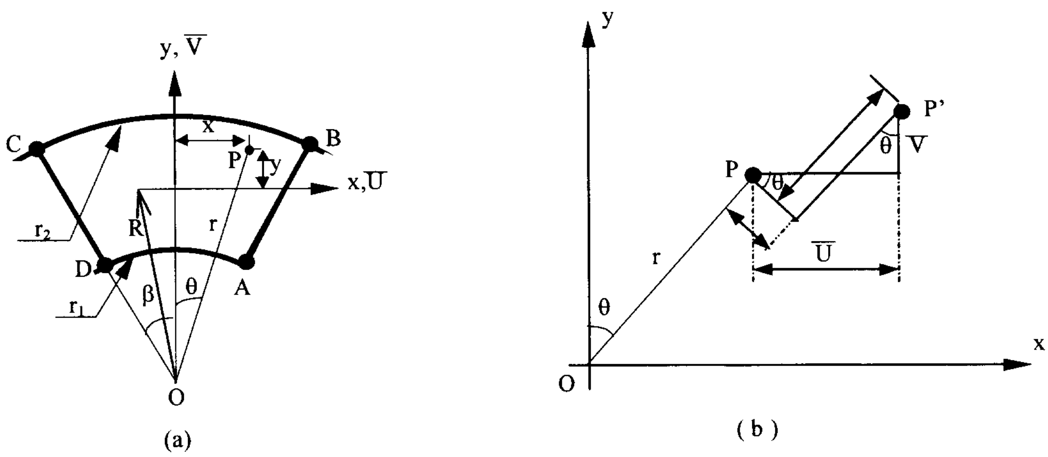

Fig.2.1: Coordinates systems and displacements for the sector element

To convert the above two equations in terms of polar coordinate system, using the following expressions from Fig.2.1.(b).

$$x = r \sin\theta \tag{2.4a}$$

$$y = r \cos\theta - R \tag{2.4b}$$

Where R is the radius of curvature of the central circumferential line of the element and the polar coordinates r and θ are as shown in Fig.2.1(a) .

The displacement components in the ε_y are the direct strains, γ_{xy} is the hearing strain, and U and V are the translational displacement in the r and θ directions U and V are given by Fig.2.1(b):

$$U = \overline{U} \sin\theta + \overline{V} \cos\theta \tag{2.5a}$$

$$V = \overline{U} \cos\theta - \overline{V} \sin\theta \tag{2.5a}$$

The final displacement functions are given in terms of polar coordinates as follows:

$$U = a_1 \sin\theta + a_2 \cos\theta + a_3 R \sin\theta + a_4 r \sin^2\theta + a_5\, r \sin^2\theta\, (r \cos\theta/2 - R) + a_6 \cos\theta\, (r \cos\theta - R) + a_7 \sin\theta\, (r^2 \cos^2\theta - R^2)/2 + a_8 \sin\theta\, (r \cos\theta - R/2)$$

$$V = a_1 \cos\theta - a_2 \sin\theta + a_3\, (R \cos\theta - r\,) + a_4\, r \sin\theta \cos\theta + a_5\, r \sin\theta\, (r \cos^2\theta + r \sin^2\theta/2) + a_6 \sin\theta\, (R - r \cos\theta\,) - a_7\, (r^2 \cos^3\theta - R^2 \cos\theta + 2\, r^2 \sin^2\theta \cos\theta - 2rR\,)/2 + a_8\, (\cos 2\theta - R \cos\theta)/2$$

2.2.3. Bouzerira Element [BOU 87]

Bouzerira has developed a twelve degrees of freedom strain based sector element, the strain field proposed is:

$$\begin{aligned} \varepsilon_r &= a_4 + a_5\theta + a_6 r \\ \varepsilon_\theta &= a_7 + a_8\theta + {}^{a_9}\!/_{r} + (a_6 r) \\ \gamma_{r\theta} &= a_{10} + {}^{a_{11}\theta}\!/_{r} + a_{12} r + \left({}^{a_6 r\theta}\!/_{2}\right) \end{aligned} \tag{2.6}$$

However the results obtained by this element when analysing some plane elasticity problems were shown to be unsatisfactory, particularly for the deflection convergence.

2.2.4. Djoudi Elements [DJO 90]

Djoudi has developed two sector elements:

The first element is developed by using the second approach and using the shape functions of the SBRIEIR developed by Sabir [SAB 86], the strain filed

$$\varepsilon_x = a_4 + a_6 y + a_{10} y^2 + 2a_{11} xy^3 \tag{2.7a}$$

$$\varepsilon_y = a_7 + a_8 x - a_{10} x^2 - 2a_{11} yx^3 \tag{2.7b}$$

$$\gamma_{xy} = 2\, a_5 + a_6 x + a_8 y + 2a_9 y + 2a_{12} x \tag{2.7c}$$

The Second element is developed by using the first approach and using the shape functions of Bouzerira element [BOU 87], the strain filed is

$$\varepsilon_r = a_4 + a_5\theta + a_6 r \tag{2.8a}$$

$$\varepsilon_\theta = a_7 + a_8\theta + {}^{a_9}\!/_{r} + (a_6 r) \tag{2.8b}$$

$$\gamma_{r\theta} = a_{10} + {}^{a_{11}\theta}\!/_{r} + a_{12} r + \left({}^{a_6 r\theta}\!/_{2}\right) \tag{2.8c}$$

We note here that these two elements ameliorate the results, but still unstable against aspect ratio.

2.2.5. Belarbi Element SBS4 [BEL 98a]

Belarbi and Charif have used the same approach as Raju and Rao [RAJ 69], and developed a strain based sector element. It has Three degrees of freedom at each corner node. The displacement fields proposed in Cartesian coordinates are:

$$\begin{aligned}
\overline{U} &= a_1 - a_3 y + a_4 x + a_5 y + a_6 xy + a_8 \frac{y^2}{2} + a_9 y^2 + a_{10} xy^2 + a_{11} x^2 y^3 \\
\overline{V} &= a_2 + a_3 x + a_5 x + a_6 \frac{x^2}{2} + a_7 y + a_8 xy - a_{10} x^2 y - a_{11} y^2 x^3 + a_{12} x^2 \\
\theta_z &= a_3 - a_9 y - 2a_{10} xy - 3a_{11} x^2 y^2 + a_{12} x
\end{aligned} \tag{2.9}$$

By replacing x and y with r and θ ; hence the displacement field would be:

$$\begin{aligned}
U_r &= a_1 - a_3\theta + a_4 r + a_5\theta + a_6 r\theta + a_8 \frac{\theta^2}{2} + a_9\theta^2 + a_{10} r\theta^2 + a_{11} r^2\theta^3 \\
V_\theta &= a_2 + a_3 r + a_5 r + a_6 \frac{r^2}{2} + a_7\theta + a_8 r\theta - a_{10} r^2\theta - a_{11}\theta^2 r^3 + a_{12} r^2 \\
\theta_z &= a_3 - a_9\theta - 2a_{10} r\theta - 3a_{11} r^2\theta^2 + a_{12} r
\end{aligned} \tag{2.10}$$

2.3. Formulation of the New Mixed Sector Element SBMS-BH

2.3.1. Satisfaction of rigid body movements (RBM)

Consider the rectangular element shown in Fig.2.2 (a): the three components of strain at any point in the Cartesian coordinate system x and y will be given by

$$\varepsilon_x = \frac{\partial U}{\partial x} \tag{2.11a}$$

$$\varepsilon_y = \frac{\partial V}{\partial y} \tag{2.11b}$$

$$\gamma_{xy} = \frac{\partial U}{\partial y} + \frac{\partial V}{\partial x} \tag{2.11c}$$

Where ε_x and ε_y are the direct strains, γ_{xy} is the hearing strain, and U and V are the translational displacement in the x and y directions respectively

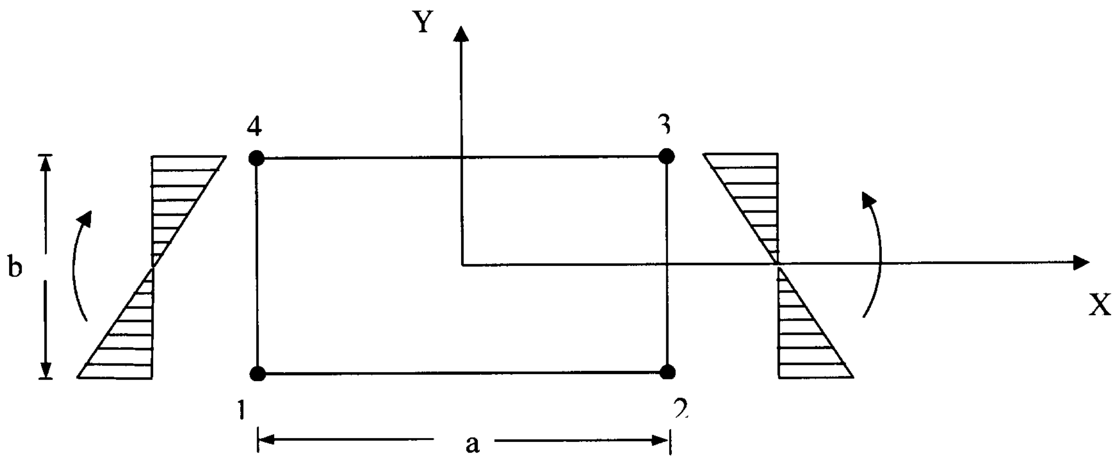

(a) Before bending

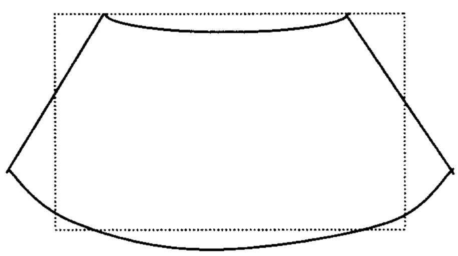

(b) Deformed shape
«Strain based approach

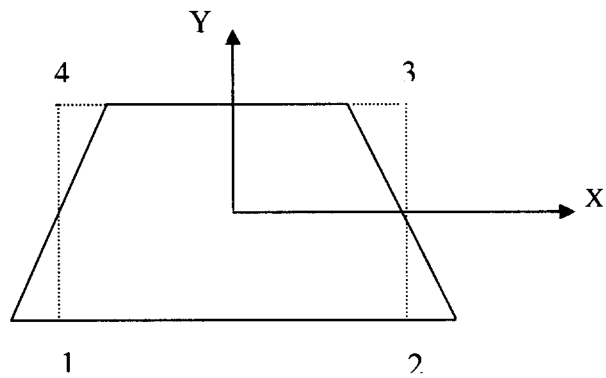

(c) Deformed shape
«Displacement approach » bilinear

Fig .2.2: Pure bending state

If we consider a rigid body movements Fig.2.2, i.e. displacements of an element without straining, we will have:

$$\varepsilon_x = 0 \tag{2.12a}$$

$$\varepsilon_y = 0 \tag{2.12b}$$

$$\gamma_{xy} = 0 \tag{2.12c}$$

Integrating the first two equations (2.12a) and (2.12b), we obtain the following expression for U and V

$$U = a_1 + f_1(y) \tag{2.13a}$$

$$V = a_2 + g_1(x) \tag{2.13b}$$

Then differentiating equations (2.13) and substituting in the equation (2.12c), we obtain the following equation

$$f'_1(y) + g'_1(x) = 0 \tag{2.14}$$

We should mention here that $f'_1(y)$ and $g'_1(x)$ must be constant, then if we take

$$f'_1(y) = -a_3 \tag{2.15a}$$

$$g'_1(x) = a_3 \tag{2.15b}$$

Then integrating the two above equations we find:

$$f_1(y) = -a_3 y \tag{2.16a}$$

$$g_1(x) = a_3 x \tag{2.16b}$$

Substituting $f_1(y)$ and $g_1(x)$ in equations (2.13), we obtain the rigid body movements

$$U = a_1 - a_3 y \tag{2.17a}$$

$$V = a_2 + a_3 x \tag{2.17b}$$

Equations (2.17) represent the displacement fields for the sector element in terms of its three rigid body movement components a_1, a_2 and a_3. Where a_1 and a_2 are the translations in the in x and y directions respectively, wile the component a_3 is the in plane rotation see Fig.2.3

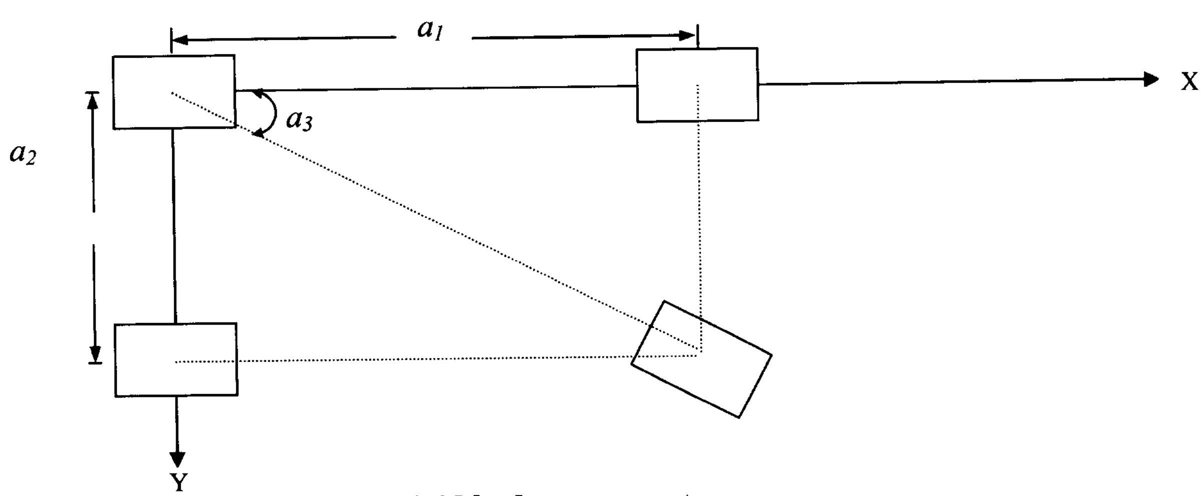

Fig.2.3: Rigid body movements

2.3.2. Displacement functions for The R4BM element

Belarbi and Maalem have developed a membrane finite element for plane elasticity analysis [BEL 2005]. This element is rectangular with four corner nodes and a central node, each node has two degrees of freedom and based on the strain approach as shown in Fig.2.4 a. The suitable shape function assumed is given as follows:

$$\varepsilon_x = a_4 + a_5 y + a_9 x \tag{2.18a}$$

$$\varepsilon_y = a_6 + a_7 x + a_{10} y \tag{2.18b}$$

$$\gamma_{xy} = a_8 \tag{2.18c}$$

In equations (2.18) the three strain components can not be taken arbitrarily, they must satisfy the compatibility equation

$$\frac{\partial^2 \varepsilon_x}{\partial y^2} + \frac{\partial^2 \varepsilon_y}{\partial x^2} - \frac{\partial^2 \gamma_{xy}}{\partial x \partial y} = 0 \tag{2.19}$$

By integrating equations (2.18), the displacement functions are obtained as follows:

$$U = a_4 x + a_5 xy - 0.5\, a_7 y^2 + 0.5\, a_8 y + 0.5\, a_9 x^2 \tag{2.20a}$$

$$V = -0.5\, a_5 x^2 + a_6 y + a_7 xy + 0.5\, a_8 x + 0.5\, a_{10} y^2 \tag{2.20b}$$

The final displacement functions are obtained by adding equations (2.17) and (2.20):

$$U = a_1 - a_3 y + a_4 x + a_5 xy - 0.5\, a_7 y^2 + 0.5\, a_8 y + 0.5\, a_9 x^2 \tag{2.21a}$$

$$V = a_2 + a_3 x - 0.5\, a_5 x^2 + a_6 y + a_7 xy + 0.5\, a_8 x + 0.5\, a_{10} y^2 \tag{2.21b}$$

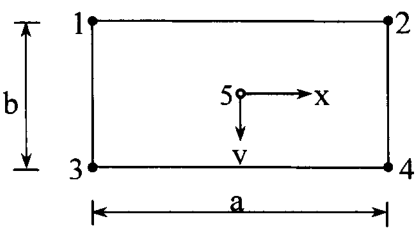

Fig.2.4: Co-ordinates and nodal points for the rectangular R4BM element

2.3.3. Displacement functions for the New Sector Element SBMS-BH

The second approach mentioned above is used to develop a new sector element based on the shape functions of R4BM element [BEL 2005a]. This element has four nodes in addition to the central node, and two degrees of freedom per node U and V (Fig.2.5), by replacing x and y with r and θ; hence

$$U_r = a_1 - a_3\,\theta + a_4 r + a_5 r\theta - 0.5\,a_7\,\theta^2 + 0.5\,a_8\,\theta + 0.5\,a_9 r^2 \tag{2.22a}$$

$$V_\theta = a_2 + a_3 r - 0.5\,a_5 r^2 + a_6\,\theta + a_7 r\theta + 0.5\,a_8\, r + 0.5\,a_{10}\theta^2 \tag{2.22b}$$

The stiffness matrix $[K_e]$ for the sector element can now be calculated from the well-known expression

$$[K_e] = [A^{-1}]^T \left[\iint_S [B]^T [D][B] r.dr.d\theta \right] [A^{-1}] \tag{2.23a}$$

$$[K_e] = [A^{-1}]^T [K_0] [A^{-1}] \tag{2.23b}$$

With: $$[K_0] = \int_{-\beta}^{\beta}\int_{r_1}^{r_2} [B]^T [D][B] r.dr.d\theta \tag{2.23c}$$

Where [D] is the rigidity matrix, [A] is the transformation matrix and [B] is the strain matrix.

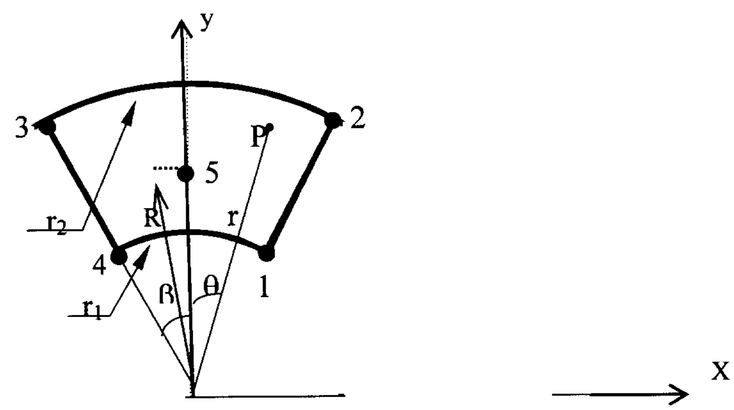

Fig.2.5: Coordinate system and displacements for the sector element SBMS-BH

In polar coordinates the strain displacement relationships are given by

$$\varepsilon_r = \frac{\partial U_r}{\partial r} \tag{2.24a}$$

$$\varepsilon_\theta = \frac{U_r}{r} + \frac{\partial U_r}{r\partial\theta} \tag{2.24b}$$

$$\gamma_{r\theta} = \frac{\partial U_r}{r\partial\theta} + \frac{\partial V_\theta}{\partial r} - \frac{V_\theta}{r} \tag{2.24c}$$

Where ε_r and ε_θ are the direct radial and circumferential strains and $\gamma_{r\theta}$ is the shearing strain.

From Eqs. (2.22) and (2.24) the strain matrix [B] can be derived. See **Appendix A.1**

For the case of plane stress problems where:

$$[\mathrm{D}] = \begin{bmatrix} \mathrm{D11} & \mathrm{D12} & 0 \\ \mathrm{D12} & \mathrm{D22} & 0 \\ 0 & 0 & \mathrm{D33} \end{bmatrix} \tag{2.25}$$

Where: $D11 = D22 = \dfrac{E}{\left(1-\nu^2\right)}$ $\quad D12 = \dfrac{\nu.E}{\left(1-\nu^2\right)}$ $\quad D33 = \dfrac{E}{2(1+\nu)}$

The result of the matrix multiplication and integration required to obtain the bracketed part $[K_0]$ is given explicitly in the **Appendix A.2.** $[K_e]$ is then calculated by carrying out the multiplication by $[A^{-1}]$ and its transpose in the usual way.

2.3.4. Evaluation of Stresses

Having obtained the displacements, the stresses are evaluated by using the stress-strain relationships, the stresses within the element can then be obtained by the strain filed derived from the following displacement functions [BEL 98a].

$$\begin{aligned} U_r &= a_1 - a_3\theta + a_4 r + a_5\theta + a_6 r\theta + a_8\frac{\theta^2}{2} + a_9\theta^2 + a_{10}r\theta^2 + a_{11}r^2\theta^3 \\ V_\theta &= a_2 + a_3 r + a_5 r + a_6\frac{r^2}{2} + a_7\theta + a_8 r\theta - a_{10}r^2\theta - a_{11}\theta^2 r^3 + a_{12}r^2 \\ \theta_z &= a_3 - a_9\theta - 2a_{10}r\theta - 3a_{11}r^2\theta^2 + a_{12}r \end{aligned} \tag{2.26}$$

Results and convergence curve for deflections and stresses are given and compared with the exact solution and those obtained from other sector elements.

2.4. Validation test

The performance of the developed sector element **SBMS-BH** is tested by applying it to a thick cylinder under internal pressure.

The dimension, loading and elastic properties for this rotationally symmetric plane stress problem are given in Fig.2.6. Due to symmetry only one quarter of the cylinder is considered in the finite element idealisations Fig2.6. (b).

Internal radius $a = 20$ mm   Thickness $t = 1$ mm

External radius $b = 40$ mm   Poisson ratio $\nu = 0{,}3$

Young's modulus $E = 2\ 10^5$ MPa (Steel)

$\sigma_e = 210$ MPa $\alpha = \pi/4$

Condition of symmetry:

AB and CD $V_\theta = 0$ Internal pressure $q = 0{,}1$ KN/mm^2

Fig.2.6: Thick cylinder under internal pressure.

The results obtained for the radial deflections Ur and the stresses σ_r and σ_θ are compared to the analytical solution given by Rekatch [REK 80]:

$$
\begin{aligned}
U_r &= \frac{(1+\nu)}{E(b^2-a^2)}\left[(1-2\nu)(a^2P_i - b^2P_e)r + \frac{a^2b^2}{r}(P_i - P_e)\right] \\
V_\theta &= 0 \\
\sigma_r &= \frac{1}{(b^2-a^2)}\left[a^2P_i - b^2P_e + \frac{a^2b^2}{r^2}(P_e - P_i)\right] \\
\sigma_\theta &= \frac{1}{(b^2-a^2)}\left[a^2P_i - b^2P_e - \frac{a^2b^2}{r^2}(P_e - P_i)\right]
\end{aligned}
\qquad (2.27)
$$

In this case: $P_i = q$; $P_e = 0$

The following are calculated for the mid point E (r=30mm) along the radial section m-n.,

Ur: The radial deflection

σ_r : The radial stress this

σ_θ : The tangential stress

The convergence of radial deflection U_r, and the stresses σ_r and σ_θ at point E (r = 30 mm) are presented in Table 2.1 and also plotted by using different mesh size.

Mesh	Radial deflection U_r (mm)	Radial Stress σ_r (MPa)	Tangentielle Stress σ_θ (MPa)
2 x 2	1,4146	38,828	86,997
4 x 2	1,4155	28,883	91,320
6 x 2	1,4155	27,228	92,033
8 x 2	1,4156	26,633	92,288
10 x 2	1,4157	26,383	92,404
12 x 2	1,4156	26,248	92,458
14 x 2	1,4156	26,174	92,486
Exact Sol.	**1,4155**	**25,9259**	**92,5900**

Table 2.1: Thick cylinder under internal pressure

The computed results for the radial deflection at mid point along the radial section m-n are shown in table 2.1. The figure 2.7 shows that the results from **SBMS-BH** converge to the analytical results when the cylinder is divided into a small number of elements (2x2), which illustrates the high degree of accuracy obtained from element **SBMS-BH,** for instance for a mesh size 2x2 elements the error accounts is equal to **0.063 %** of the exact solution.

Furthermore, the results obtained for the various components of stresses satisfactory and converge to the theoretical solution as the number of elements is increased.

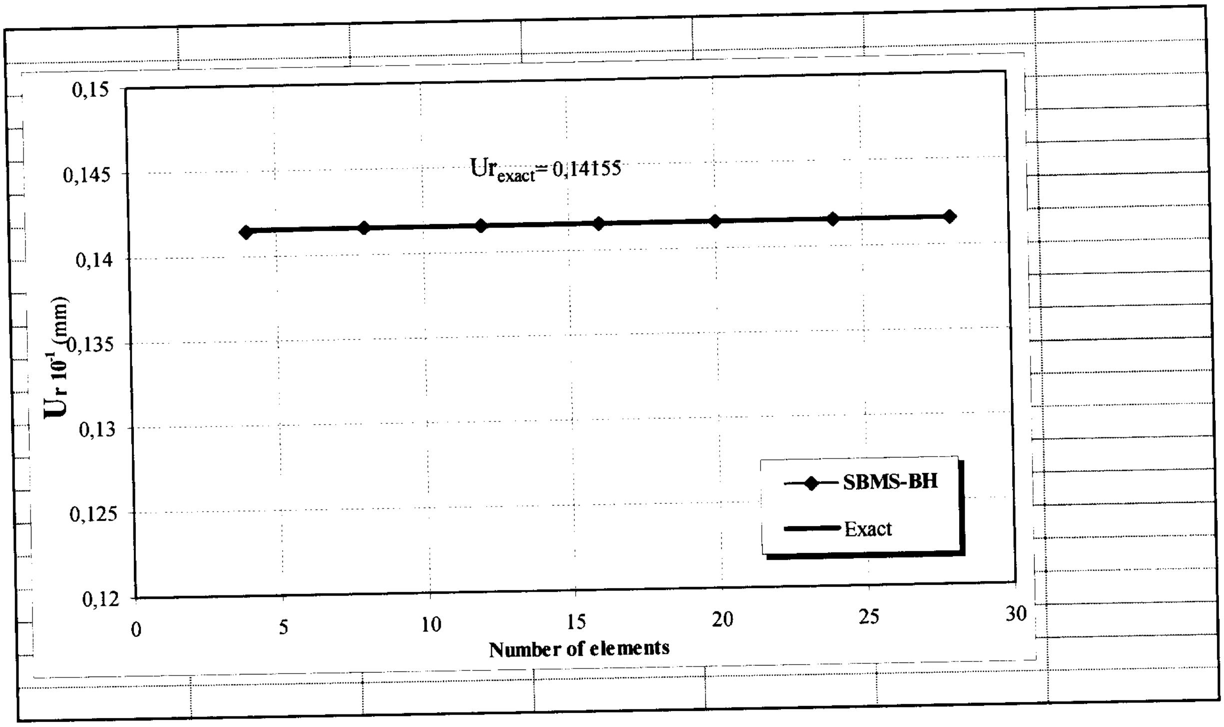

Fig.2.7: Convergence curve for the radial deflection U_r at point E

2.5. Conclusion

The inclusion of the internal node ameliorates the results obtained.

The results obtained from the developed element **SBMS-BH** are shown to converge to the theoretical solution for the problem considered.

We should mention here that the convergence is monotone for both deflections and stresses

The good performance of the developed sector element **SBMS-BH** is confirmed.

CHAPTER 3

A NEW INTEGRATION SOLUTION ROUTINE FOR QUADRILATERAL AND TRIANGULAR SHAPES

CHAPTER 3

A NEW INTEGRATION SOLUTION ROUTINE FOR QUADRILATERAL AND TRIANGULAR SHAPES

3.1. Introduction

Analytical expressions for the fully integrated stiffness matrix of a rectangular four node element have been published by Hacker and Schreyer [HAC 89] and analytical integration formulae for linear isoparametric elements by Babu and Pinder [BAB 84] and Rathod [RAT 88], Griffiths describes how the stiffness matrix of a general quadrilateral element can be expressed in closed form by expending and simplifying the four terms in the numerical integration summation [GRI 88]. Most of the finite elements based on assumed strains have been developed since 1972 by many researchers, Sabir and Ashwell [ASH 72], Sabir and Salhi [[SAB 86]], Belarbi [BEL 98a], [BEL 99], Djoudi and Bahai [DJO 2004a], [DJO 2004b] and others. Many of them were undertaking their research work at Cardiff University in the U.K. These elements were characterized by a regular form and appropriate coordinates with the form of the element; these coordinates can be Cartesian, polar, spherical, cylindrical or else conical. With the continuation of the development of the strain based approach many elements for general plane elasticity as well as shells have been derived by Sabir et al [SAB 85a], [SAB 85b] and [SAB 95].

To model a structure which has complex geometrical shape in real problem, by a limited number of elements as cited above; is not sufficient at all. To overcome this geometrical inconvenience; this chapter presents a new integration solution routine. This solution is adopted for two reasons. First, to know how these elements will behave when they have irregular forms. And second, in the positive case, to extend their applications domain for the structures no matter what the geometrical shape might be [BEL 2003]. The performance of this new solution routine is tested by applying to the analysis of the problems used in previous publications and to obtain solutions for practical problems in engineering.

3.2. Integration method

3.2.1. Numerical integration

The element stiffness matrix [Ke] can be calculated using the well known Eq.(3.1)

$$[K_e] = \iint_S [B]^T [D][B] \det J.d\xi.d\eta \qquad (3.1)$$

Where:

[B]: the strain matrix

[D]: the rigidity matrix

det J: the determinant of Jacobian matrix

To carry out the integral, we have to choose either numerical integration (e.g Gauss integration) or analytical integration. One of the disadvantages of the numerical integration is the high order of the monomials after the three multiplications of integral matrices Eq.(3.1), which would signify many integration points.

3.2.2. Sabir approach [SAB 85a]

If we consider the triangular element shown in Fig.3.1, the element stiffness matrix can be calculated using Eq.(3.2)

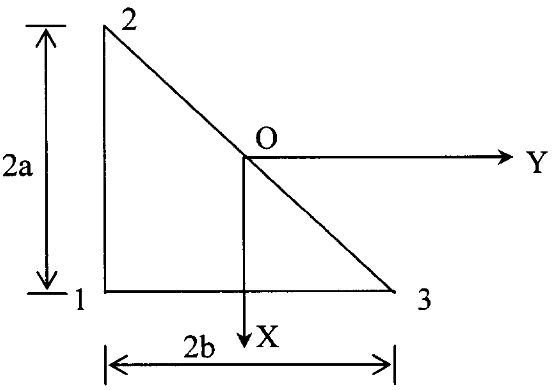

Fig.3.1: Triangular element, Coordinate axes

$$[K_e] = \left[A^{-1}\right]^T \left[\int_{-b}^{b} \int_{\frac{ay}{b}}^{a} [Q]^T [D].[Q]..dx.dy \right] \left[A^{-1}\right] \qquad (3.2)$$

Where:

[A]: Transformation matrix

[Q]: Strain matrix

The multiplication and integration of the terms within the brackets Eq.(3.2) are carried out explicitly. In order to use the nodal Sabir solution routine and to simplify the assembly of the finite elements, for the problem considered, Sabir used the following technique in which two triangles are combined together to form a rectangular element as shown in Fig.3.3. This was achieved by substituting the coefficients of each node from the element stiffness matrices of the two triangles into their corresponding place in the element stiffness matrix of the two combined elements as shown in Fig.3.2 and Fig.3.3. The stiffness matrix of the combined elements will then be used in the assembly of the overall stiffness matrix of the structure. Unfortunately, the above technique is suitable only for a rectangle triangular element (rectangular form) which decreases its utilization domain:

Firstly according to the integral limits, the obtained element has a simple shape which is a rectangle triangle.

Secondly, according to quadrilateral shapes, the element obtained is a simple rectangle. Hence the applied domain will be limited.

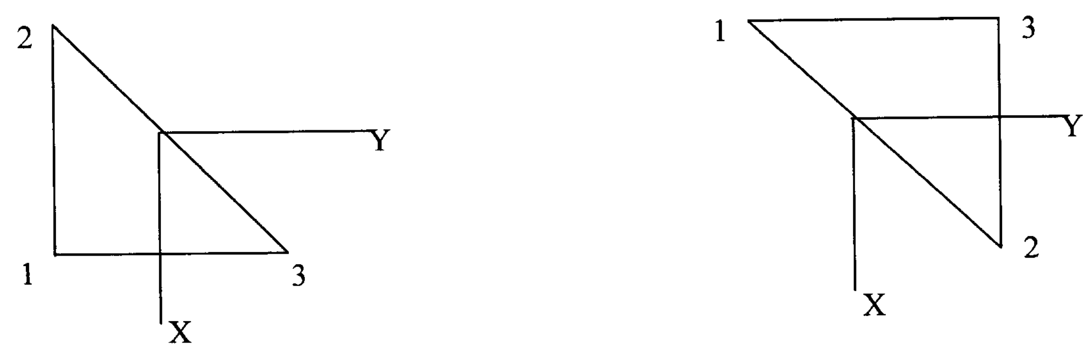

A	B	C
D	E	F
G	H	I

a	b	c
d	e	f
g	h	i

Fig.3.2: Stiffness matrix of each triangle element

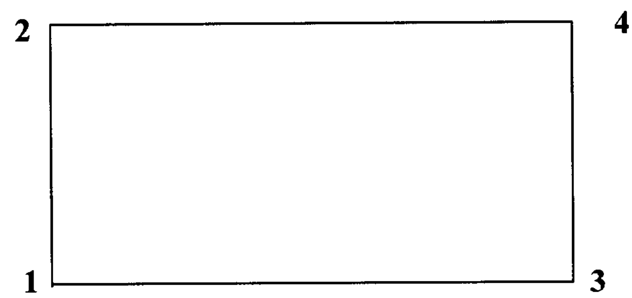

	B	C	
A	E+a	F+b	C
G	H+d	I+e	F
	G	H	I

Fig.3.3: Stiffness matrix of the combined elements

3.2.3. A new approach

The evaluation of the element stiffness matrix is summarized with the evaluation of the following expression:

$$[K_e] = [A^{-1}]^T \left[\iint_S [Q]^T [D][Q].dx.dy \right] [A^{-1}] \tag{3.3a}$$

$$[K_e] = [A^{-1}]^T [K_0] [A^{-1}] \tag{3.3b}$$

With: $$[K_0] = \iint_S [Q]^T [D].[Q].dx.dy \tag{3.3c}$$

Since [A] and its inverse can be evaluated numerically, the evaluation of the integral (3.3c) becomes the key of the problem.

In general, the multiplication $\mathbf{Q}^T$ **D Q** can be done manually, we will end up by calculating the double integrals of the form:

$$I = [K_0] = \iint_S C.x^{\alpha} y^{\beta}\, dx.dy \tag{3.4}$$

Knowing that, for certain elements, a too great distortion can lead to erroneous numerical results particularly in the calculation of the Jacobien, an expression that is general, and easy to implement numerically being formulated. It allows the evaluation of the matrix $[K_0]$ in an automatic way whatever the degree of the polynomial of the kinematics field and the distortion of the element (Fig. 3.4)

The calculation of integral **I** is the principal problem of the calculation of the element stiffness matrix [Ke].

In a very simple and effective manner, the integral is solved by the subroutine "INTEGRATION". To illustrate the step of calculation of the integral in detail, let us take the case of an arbitrary element as shown in Fig.3.4. The integral is composed of three parts symbolized on the figure by Roman numerals $\mathbf{I_1}$ $\mathbf{II_2}$ and $\mathbf{III_3}$, each integral must be calculated separately.

The integral will be solved easily if one can determine the limits of the integral with precaution, which is far from being obvious. The fact that the limits can change with the geometry of the element raises difficulties, which make the programming enormously complex.

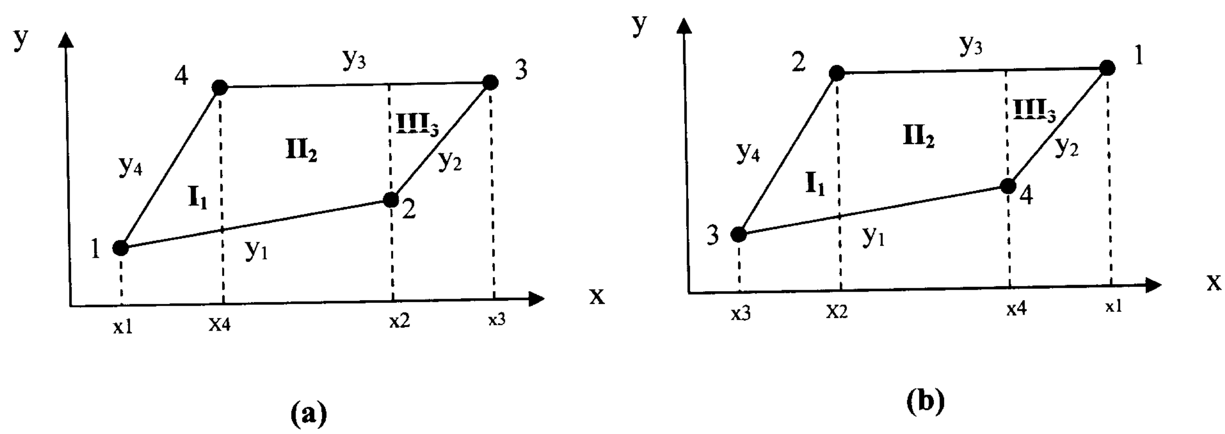

Fig.3.4: Quadrilateral element

$$I = I_1 + II_2 + III_3 \qquad (3.5)$$

Where:

$$I_1 = C.\int_{x_1}^{x_4}\int_{y_1}^{y_4} x^{\alpha} y^{\beta} dxdy \qquad (3.6a)$$

$$I_2 = C.\int_{x_4}^{x_2}\int_{y_1}^{y_3} x^{\alpha} y^{\beta} dxdy \qquad (3.6b)$$

$$I_3 = C.\int_{x_2}^{x_3}\int_{y_2}^{y_3} x^{\alpha}y^{\beta}dxdy \tag{3.6c}$$

This means calculating the double integrals of the following form:

$$I= \iint_S C.x^{\alpha} y^{\beta}\, dx.dy \tag{3.7a}$$

Where

C: constant

y: the ordinate of the segment of equation $y = ax + b$ (3.7b)

$y^2 = (ax + b)^2 = \mathbf{1}a^2x^2 + \mathbf{2}abx + \mathbf{1}b^2$ (3.7c)

$y^3 = (ax + b)(ax + b)^2 = \mathbf{1}\, a^3x^3 + \mathbf{3}a^2\, bx^2 + \mathbf{3}ab^2x + \mathbf{1}b^3$ (3.7d)

We will end up with the general form of y^{β} :

$$y^{\beta} = \sum_{k=1}^{\beta+1} C(k).a^{\beta+1-k}.b^{k-1}.x^{\beta+1-k} = \sum_{k=1}^{\beta+1} C(k).a^{k-1}.b^{\beta+1-k}.x^{k-1} \tag{3.8}$$

Where:

C(k): Coefficients function of β (see Table 3.1), is for example:

if β=1 we will have 2 coefficients (see (3.7b)).

if β=2 we will have 3 coefficients (see (3.7c)).

if β=3 we will have 4 coefficients (see (3.7d)).

	$C(k)_{K=1,6}$					
β	C(1)	C(2)	C(3)	C(4)	C(5)	C(6)
0	1	-	-	-	-	-
1	1	1	-	-	-	-
2	1	2	1	-	-	-
3	1	3	3	1	-	-
4	1	4	6	4	1	-
5	1	5	10	10	5	1

Table 3.1: C(k) coefficients relating to the expression (3.8)

In which:

$$\int y^{\beta}dy = \frac{1}{\beta+1}y^{\beta+1} = \frac{1}{\beta+1}(ax+b)^{\beta+1} = \frac{1}{\beta+1}\sum_{k=1}^{\beta+2}C(k).a^{k-1}.b^{\beta+2-k}.x^{k-1} \tag{3.9}$$

Therefore

$$\int_{y_i}^{y_j} y^{\beta}dy = \frac{1}{\beta+1}\sum_{k=1}^{\beta+2}C(k).\left(a_j^{k-1}.b_j^{\beta+2-k} - a_i^{k-1}.b_i^{\beta+2-k}\right).x^{k-1} \tag{3.10}$$

$$\iint x^{\alpha}y^{\beta}dx.dy = \int_m^n \frac{1}{\beta+1}\sum_{k=1}^{\beta+2}C(k).\left(a_j^{k-1}.b_j^{\beta+2-k} - a_i^{k-1}.b_i^{\beta+2-k}\right).x^{k+\alpha-1}.dx \tag{3.11}$$

$$\iint x^{\alpha}y^{\beta}dx.dy = \frac{1}{\beta+1}\sum_{k=1}^{\beta+2}\frac{1}{k+\alpha}C(k).\left(a_j^{k-1}.b_j^{\beta+2-k} - a_i^{k-1}.b_i^{\beta+2-k}\right)\left(x_n^{k+\alpha} - x_m^{k+\alpha}\right) \tag{3.12}$$

In our case:

$$I = \sum_{P=1}^{3} I_P \tag{3.13}$$

The general expression of I_P for a quadrilateral would be:

$$I_P = \frac{C}{\beta+1}\sum_{k=1}^{\beta+2}\frac{1}{k+\alpha}.C(k)\left(a_j^{k-1}.b_j^{\beta+2-k} - a_i^{k-1}.b_i^{\beta+2-k}\right)\left(x_n^{k+\alpha} - x_m^{k+\alpha}\right) \tag{3.14}$$

That is to say the expression of I for a triangle is:

$$I = \sum_{P=1}^{2} I_P \tag{3.15}$$

3.3. Programming the integral expression (3.14)

3.3.1. Determination of the integral limits

The limits of the volumetric integral of the equation (3.4) depend on the element geometry. In the following figures (Figs. 3.5 to 3.12) all the possible cases that must be distinguished when calculating the integral are schematized. The different figures are characterized by their integration limits. Let us take for example Fig. 3.5 and 3.6; to calculate the integral of the first part, I1 should be solved by the following equations:

$$I_1 = \int_{x(A)}^{x(B)} \int_{y_1}^{y_4} x^{\alpha} y^{\beta} dx dy \qquad \text{In the case of Fig. 3.5} \tag{3.16}$$

$$I_1 = \int_{x(A)}^{x(D)} \int_{y_1}^{y_4} x^{\alpha} y^{\beta} dx dy \qquad \text{In the case of Fig. 3.6} \tag{3.17}$$

There is obviously a change of the limits of co-ordinates x. Figures 3.5 to 3.12 show all the possible cases: to form a distorted element, there are theoretically 6 possibilities (Fig.3.5 to 3.10). As the distortion of the elements of Figs.3.11 and 3.12 is exaggerated, we can ignore the study of these two cases. We will accept only the use of the elements whose distortion remains moderate.

There remain only the 5 cases of a distorted element (Figs. 3.5 to 3.9) and the particular case of a rectangular element, illustrated in Fig.3.10.

Let us examine initially the case of the distorted elements (Fig.3.5 to 3.9). Illustrated in the figures in Roman numerals, the integration is composed of three different parts. To calculate the integral of these elements, we need a routine which is able to make the distinction between the 4 possible cases, and which provide the limits of integration. The programming of such a routine is not obvious. The numbering of the nodes varies from 1 to 4 but *a priori* we do not know which node has which numbering. To illustrate the problems, let us look at figure 3.5. To calculate the integral $\mathbf{I_1}$ we should solve the following integral:

$$I_1 = \int_{x(A)}^{x(B)} \int_{y_1}^{y_4} x^{\alpha} y^{\beta} dx dy \tag{3.18}$$

Neither the lines y_1 and y_4 nor the limits x (A) and x (B) are easy to determine. The numbering of nodes A and D is unknown. We do not know which nodes are hidden behind the nodes A and B. We thus need a routine which determines the numbering and assigns it with the nodes A, B, C and D.

To simplify the problem, we introduce a convention to number the nodes in anticlockwise direction.

Although this convention was adopted by several authors; it does not solve the whole problem. We cannot still identify the various nodes.

To finally solve the problem, a subroutine **FORM_ICORD** is introduced into the programming. The purpose of this subroutine is to find the sequence of the nodes and to provide the order of the nodes of the element arranged by co-ordinates **x** (according to the ascending order).

Let us look at figure 3.4 which shows an element having an arbitrary numbering. The subroutine **FORM_ICORD** introduces a Icord vector of dimension 4. In the example of the figure 3.4, Icord stores the following values:

Icord	Icord(1)	Icord(2)	Icord(3)	Icord(4)
Number of the node	1	4	2	3

Icord(1) contains the node number with the lowest co-ordinate **x** .

Icord(4) contains the node number with the highest co-ordinate **x**.

Using the Icord vector we can determine the limits of the integral easily. For example the integral $\mathbf{I_1}$ of the example of figure 3.5 is calculated in the following way:

$$I_1 = C \int_{x(Icord(1))}^{x(Icord(2))} \int_{y_1}^{y_4} x^\alpha y^\beta dxdy \tag{3.19a}$$

The key point of this step is to introduce into the limits of the co-ordinates of **x** the Icord vector. For the calculation of the above integral **I** , it is necessary to integrate the node with the lowest co-ordinates of **x** until the node which follows: x(Icord(1)) $\rightarrow$ x(Icord(2)).

The second integral $\mathbf{II_2}$ is calculated with the same method.

$$II_2 = C \int_{x(Icord(2))}^{x(Icord(3))} \int_{y_2}^{y_4} x^\alpha y^\beta dxdy \tag{3.19b}$$

The limits of the co-ordinates of x are replaced by x(Icord(2)) $\rightarrow$ x(Icord(3)). Likewise, it is necessary for the third integral $\mathbf{III_3}$ to replace the limits by x(Icord(3)) $\rightarrow$ x(Icord(4)).

$$III_3 = C \int_{x(Icord(3))}^{x(Icord(4))} \int_{y_3}^{y_4} x^\alpha y^\beta dxdy \tag{3.19c}$$

Now we know the limits of co-ordinates **x**, but we cannot still calculate the lines y_1 to y_4.

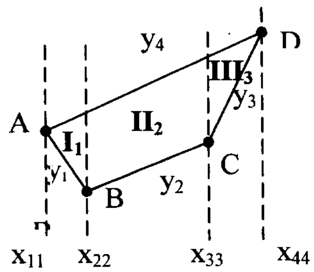

Fig. 3.5: Shape 1

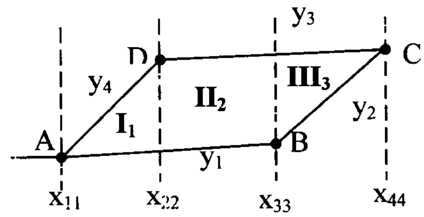

Fig.3.6: Shape 2

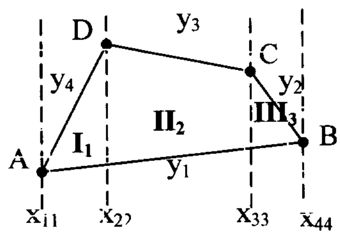

Fig. 3.7: Shape 3

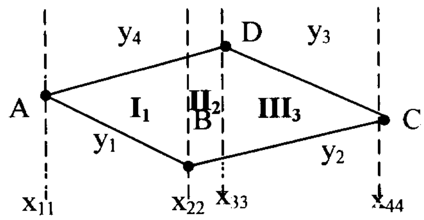

Fig.3.8: Shape 4

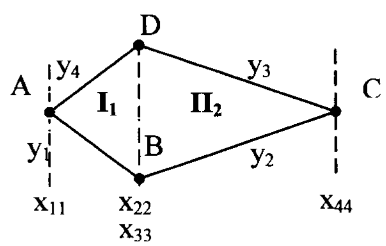

Fig. 3.9: Shape 5

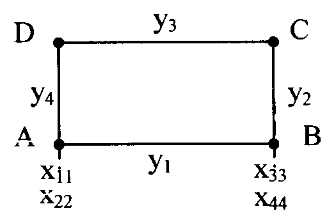

Fig. 3.10: Shape 6

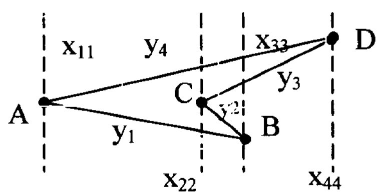

Fig. 3.11: Shape 7

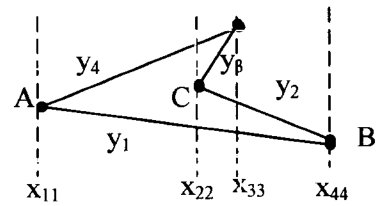

Fig. 3.12: Shape 8

For the case of triangular shapes, we have the following figures (3.13, 3.14).

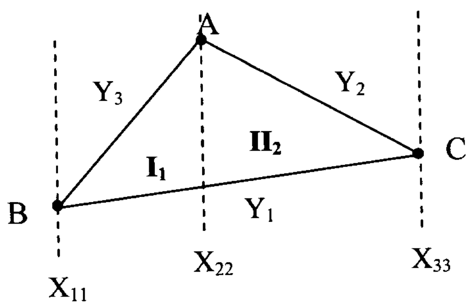

Fig.3.13: Shape 1

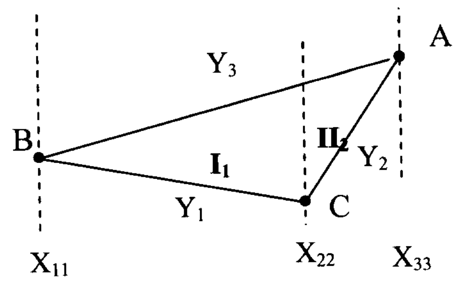

Fig.3.14: Shape 2

3.3.2. Determination of the lines y_1 to y_4 (y_3)

a) Case of quadrilateral shapes

Numbering the nodes in anticlockwise direction simplifies the determination of lines y_1 to y_4. Let us take the element of figure 3.6. In the drawing we can see the true numbering of the nodes and the numbering with the Icord vector. We can observe that the lines y_1 to y_4 do not change with the geometry of the element. The starting point of line y_1 is always the node stored in Icord(1). In the example of figure 3.4(a) the value stored in Icord(1) is 1. We can easily calculate the second point of the line using the equation:

$$2\ ^{2nd}\ \text{node} = \text{Icord}(1) + 1 = 2$$

In the case of figure 3.4(b) the value stored in Icord(1) is 3. The second point of the line can be calculated using the equation:

$$2\ ^{2nd}\ \text{node} = \text{Icord}(1) + 3 = 4$$

The other lines y_2 and y_3 are determined in the same way. Any handling of the Icord vector must hold account of which the node numbering is between 1 and 4. If for instance, the node 4 is hidden behind Icord(1), the complement Icord(1) +1 will be 5, which is obviously false. A correction is programmed easily with the order <u>IF of FORTRAN77.</u>

In the case of a rectangular element a subroutine must take account that the slope of the lines y_1 and y_2 is infinite, a value which does not exist in the programming languages.

The subroutine treating the calculation of the lines is called COEFF.

b) Case of triangular shapes

The triangular element is similar to the quadrilateral in point view of numbering of nodes in Icord vector (Fig.3.13 and 3.14), within a minimum of geometric forms can be used. For the two possible cases illustrated, the integration procedure can be used in two parts whatever the position of the nodes.

3.4. Calculation of the integral for the distorted elements

With the explanations of the preceding paragraphs, it is now possible to determine the limits of the integral: the lines $y_1$to y_4 and the limits of the co-ordinates of **x.** For the case of quadrilateral shapes a routine which carries out the integration "INTEGRATION" is given in **Appendix B.1** with the related subroutines.

3.5. Numerical applications

In order to illustrate the interest of the integration subroutine, **"INTEGRATION"** is thus developed. We have chosen to test the Sabir membrane element **SBRIEIR** [SAB 85a] through three case tests of isotropic plane elasticity, taking into account the geometrical distortions. These tests are regarded as a tool to validate of the membrane elements. The displacement field for the element **"SBRIEIR"** is as follows [SAB 85a]:

$$u = a_1 - a_3 y + a_4 x + a_8 y/2 + a_5 xy + a_{10} y^2/2 + a_{11} x y^2 + a_{12} x^2 y^3$$

$$v = a_2 + a_3 x + a_6 y + a_8 x/2 + a_7 xy + a_9 x^2/2 - a_{11} x^2 y - a_{12} x^3 y^2 \qquad (3.20)$$

$$\phi = a_3 - a_5 x/2 + a_7 y/2 + a_9 x/2 - a_{10} y - 2a_{11} xy - 3 a_{12} x^2 y^2$$

After the programming of the routines which calculate the integral, we can finally carry out the calculation of the element stiffness matrix $[K_0]$, **see Appendix B.2**

Note 1: The distorted version of the element **"SBRIEIR"** will be baptized **"SBQIEIR"**

3.5.1. High Order Patch Test: Pure bending of a cantilever

The cantilever is modeled by two membrane rectangular elements (regular mesh) or trapezoidal (distorted mesh); various cases of boundary conditions [SZE 92] are shown in the figures 3.15a, 3.15b and 3.15c.

The results obtained with the element **"SBQIEIR"** are compared with those obtained with other known quadrilateral elements (Q4, 07β MAQ, AQ and PS5β) (Figs.3.16 and 3.17).

Note 2 Q4 and PS5β are elements without rotation dof.

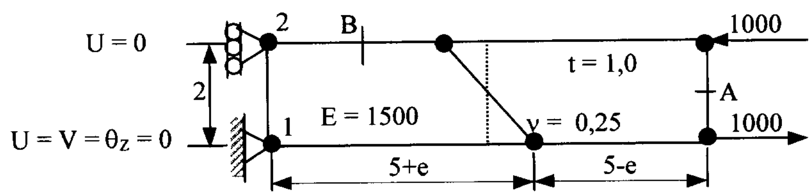

Fig. 3.15a: Pure bending of a cantilever; Data and mesh.
Rotation θ_Z is free at 2.

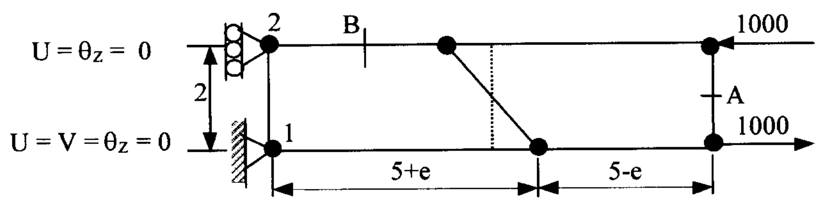

Fig.3.15b: Pure bending of a cantilever; Data and mesh.
Rotation θ_Z is fixed at 1 and 2.

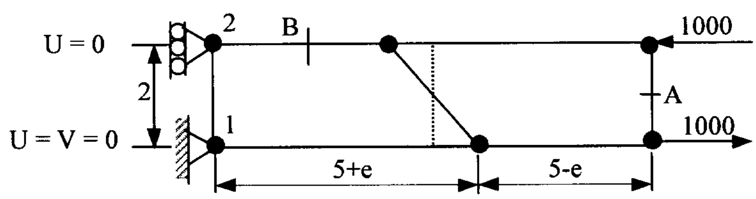

Fig.3.15c: Pure bending of a cantilever; Data and mesh.
Rotation θ_Z is free at 1 and 2.

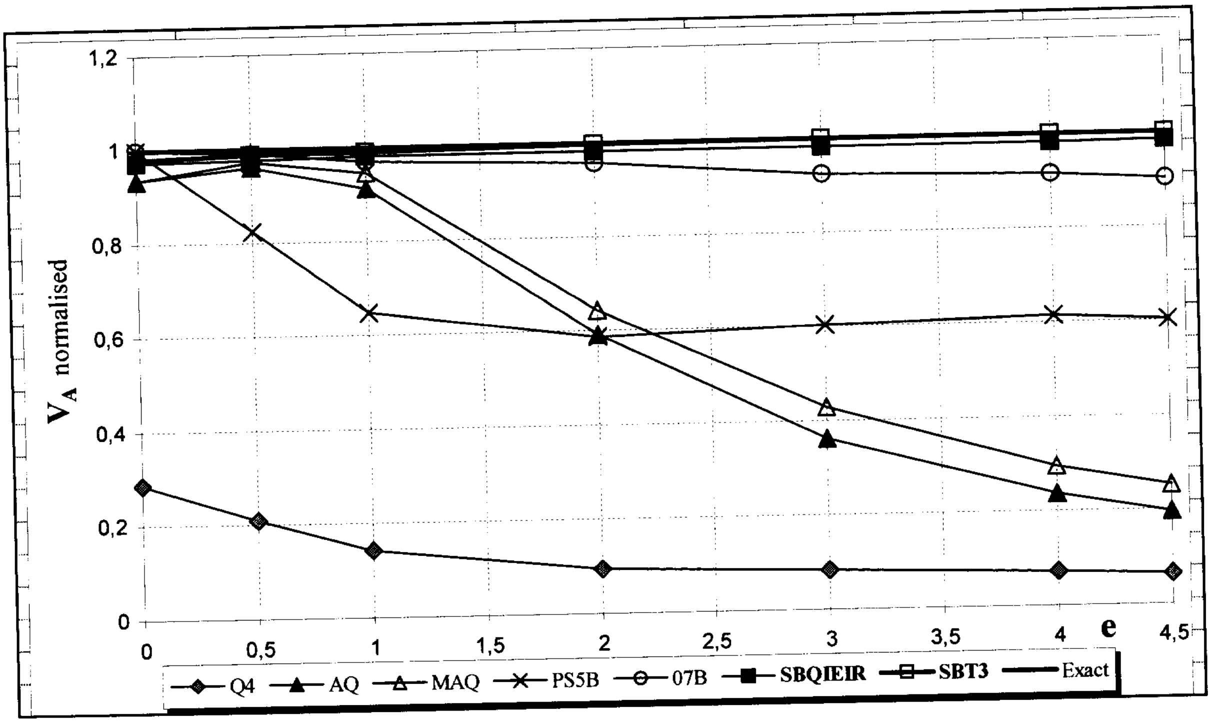

Fig. 3.16a: Pure bending of a cantilever; Rotation θ_Z is free at 2. Vertical displacement at A. (Fig.3.15a)

For the case of the regular mesh (Fig.3.15a; e = 0), a good results are obtained for all the elements except for the standard element Q4 which gives unacceptable results. However, for the case of the distorted mesh characterized by the distance "e" (e > 0), the results of **SBQIEIR** are powerful and comparable with the robust element 07β. Elements AQ, PS5β and MAQ remain sensitive to the distortions of the mesh. For the standard element Q4, the precision is always largely insufficient (Figs.3.16a and 3.16b).

In the case of the figure 3.15b, the robustness of this element *via* the regular and distorted mesh is confirmed. The figures 3.17a and 3.17b show the stability, the reliability and the good performance of **SBQIEIR** no matter what the geometrical distortion might be (only one element on h!). This is explained probably partly by the nature of analytical integration carried out. The distortion has a considerable influence on elements AQ and MAQ, while 07β element is not very sensitive to the geometrical distortions (Fig.3.17). These results confirm that the modified version of element **SBRIEIR (SBQIEIR)** satisfied the High Order Patch Test [SAB 85a] and [SAB 85b].

The figure 3.17c confirms the good performance and the stability of **SBQIEIR** element.

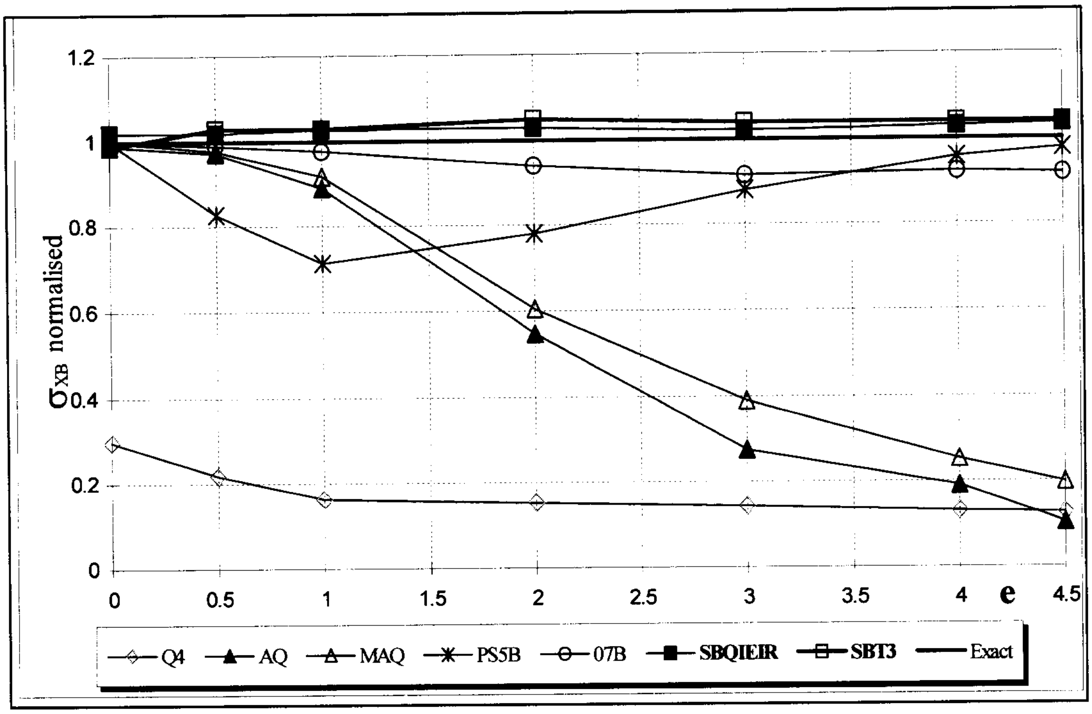

Fig.3.16b: Pure bending of a cantilever; Rotation θ_Z is free at 2. Normal stress at point B. (Fig.3.15a)

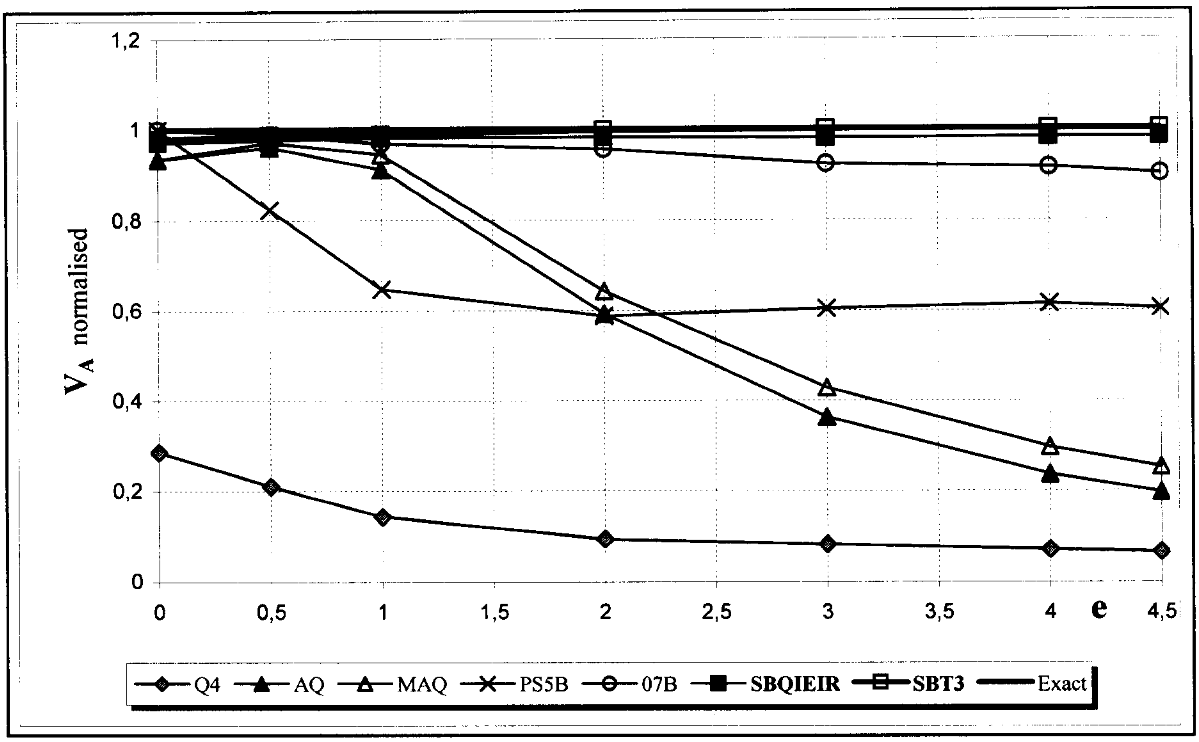

Fig.3.17a: Pure bending of a cantilever; Rotation θ_Z is free at 1 and 2. Vertical displacement at A. (Fig.3.15b)

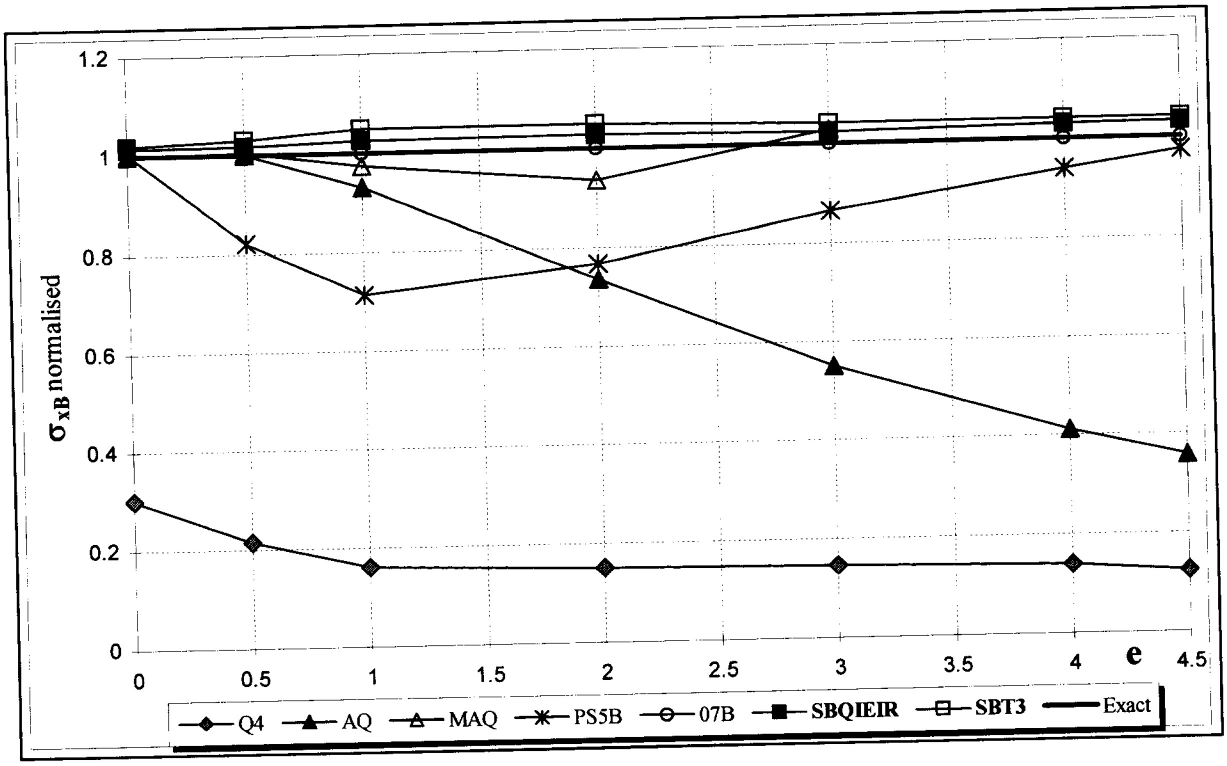

Fig.3.17b: Pure bending of a cantilever; Rotation θ_Z is fixed at 1 and 2. Normal stress at point B. (Fig.3.15b)

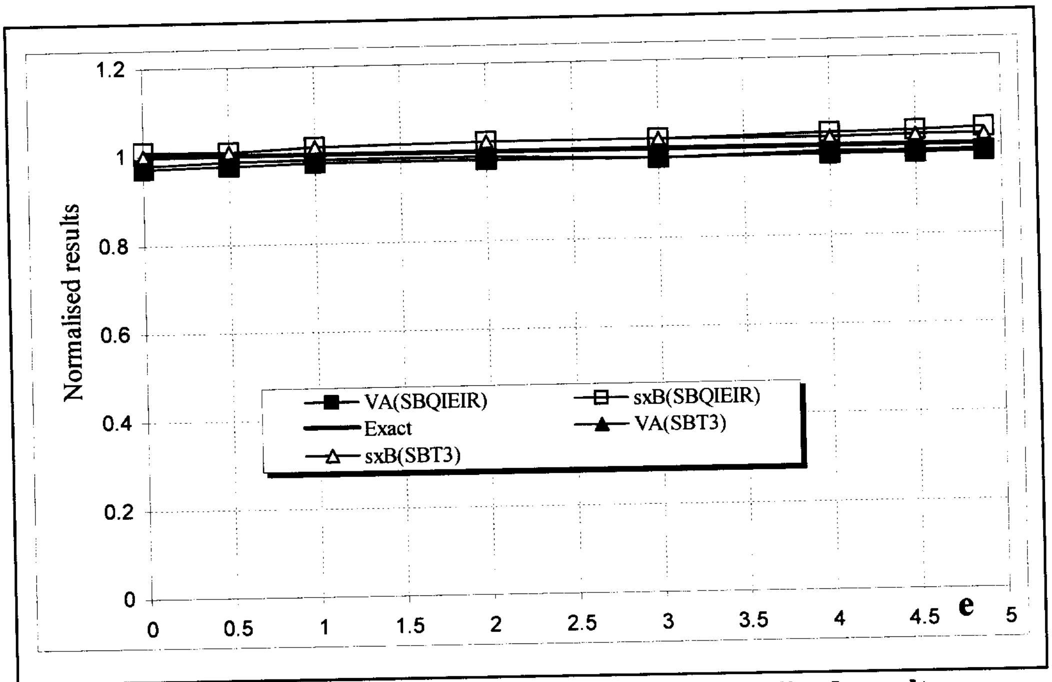

Fig.3.17c: Pure bending of a cantilever. Normalized results Rotation is free at 1 and 2. (Fig.3.15c)

3.6. Conclusion

The interest of the subroutine "**INTEGRATION**" was shown.

The results demonstrate the stability of the element "**SBQIEIR**" whatever the value "e". This is partly explained probably by the nature of analytical integration carried out.

CHAPTER 4

A NEW QUADRILATERAL FINITE ELEMENT FOR GENERAL PLANE ELASTICITY PROBLEMS

CHAPTER 4

A NEW QUADRILATERAL FINITE ELEMENT FOR GENERAL PLANE ELASTICITY PROBLEMS

4.1. Introduction

The strain based approach was used by Sabir [SAB 83] to develop a new class of elements for general plane of elasticity problems in Cartesian coordinates. A basic rectangular element having the only essential nodal degrees of freedom (2 d.o.f / node) and satisfying the requirements of the strain free rigid body modes is developed. The compatibility within the element is first established. Other elements meeting the above basic considerations together with equilibrium within the element are also developed. A simple and efficient rectangular element including the in-plane rotation is derived. This element was first applied to the simple problem of cantilevers and simply supported beams, where the results for deflections as well as stresses were satisfactory and converged to the exact solution. With the continuation of the development of the strain based approach many elements for general plane elasticity as well as shells have been derived by Sabir [SAB 85a], [SAB 85b], [SAB 86] and [SAB 95].

Several models such as rectangular elements were developed, among them the elements of Sabir SBRIE (Strain Based Rectangular In-plane Element) and SBRIE1 (Strain Based Rectangular In-plane Element with An Internal Node) [SAB 95]. The first element is based on linear variation of direct strains and constant shearing strain. The second is based on linear variation of all three strain components. Attention was therefore focused on the development of more sophisticated elements based on the strain approach by Belarbi [BEL 98a], [BEL 99] [BEL 2000] and [BEL 2002].

In the present chapter, an improved quadrilateral strain based element that satisfies the equilibrium equations is formulated, in order to give supplementary amelioration. This element has two degrees of freedom (d.o.f) at each corner node in addition to the internal node. Through the introduction of additional internal node an element that proved to be more accurate was developed, even though it requires static condensation [BATH 76].

The element is applied to the analysis of some civil engineering problems and it is shown that satisfactory results can be obtained without the use of large number of elements. The efficiency of this element was established and the convergence of the results for stresses and displacements to a satisfactory degree of accuracy was shown to be faster when compared with the quadrilateral standard element Q4, moreover the results obtained are comparable with those obtained when using the robust element Q8.

The performance o this element is tested by applying it to the analysis of the problems used in previous publications. A comparison with existing results is given. This element produces rapid convergence of deflections as well as stresses.

4.2. Description of "SBRIE2 "element [SAB 95]

Consider the rectangular element shown in Figure 4.1; the three components of the strain at any point in the Cartesian coordinate system are given in terms of the displacements U and V:

$$\varepsilon_{xx} = U_{,x} \tag{4.1a}$$

$$\varepsilon_{yy} = V_{,y} \tag{4.1b}$$

$$\gamma_{xy} = U_{,y} + V_{,x} \tag{4.1c}$$

If the strains given by equations (4.1) are equal to zero, the integration of these equations allows obtaining the following expressions:

$$U = a_1 - a_3 y \tag{4.2a}$$

$$V = a_2 + a_3 x \tag{4.2b}$$

Equations [2] represent the displacement field in terms of its three rigid body displacements.

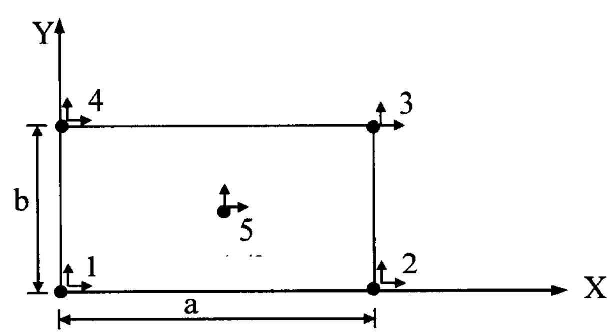

Fig. 4.1: Co-ordinates and nodal points for the rectangular element "SBRIE2"

The assumed strains for SBRIE2 element [SAB 95] are:

$$\varepsilon_{xx} = a_4 + a_5\, y - a_7 x - (1\text{-}v/2v)\, a_{10}\, x \tag{4.3a}$$

$$\varepsilon_{yy} = a_6 + a_7\, x - a_5\, y - (1\text{-}v/2v)\, a_9\, y \tag{4.3b}$$

$$\gamma_{xy} = a_8 + a_9\, x + a_{10}\, y \tag{4.3c}$$

Such assumption will lead to the displacement fields given below

$$U = a_1 - a_3 y + a_4 x + a_5\, x\, y - a_7 (x^2 + y^2)/2 + a_8 y/2 - a_{10}[\,(1\text{-}v)x^2/4v - y^2/2] \tag{4.4a}$$

$$V = a_2 + a_3 x - a_5 (x^2 + y^2)/2 + a_6 y + a_7 xy + a_8 x/2 - a_9 [(1\text{-}v)y^2/4v - x^2/2] \tag{4.4b}$$

Unfortunately this element baptized SBRIE2 does not satisfied equilibrium equations, further more it has a rectangular shape which limited its application domain.

4.3. Variational formulation of the new element "Q4SBE1"

The present element is a quadrilateral with four corner nodes and a central node, each node has two degrees of freedom. Thus, the displacement field should contain ten independent constants. Figure 4.2 shows the geometry of the "Q4SBE1" element and the corresponding nodal displacements.

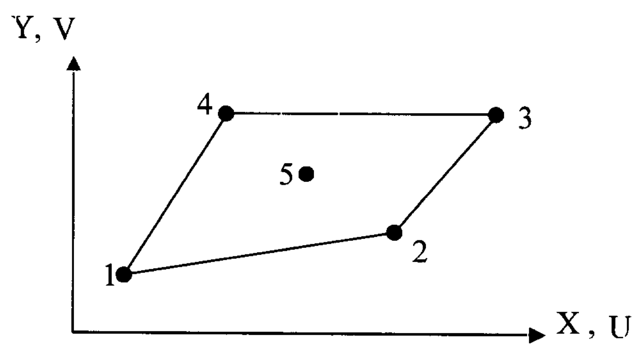

Fig.4.2: Co-ordinates and nodal points for the quadrilateral element" Q4SBE1"

The three components of the strain field at any point are given by equation (4.1). The components of the displacements in the directions x and y are U and V respectively.

The strains in equation (4.1) can not be considered independent, they are in terms of two displacements U, V and hence the strains must satisfy an additional equation called the compatibility equation. This equation can be obtained by eliminating U, V from equation (4.1), hence:

$$\frac{\partial^2 \varepsilon_x}{\partial y^2} + \frac{\partial^2 \varepsilon_y}{\partial x^2} - \frac{\partial^2 \gamma_{xy}}{\partial x \partial y} = 0 \tag{4.5}$$

Equation (4.2) gives the three components of the rigid body displacements and requires three independent constants (a_1, a_2, a_3). Thus it is left seven constants (a_4, a_5... a_{10}) for expressing the displacement due to straining of the element. These seven independent constants are apportioned among the three strains as follow:

$$\begin{cases} \varepsilon_x = a_4 + a_5 y + a_9 x \\ \varepsilon_y = a_6 + a_7 x + a_{10} y \\ \gamma_{xy} = -a_5 x R - a_7 y R + a_8 - a_9 H y - a_{10} H x \end{cases} \tag{4.6}$$

With: $H = \frac{2}{(1-v)}$; $R = \frac{2v}{(1-v)}$

These strains given by equations (4.6) satisfy both the compatibility equation (4.5) and the two- dimensional equilibrium equations (4.7a) and (4.7b)

$$\frac{\partial \sigma_x}{\partial x} + \frac{\partial \tau_{xy}}{\partial y} = 0 \tag{4.7a}$$

$$\frac{\partial \sigma_y}{\partial y} + \frac{\partial \tau_{xy}}{\partial x} = 0 \tag{4.7b}$$

By integrating equations (4.6) we obtain:

$$U = a_4 x + a_5 xy - a_7 y^2 (R+1)/2 + a_8 y/2 + a_9 (x^2 - H y^2)/2 \tag{4.8a}$$

$$V = - a_5 x^2 (R+1)/2 + a_6 y + a_7 xy + a_8 x/2 + a_{10} (y^2 - Hx^2)/2 \tag{4.8b}$$

The final displacement functions are obtained by adding equations (4.2) and (4.8) to obtain the following:

$$\begin{cases} U = a_1 - a_3 y + a_4 x + a_5 xy - a_7 \frac{y^2 (R+1)}{2} + a_8 \frac{y}{2} + a_9 \frac{1}{2}(x^2 - Hy^2) \\ V = a_2 + a_3 x - a_5 \frac{x^2 (R+1)}{2} + a_6 y + a_7 xy + a_8 \frac{x}{2} + a_{10} \frac{1}{2}(y^2 - Hx^2) \end{cases} \tag{4.9}$$

Another version of this element "Q4SBE2" having the same strain assumptions as above, with a rearrangement of the different coefficients, the strain field will be:

$$\varepsilon_{xx} = a_4 + a_5 R\, y + a_9 H x \tag{4.10a}$$

$$\varepsilon_{yy} = a_6 + a_7 R\, x + a_{10} H y \tag{4.10b}$$

$$\gamma_{xy} = - a_5 x - a_7 y + a_8 - a_9 y - a_{10} x \tag{4.10c}$$

With: $H = (1\text{-}2v)/2(1\text{-}v)$; $R = (1\text{-}2v)/2v$

The final displacement field is:

$$U = a_1 - a_3 y + a_4 x + a_5 R\, x\, y - a_7 y^2 (R+1)/2 + a_8 y/2 + a_9 (H x^2 - y^2)/2 \tag{4.11a}$$

$$V = a_2 + a_3 x - a_5 x^2 (R+1)/2 + a_6 y + a_7 R\, x\, y + a_8 x/2 + a_{10} (H y^2 - x^2)/2 \tag{4.11b}$$

This version produces similar results to those obtained by (4.9).

The stiffness matrix can be calculated from the well known expression:

$$[K_e] = [A^{-1}]^T [K_0] [A^{-1}] \tag{4.12a}$$

$$[K_0] = \iint_S [Q]^T [D][Q]\, dx.dy \tag{4.12b}$$

With:

$$[Q] = \begin{bmatrix} 0 & 0 & 0 & 1 & y & 0 & 0 & 0 & x & 0 \\ 0 & 0 & 0 & 0 & 0 & 1 & x & 0 & 0 & y \\ 0 & 0 & 0 & 0 & -xR & 0 & -yR & 1 & -Hy & -Hx \end{bmatrix} \tag{4.13}$$

And $[D] = \begin{bmatrix} D11 & D12 & 0 \\ D12 & D22 & 0 \\ 0 & 0 & D33 \end{bmatrix}$ the usual constitutive matrix

Where: $D11 = D22 = \dfrac{E}{(1-\nu^2)}$; $D12 = \dfrac{\nu.E}{(1-\nu^2)}$; $D33 = \dfrac{E}{2(1+\nu)}$

For [A] and [K_0] see the **Appendix C.1**

We notice that the final functions of displacement (4.9) contain quadratic terms thus allowing the change of curvature.

If the classical formulation is adopted, two problems can arise:

The first one is the geometrical problem of distortion for some finite elements of higher degree (loss of precision); the second is the problem of locking for the finite elements of degree relatively low.

The adoption of a strain approach with an analytical integration method would allow avoiding these problems Belarbi [BEL 2000].

4.4. Analytical evaluation of the $[K_0]$ matrix

The evaluation of the element stiffness matrix is summarized with the following expression:

$$[K_e] = [A^{-1}]^T \left[\iint_S [Q]^T [D][Q].dx.dy \right] [A^{-1}] \tag{4.14a}$$

$$[K_e] = [A^{-1}]^T [K_0] [A^{-1}] \tag{4.14b}$$

With: $$[K_0] = \iint_S [Q]^T [D].[Q].dx.dy \tag{4.14c}$$

Since [A] and its inverse can be evaluated numerically, the evaluation of the integral (4.14c) becomes the key of the problem.

Knowing that, for certain elements, a too great distortion can lead to erroneous numerical results particularly in the calculation of the Jacobien, an expression that is general, and easy to implement numerically being formulated. It allows the evaluation of the matrix $[K_0]$ in an automatic way whatever the degree of the polynomial of the kinematics field and the distortion of the element [Chapter 3], Fig.4.3.

$$I = [K_0] = \iint_S C.x^{\alpha} y^{\beta} \, dx.dy \tag{4.15}$$

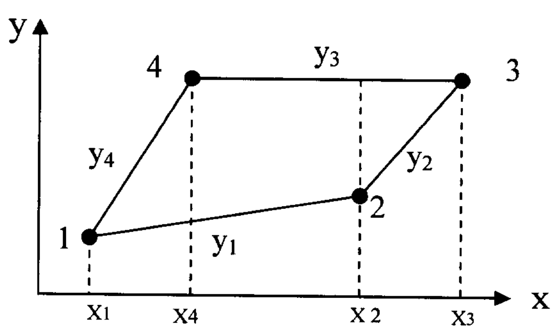

Fig.4.3: Quadrilateral element

x_1, x_2, x_3 and x_4 are the coordinates of the nodes 1, 2, 3 and 4 in X direction, y_1, y_2, y_3 and y_4 are the functions of the quadrilateral sides, 1-2, 2-3, 3-4, 4-1 respectively as shown in figure 3.

The general expression of the equation (4.15) for a quadrilateral is:

$$I = \sum_{P=1}^{3} I_P \tag{4.16}$$

With: $$I_P = \frac{C}{\beta+1}\sum_{k=1}^{\beta+2}\frac{1}{k+\alpha}.C(k)\left(a_j^{\,k-1}.b_j^{\,\beta+2-k} - a_i^{\,k-1}.b_i^{\,\beta+2-k}\right)\left(x_n^{\,k+\alpha} - x_m^{\,k+\alpha}\right) \tag{4.17}$$

The stiffness matrix is derived without using any tricks, which implies that it is obtained using exact and not reduced integration, see **Appendix C.2**.

4.5. Numerical tests

In first, the numerical results of several quadrilateral plane elements are used and compared with those obtained from the present Q4SBE1 element, and in the second, the behaviour of the formulated element with irregular forms (distorted shape) is tested.

The present element is compared to the following elements:

SBRIE: the strain based rectangular in-plane element Sabir [SAB 86].

SBRIE2: The strain based rectangular in-plane element with an internal node Sabir [SAB 95].

Q4: the standard four-node isoparametric element.

Q8: the standard eight -node isoparametric element.

PS5β: Pian and Sumihara's four- node five-beta mixed element Pian [PIA 84]

AQ: Cook's quadrilateral counterpart Cook [COO 86] of Allman's triangle [ALL 84]

MAQ: a mixed counterpart of AQ using complete linear stress modes (in term of isoparametric coordinates) for all stress components Yunus [YUN 89].

Q4Rβ: the quasi-conforming counterpart of AQ proposed by Lin *et al.* [LIN 90].

Q4S: Mac-Neal and Harder's refined membrane element with drilling degree of freedom Mac. *et al.* [MAC 89].

07β: the Sze element [SZE 92].

Q8: the Mac -Neal element [MAC 88].

Allman element [ALL 88b]

Most of the examples dealt with have been proposed at various stages in open literature to validate element performance. It will be seen that the SBRIE and the SBRIE2 versions show the same results for all cases.

4.5.1. High Order Patch Test: Pure bending of a cantilever beam

It is useful to know the behaviour of a finite element presenting an important geometrical distortion. Sze, Chen and Cheung [SZE 92] studied this Problem in order to test the performance and the precision of the elements 07β and 07β*.

A cantilever beam with a rectangular section (l x t x h = 10 x 1 x 2) is subjected to two nodal forces (P =1000) forming a couple to produce pure bending (Fig.4.4a).

Two meshes (rectangular, trapezoidal) are considered and the boundary conditions are taken as shown in Fig.4.4a. The results obtained with "Q4SBE1" are compared with the analytical solution given by Ibrahimbegovic [IBR 93a]. and the quadrilateral element Q4, figures (4.4b and 4. 4c).

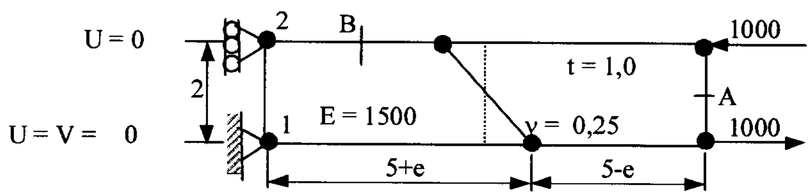

a) Pure Bending of a Cantilever beam; Data and Meshes.

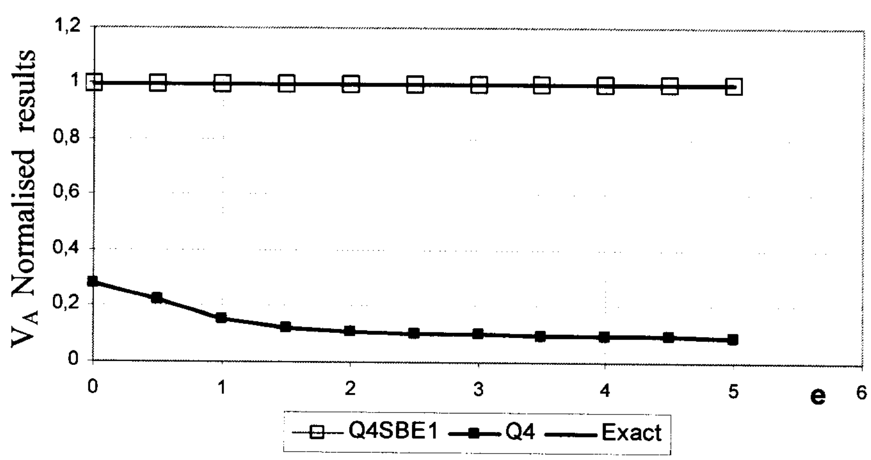

b) Vertical Displacement at Point A. Normalised results

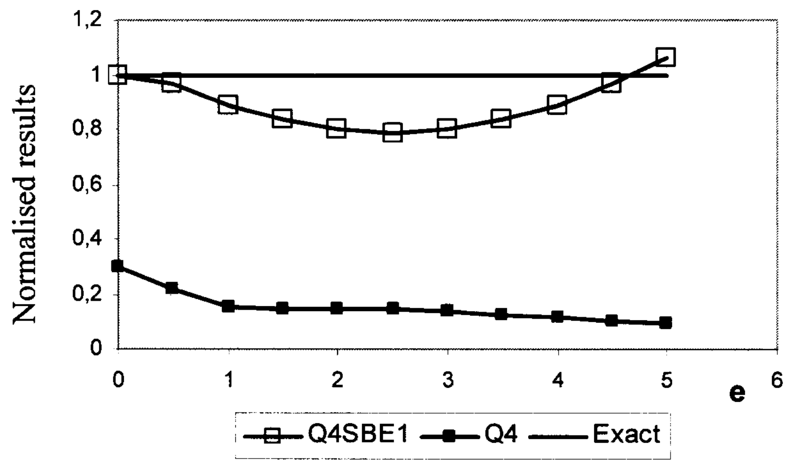

c) Normalised stress at Point B. Normalised results

Fig.4.4: Pure bending of a cantilever beam

For the case of the regular mesh (Figs.4.4b, 4.4c; e = 0), good results are obtained for "Q4SBE1" element; whereas the standard element Q4 gives unacceptable results. For the case of the distorted mesh characterized by the distance «e" (e > 0), the results of "Q4SBE1" are powerful and comparable with the exact solution for standard quadrilateral element Q4, the precision is always largely insufficient (Figs.4.4b and 4.4c).

The Figures 4.4b and 4.4c show the stability, the reliability and the good performance of "Q4SBE1" element no matter what the geometrical distortion might be (only one element on h!), this is explained probably partly by the nature of analytical integration carried out. These results confirm that the formulated element Q4SBE1 satisfies the High Order Patch Test Taylor et al. [TAY 86] and Batoz et al [BAT 90b].

The robustness of this element "Q4SBE1" via the regular and distorted mesh is confirmed.

4.5.2. Allman's cantilever beam (Distortion sensitivity study)

In the following example, it is a question of evaluating the vertical displacement V_A at the free end of a short cantilever Fig.4.5 subject to a uniform vertical load (resultant W).

This test is considered by many researchers as a tool to validate the plane elements. It makes it possible to examine the aptitude of an element of the membrane type to simulate the problems dominated by bending.

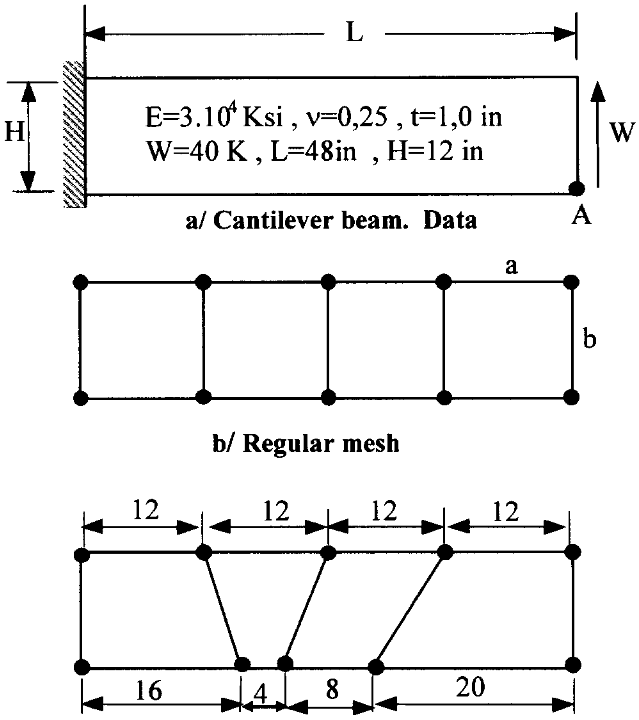

Fig.4.5. Allman's cantilever beam; Data and mesh

The analytical solution for the vertical deflection at point A is calculated by the following equation [TIM 51]:

$$V_A = \frac{PL^3}{3EI} + \frac{(4+5\upsilon)}{2EH}PL = 0{,}3553 \tag{4.18}$$

The results obtained for the two cases of meshes (regular and distorted) are listed on Table 4.1.

Formulation/ Element	Mesh	Normalized vertical displacement at A
Mac-Neal [MAC 88a]	Reg.	0,959
Mac-Neal [MAC 88a]	Dist.	0,838
Allman [ALL 88b]	Reg.	0,852
Allman [ALL 88b]	Dist.	-
PS5β	Reg.	0,978
PS5β	Dist.	0,925
AQ	Reg.	0,918
AQ	Dist.	0,947
MAQ	Reg.	0,918
MAQ	Dist.	0,952
QR4b	Reg.	0,978
QR4b	Dist.	0,977
Q4S	Reg.	0,978
Q4S	Dist.	0,976
07β	Reg.	0,978
07β	Dist.	0,978
Q4	Reg.	0,679
Q4	Dist.	0,596
Q8 [MAC 88b]	Reg.	0,985
Q8 [MAC 88b]	Dist.	0,994
Q4SBE1	Reg.	**0,983**
Q4SBE1	Dist.	**0,995**
Exact solution [TIM 51]		**1,000** **(0,3553)**

Table 4.1: Allman's short cantilever beam

Normalised vertical displacement at point A

***Comments: Regular mesh** (Fig.4.5b)*

For the case of the regular mesh (Fig.4.5b), the results obtained for Q4SBE1 are powerful and comparable with those given by the robust element Q8, in terms of total number of degrees of freedom.

***Comments: Distorted mesh** (Fig.4.5c)*

For the case of the distorted mesh (Fig.4.5c), the very good performance of element Q4SBE1 is confirmed. The corresponding results are more precise than the results of the other elements [MAC 88a], PS5ß, MAQ, QR4b, Q4S, 07ß, Q4 (Table 4.1) and comparable with those given by the robust element Q8, in terms of total number of degrees of freedom.

4.5.3. Mac-Neal's elongated cantilever beam

Let us consider the example of the elongated cantilever beam of Mac-Neal and Harder [MAC 85], with rectangular section (6 x 2 x 1) deformed in pure bending by one moment at the end (M =10) and by a load applied at the free end (P=1).

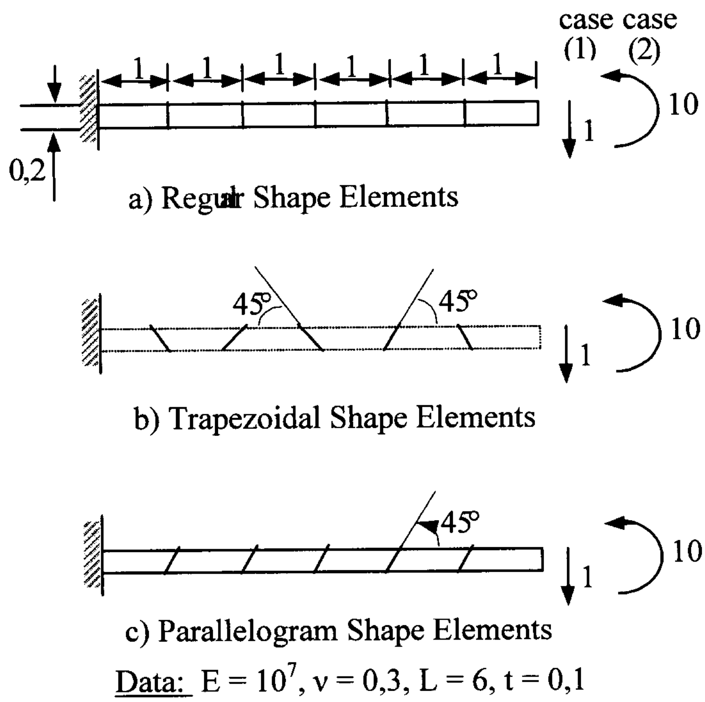

Data: $E = 10^7$, $\nu = 0,3$, $L = 6$, $t = 0,1$

Fig.4.6: Mac-Neal's elongated beam subject to (1) end shear and (2) end bending.

The cantilever is modelled by six membrane elements rectangular (Fig.4.6a), trapezoidal (Fig.4.6b) and parallelogram (Fig.4.6c).

The results obtained for Q4SBE1 are compared with those obtained with other known quadrilateral elements (Table 4.2).

Mac-Neal [MAC 87] affirms that the trapezoidal shape of the membrane finite elements with four nodes without degrees of freedom of rotation (with linear fields) generates a locking even if these elements pass the patch-test. This problem is known as "trapezoidal locking"

NOTE. — This rule does not apply to the finite elements based on the strain approach.

Element	Pure bending			End shear		
	Regular	Trapezoidal	Parallel	Regular	Trapezoidal	Parallel
Q4	0,093	0,022	0,031	0,093	0,027	0,034
PS5β [PIA 84]	1,000	0,046	0,726	0,993	0,052	0,632
AQ [COO 86]	0,910	0,817	0,881	0,904	0,806	0,873
MAQ [YUN 89]	0,910	0,886	0,890	0,904	0,872	0,884
Q4 [MAC 89]	-	-	-	0,993	0,986	0,988
07β [SZE 92]	1,000	0,998	0,992	0,993	0,988	0,985
Q4SBE1	**1,000**	**1,000**	**1,000**	**0,993**	**0,994**	**0,994**
Theory		**1,000 (0,270)**			**1,000 (0,1081)**	

Table 4.2: Normalised tip deflection for Mac-Neal's elongated beam

The results obtained for elements Q4 and PS5β (Table 4.2) show well the problem of trapezoidal locking announced by Mac-Neal [MAC 87].

Through these three cases of meshes (Figs. 4.6a, 4.6b, 4.6c), the effectiveness of this **Q4SBE1** element is confirmed.

In order to test the convergence performance of **Q4SBE1** element, using four different regular mesh divisions (1x3, 1x6, 1x9, 1x12) Fig.4.6a, the normalised tip deflections are computed and compared with those obtained by other elements (Q4, SBRIE, SBRIE2) in Figs (4.7 and 4.8).

A pertinent point to note is that exact solution can be obtained for the Q4SBE1 element. The accuracy of the SBRIE2 is not sufficient

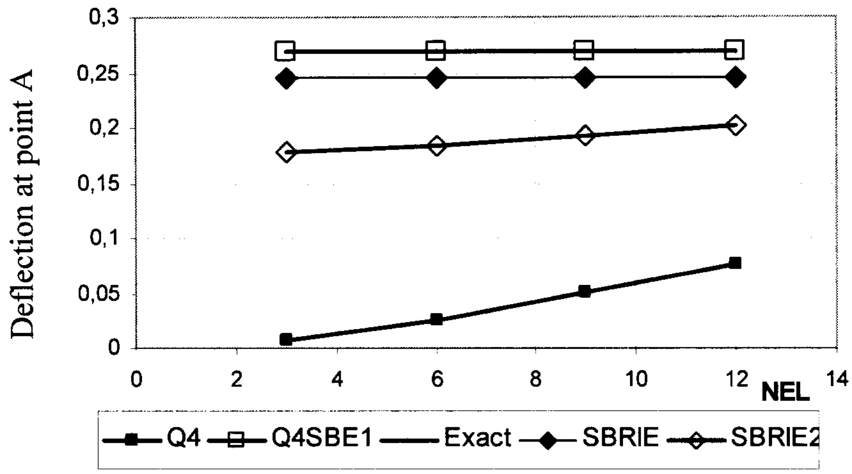

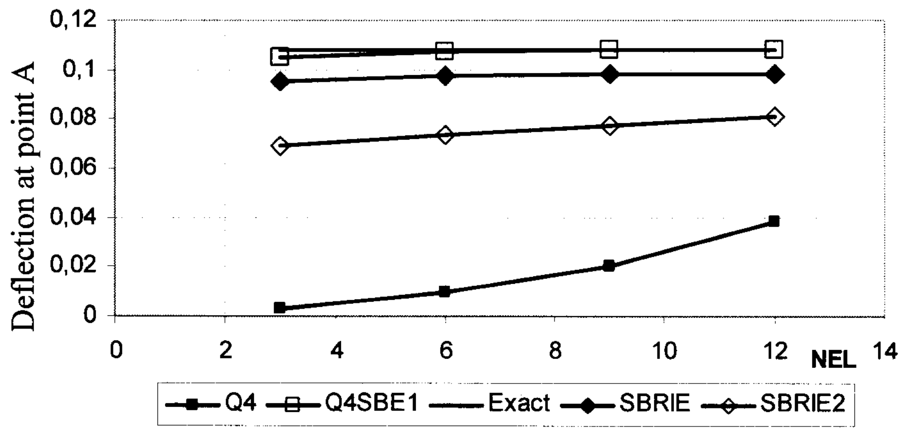

Fig.4.8: Convergence Curves for deflection at point A
Mac-Neal's cantilever beam under end shear

In conclusion, it can be said that "Q4SBE1" element is very powerful for this type of problems dominated by bending, and it remains stable with geometrical distortions.

4.5.4. Tapered Panel under End shear

This problem, proposed by Cook as a test for the accuracy of quadrilateral elements [COO 87] and Bergan et al. [BER 85], is another popular test problem.

A tapered panel of unit thickness with one edge subjected to a distributed shear load and with the other edge fully clamped (u = v = 0) is shown in Fig.4.9.

The panel is analysed by using 2 x 2 and 4 x 4 meshes (Figs. 4.9a, 4.9b). The normalised vertical deflection Vc at point C, maximum principal stress σ_{maxA} at point A and minimum principal stress σ_{minB} at point B are presented in Table 4.3. Principal stresses at points A and B are evaluated based on the averaged stress components of the elements sharing nodes A and B, respectively. The results obtained for the Q4SBE1 element are compared to the other quadrilateral elements. It can be noted that the displacement predictions of the Q4SBE1 are slightly better than the other quadrilateral elements for both meshes (Table 4.3).

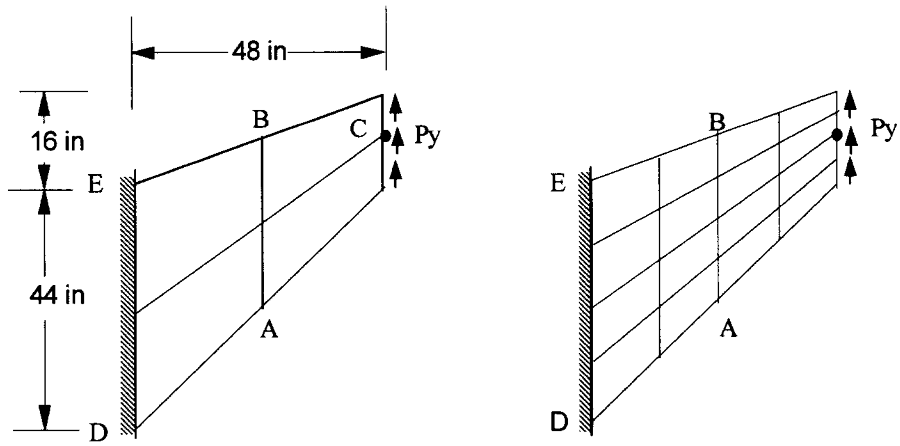

(a) 2 x 2 mesh (b) 4 x 4 mesh

Py = 1 pi (uniformly distributed load)

E = 1 psi, ν = 1/3 Thickness t =1 in

Boundary conditions:

U = V = 0 (DE)

Fig.4.9: Tapered panel subjected to end shear; data and meshes

Element model	2 x 2 mesh			4 x 4 mesh		
	V_C	σ_{maxA}	σ_{minB}	V_C	σ_{maxA}	σ_{minB}
Q4	0,496	0,437	0,533	0,766	0,756	0,719
AQ	0,890	0,780	0,900	0,965	0,936	1,010
Ref. [ALL 88b]	0,848	0,771	0,856	0,953	0,956	0,997
PS5β	0,884	0,786	0,771	0,963	0,950	0,924
MAQ	0,890	0,779	0,886	0,965	0,941	0,967
QR4b	0,941	0,879	1,059	0,980	0,990	0,997
Ref. [BER 85]	0,852	0,720	0,898	0,938	0,902	0,849
Ref [IBR 90]	0,865	-	-	0,962	-	-
Ref [SIM 89]	0,884	-	-	0,963	-	-
07β	0,945	0,835	1,069	0,981	0,982	1,012
Q4SBE1	**1,0652**	**1,508**	**1,171**	**1,011**	**1,004**	**0,992**
32 x 32 mesh Ref. [BER 85]	1,000 (23,90)	1,000 (0,236)	1,000 (-0,201)	1,000 (23,90)	1,000 (0,236)	1,000 (-0,201)

Table 4.3: Normalised prediction for tapered panel under end shear

The results obtained for the deflection and principal stresses for the refined mesh (4x4) are very good compared to an accurate solution given by Bergan and Felippa using a (32x32) mesh [BER 85] (error 1 %).

4.5.5. A simple beam

A simple beam with a length to height aspect ratio of 10 is subjected to a pure bending state. The beam is modelled by 1x 6 meshes with both regular and irregular elements as shown in Fig.4.10. Only a minimum number of restraints are imposed to eliminate rigid body movement. The load is a unit couple applied at the free end.

This beam is selected as a test problem by Ibrahimbegovic, Taylor and Wilson [IBR 90]. The results obtained for both regular and irregular mesh are compared with some of the results available in literature, and the exact solution given by beam's theory. All are presented in Table 4.4.

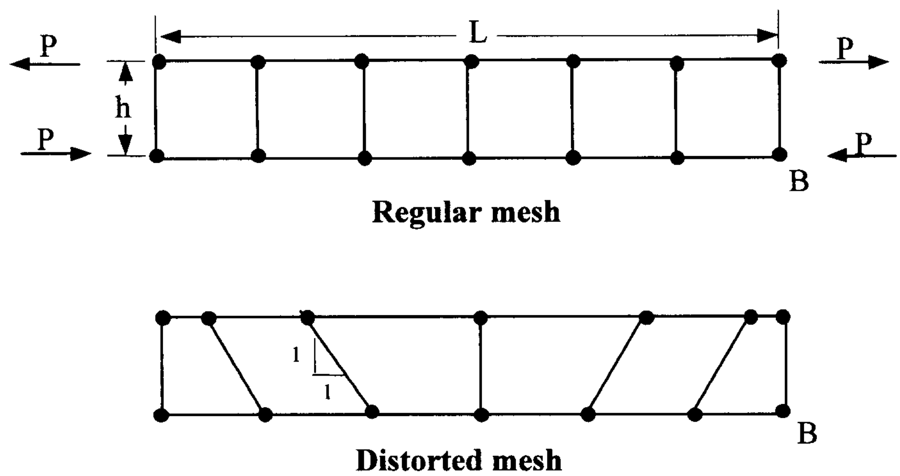

Data: **E = 100, ν = 0, P = 1, L = 10, h = 1, t = 1**

Fig.4.10: A simple beam; Data and meshes

The results obtained for the distorted element (**Q4SBE1**) are found to be more accurate than the other elements for the same finite element mesh size (Table 4.4).

It is observed that the results show very good numerical accuracy obtained for both regular and distorted mesh, and confirm the good performance of the Q4SBE1 element.

Formulation	Mesh	Vertical displacement
Mixte-type [IBR 90]	Reg.	1,50000
Mixte-type [IBR 90]	Dist.	1,14185
Displ-type [IBR 90]	Reg.	1,50000
Displ-type [IBR 90]	Dist.	1,14045
Taylor et Simo [TAY 85]	Reg.	1,50000
Taylor et Simo [TAY 85]	Dist.	1,14195
Q4	Reg.	0,62888
Q4	Dist.	0,26362
Q4SBE1	Reg.	**1,50000**
Q4SBE1	Dist.	**1,50000**
Beam's theory		**1,50000**

Table 4.4: A simple beam under pure bending Fig.4.10

4.6. Others applications (Civil engineering)

4.6.1. Solid cantilever wall [SAB 84]

In order to test the convergence performance of Q4SBE1 element, it was also applied to the analysis of a solid cantilever wall. Figure 4.11 shows the dimensions and the elastic properties of the cantilever which is subjected to a point lateral load at the top free end.

The obtained results for both membrane elements Q4SBE1 and Q4 are compared to the exact solution.

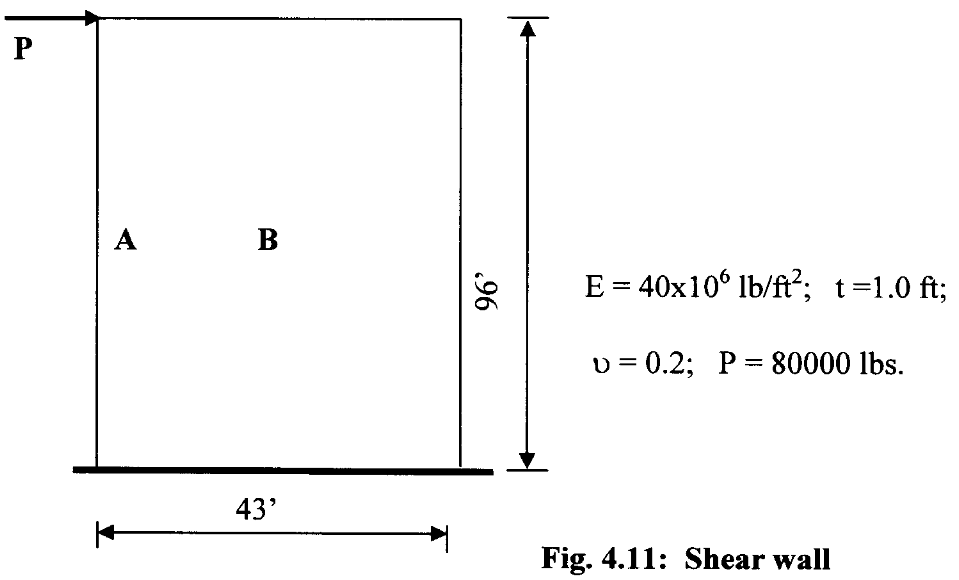

Fig. 4.11: Shear wall

Figures (4.12, 4.13 and 4.14) show respectively the convergence curves for the lateral displacement of the loaded edge, the direct bending stress at point A and the shear stress at point B.

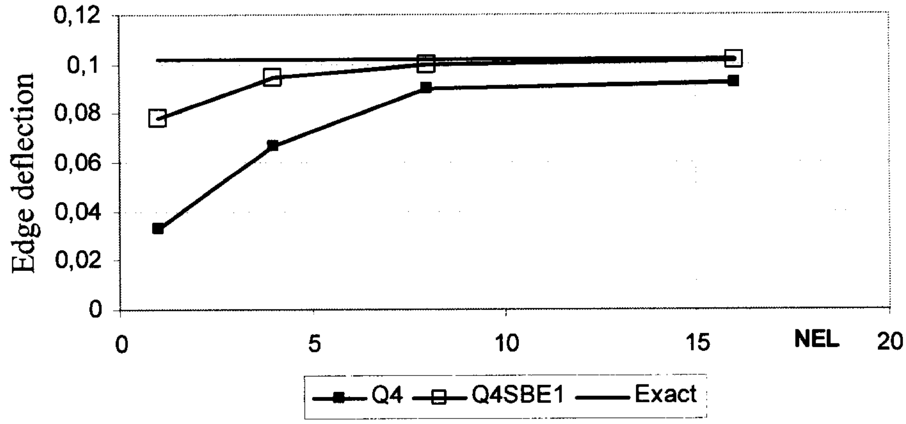

Fig.4.12: Convergence Curve for edge deflection

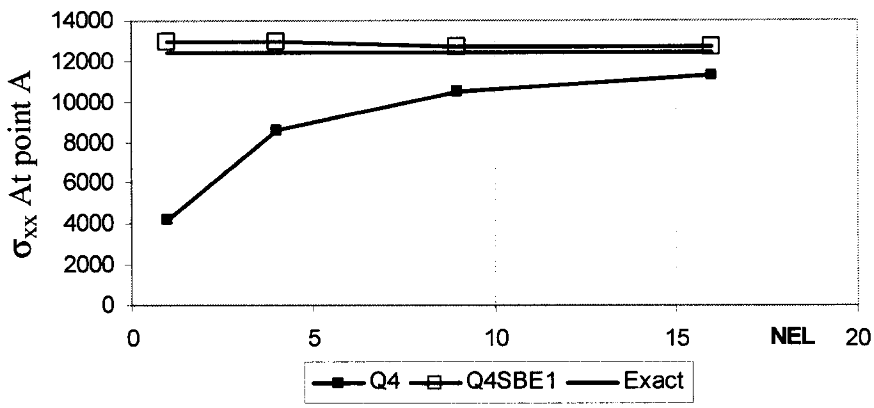

Fig.4.13: Convergence Curve for bending stress at Point A

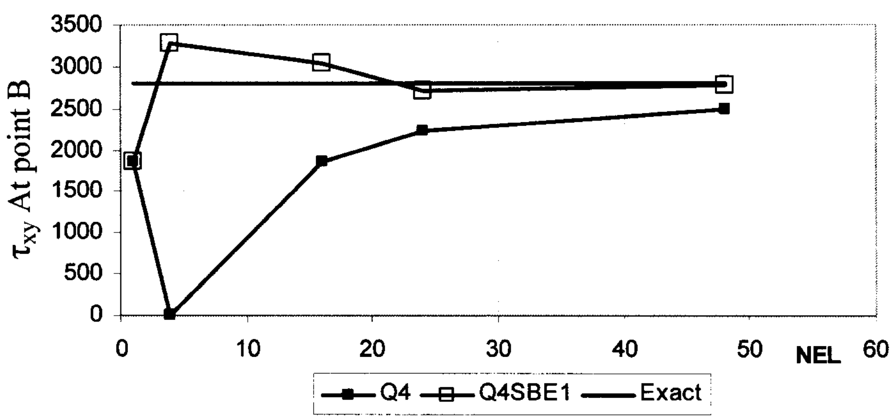

Fig.4.14: Convergence Curve for Shearing stress at Point B

4.6.2. Boussinesq problem [NOB 86]

The following example is the Boussinesq problem in the theory of linear elasticity. Suppose that a point force P is vertically applied at the center of the top surface of a semi-infinite plate. Under the generalised plane stress assumption, the stress component σ_{xx} along the x axis is given Timoshenko and Goodier [TIM 70] by the following equation:

$$\sigma_{xx} = -2P/\pi.x \tag{4.19}$$

Since infinite domains cannot be treated by the finite element approximations studied so far, we shall make a finite element model by taking only a finite portion of the semi-infinite domain shown in Fig.4.15.

Assuming homogeneity and isotropy of the material, the boundary condition has been assumed along the bottom and the right side edges. The results are shown in figure 16 for the case that:

Young's modulus E =3 2000KN/mm^2, Poisson's ratio ν =0.25,

Thickness =10 mm (generalised plane stress), Applied force P = 100 N

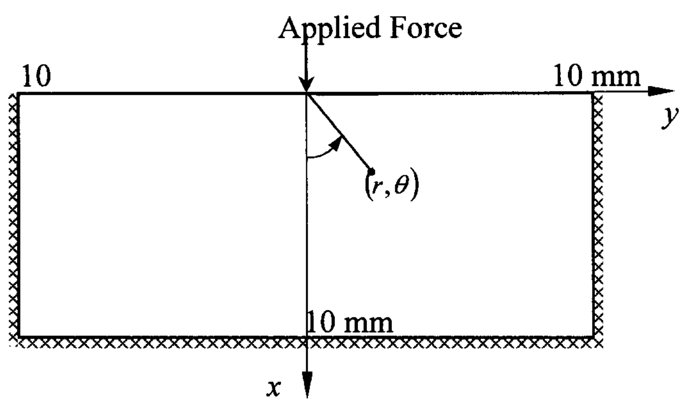

Fig.4.15: Domain for Boussinesq problem

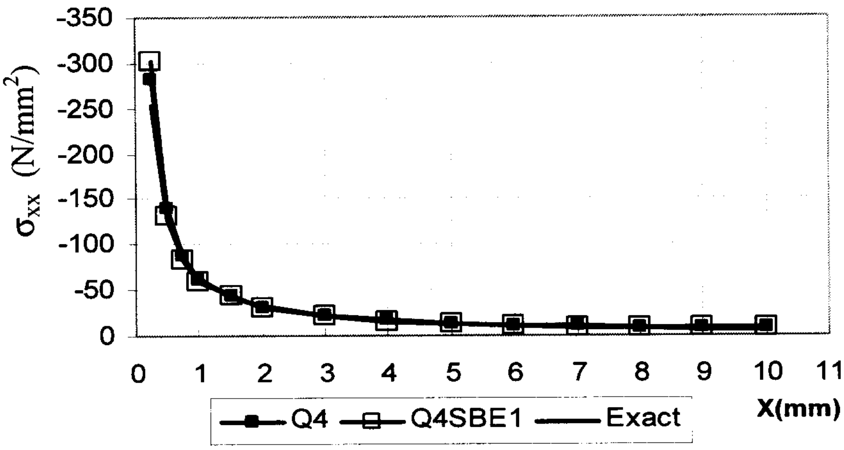

Fig.4.16. Stress σ_{xx} along x Axis (θ=90^0)

The results obtained are in close agreement with those of the analytical solution.

4.6.3. Concrete culvert [WILL 84]

The concrete culvert as shown in Fig.4.17 (a) represents a plane strain problem. Its geometry consists a half of hexagon with a semicircular opening. A uniformly distributed loading by (force per unit length) is applied to the top edge in the negative y direction. Values of physical parameters are:

Young's modulus E = 2x10^{7}KN/m^2, Poisson's ratio ν = 0.3, Thickness =1m.

Applied force b_y = 5 x 10^3 KN/m^2

For which S.I. units are used.

To analyse half the problem, we discretize the part on the right side of the centerline, as shown by the network of quadrilaterals in Fig.4.17 (b). Restraints needed for this analytical model consist of rollers at nodes on the axis (in a plane of symmetry) and pinned supports at nodes on the axis (to fix the base points).

For the purpose of design, we shall investigate the variations of the normal stress σ_y along the line *EF* Fig.4.17 (a).

Graph of stress ratios σ_y / by (on line *EF*) appear in Fig.4.18.

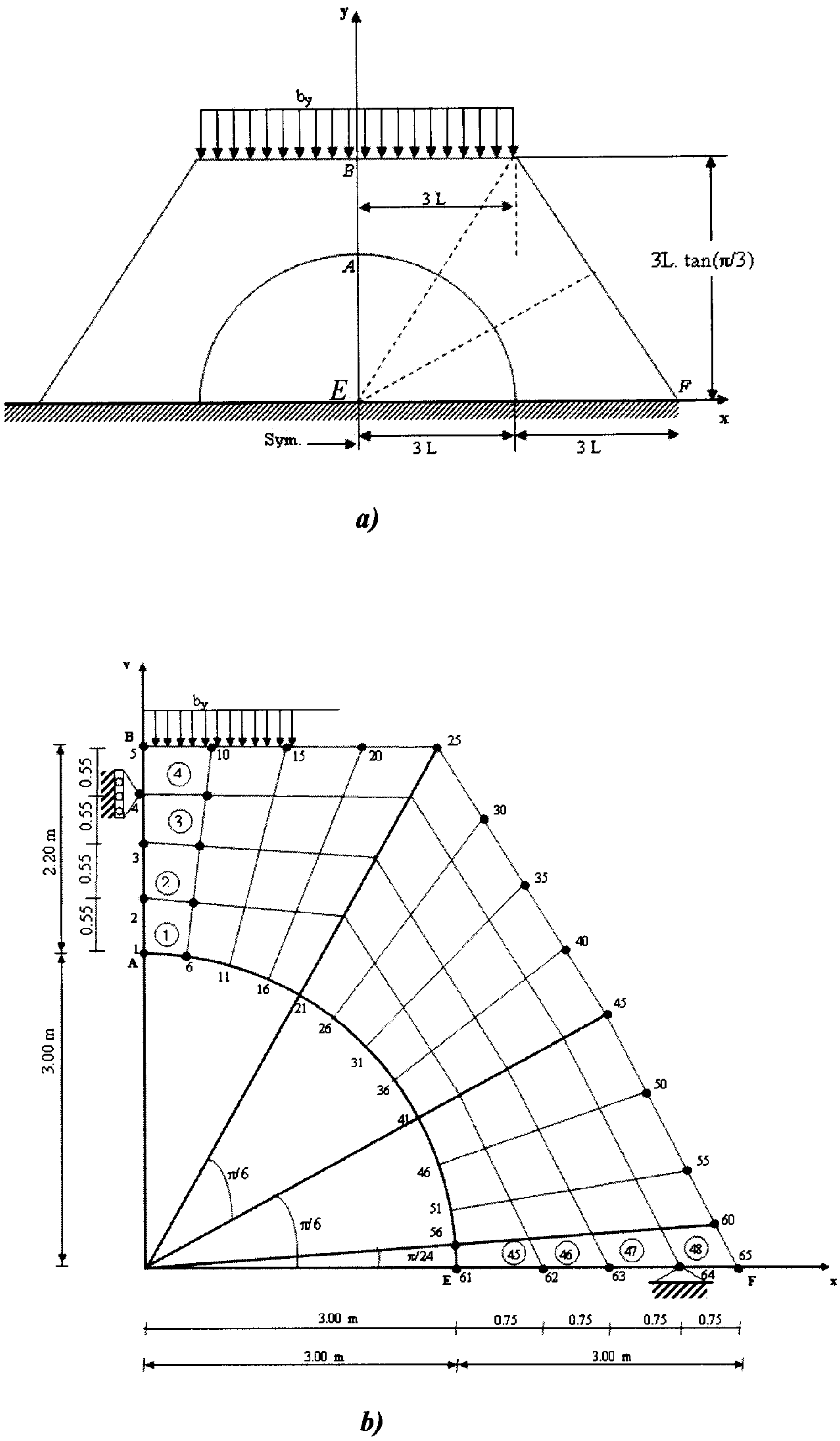

Fig.4.17: Concrete culvert

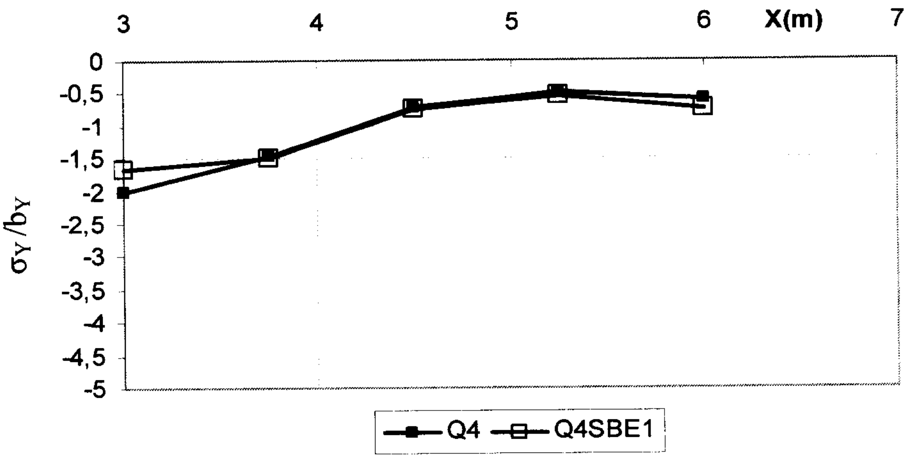

Fig.4.18: Stress Ratios on line EF

We see from this plot that the normal stresses chosen tend to be high near the opening.

4.7. Conclusion

A new strain based element is formulated for the analysis of general plane elasticity problems. It has only the customary two displacements degrees of freedom. The various numerical examples show the performances of the strain based approach. Some very good results were obtained. This element can be used for the civil engineering analysis problems. It has been shown that satisfactory finite element solutions can be obtained without the use of large number of elements.

The **Q4SBE1** element turned out to be particularly robust (Rich of membrane), much more simplified and more powerful than the standard element Q4.

CHAPTER 5

FORMULATION OF A NEW FLAT SHELL ELEMENT

CHAPTER 5

FORMULATION OF A NEW FLAT SHELL ELEMENT

5.1. Introduction

Shells possess many useful properties arising from their elastic nature and suitable design. They can be made to support large loads even when they are very thin .This property of shells is readily utilised in constructions which are strong and adaptable to a broad range of applications such as in aircraft, ships and reinforced concrete roof structures. In recent years the analysis of structures has been considerably eased by the use of computers programs especially those based on the finite element method.

The analysis of thin shell structures has generally been purely carried out on a theoretical basis and it is of importance to try to establish the validity of the theories pounded by comparing their correlation with experimental results. It will be appreciated that the numerical analysis exposed in this study has assumes that the material from which the shell was constructed is perfectly elastic. In attempting to verify this theory by experimental test it would be natural to use such perfectly elastic material. This would obviously provide the closest correlation between numerical and experimental results.

Tests on full-scale shells are few because the loading of such structures is difficult and costly. Experimental investigation of shells therefore usually resorts to small-scale tests. Therefore, the experimental work described in this study is of this type.

Direct interpolation based on strains approach instead of assumed displacement model, leads to results of stresses and displacements (obtained after integration) with a good degree of accuracy. In the assumed displacement model, based on classical formulation, the strains can be obtained by derivation of the displacement functions. The advantageous of strain based elements [BEL 99] are:

* Two criteria of the convergence conditions are related directly to strains; hence it would be easier to satisfy them (constant strains and rigid body motions) with assumed strains rather than displacements.

* The strain-displacement equations are coupled in such a way that some strains are function of more than one displacement; therefore if we make the displacements independent of each other, the strains will not be independent.

This approach usually leads to the representation of the displacements by higher order polynomial terms without the need for the introduction of the additional internal and unnecessary degrees of freedom (this enables us to deal with locking problem).

The success of the application of the strain based approach with membrane sector element **SBMS-BH** (Strain Based Mixed Sector 4-nodes) prompted the extension of the work to the development of an other quadrilateral element **Q4SBE1** (Strain Based Quadrilateral Element 4-nodes), both elements are based on assumed strains, having two degrees of freedom per node and an additional internal node.

5.2. Numerical study

5.2.1. Construction of the shell element ACM_Q4SBE1

The quadrilateral shell element used is obtained by the superposition of the **Q4SBE1** membrane strain based element with the **ACM** ([ADI 61], [MEL 63]) standard plate bending element. We have obtained a flat element shell called **ACM_ Q4SBE1.**
The **ACM_Q4SBE1** element has been obtained by using analytical integration of the membrane and bending stiffness matrix.

Description of the Q4SBE1 element

The figure 5.1 shows the geometric properties of **Q4SBE1** element, the corresponding nodal displacements. At each node (i) the degrees of freedom are U_i and V_i.

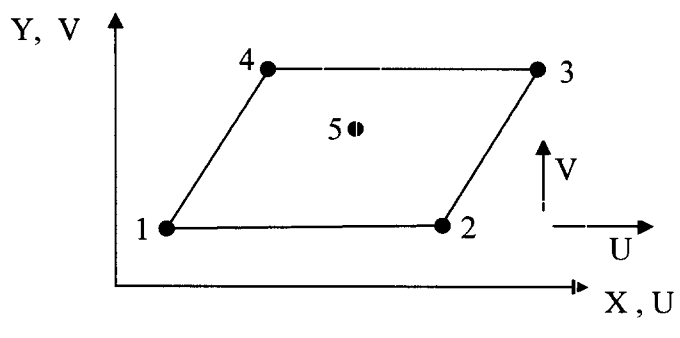

Fig.5.1: Co-ordinates and nodal points for the quadrilateral element" Q4SBE1"

Strain based element 'Q4SBE1'

In practice many engineers prefer to deal with the structures analysis by simple finite elements such as triangular elements with 3 nodes, quadrilateral with 4 nodes or solids with 8 nodes and with the same number of degrees of freedom per node .The purpose is to avoid mistakes which can be made when using complicated data elements. The displacement field of the **Q4SBE1** element is given by the following equations:

$$\begin{cases} U = a_1 - a_3 y + a_4 x + a_5 xy - a_7 \dfrac{y^2(R+1)}{2} + a_8 \dfrac{y}{2} + a_9 \dfrac{1}{2}(x^2 - Hy^2) \\ V = a_2 + a_3 x - a_5 \dfrac{x^2(R+1)}{2} + a_6 y + a_7 xy + a_8 \dfrac{x}{2} + a_{10} \dfrac{1}{2}(y^2 - Hx^2) \end{cases} \tag{5.1}$$

Rectangular plate element 'ACM'

The displacement fields of the **ACM** element (Fig.5.2) are given by the following equations:

$$\begin{aligned} W(x,y) &= a_1 + a_2 x + a_3 y + a_4 x^2 + a_5 xy + a_6 y^2 + a_7 x^3 + a_8 x^2 y \\ &\quad + a_9 xy^2 + a_{10} y^3 + a_{11} x^3 y + a_{12} xy^3 \\ \theta_x &= -(a3 + a_5 x + 2 a_6 y + a_8 x^2 + 2a_9 xy + 3 a_{10} y^2 + a_{11} x^3 \\ &\quad + 3 a_{12} xy^2) \\ \theta_y &= a_2 + 2a_4 x + a_5 y + 3a_7 x^2 + 2a_8 xy + a_9 y^2 + 3 a_{11} x^2 y + a_{12} y^3 \end{aligned} \tag{5.2}$$

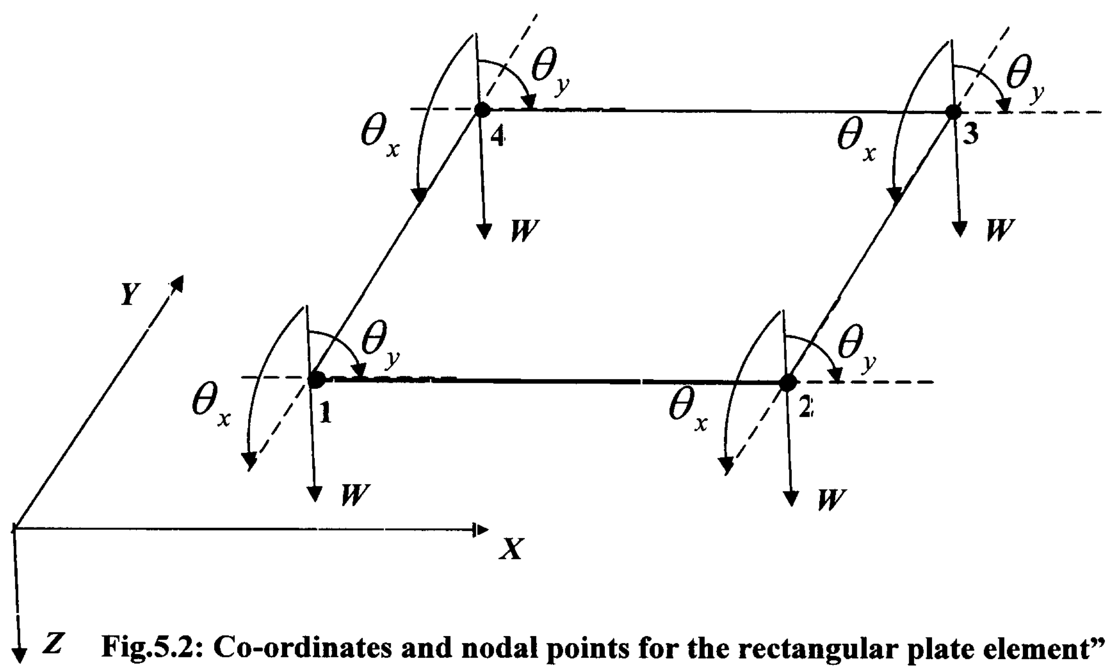

Fig.5.2: Co-ordinates and nodal points for the rectangular plate element" ACM"

The shell element **ACM_Q4SBE1** (Fig.5.3) is composed by assembling the two elements **Q4SBE1** and **ACM** in the following manner:

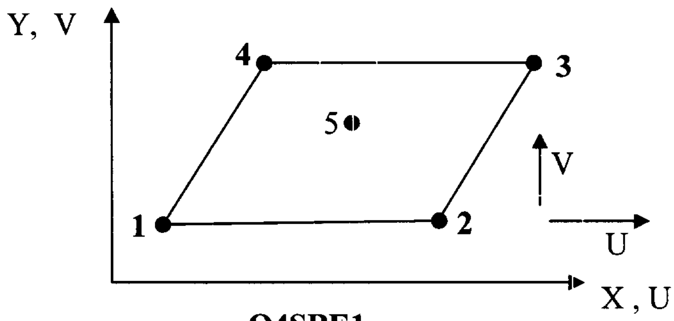

Q4SBE1

+

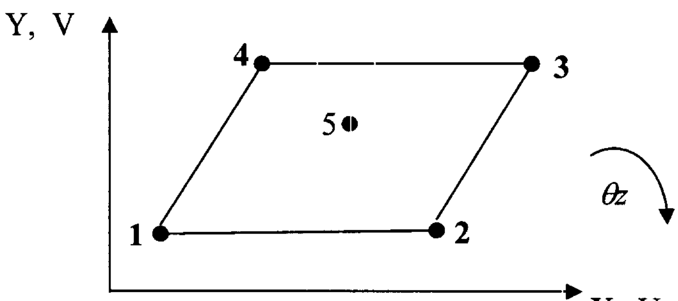

Fictive rotation θz

+

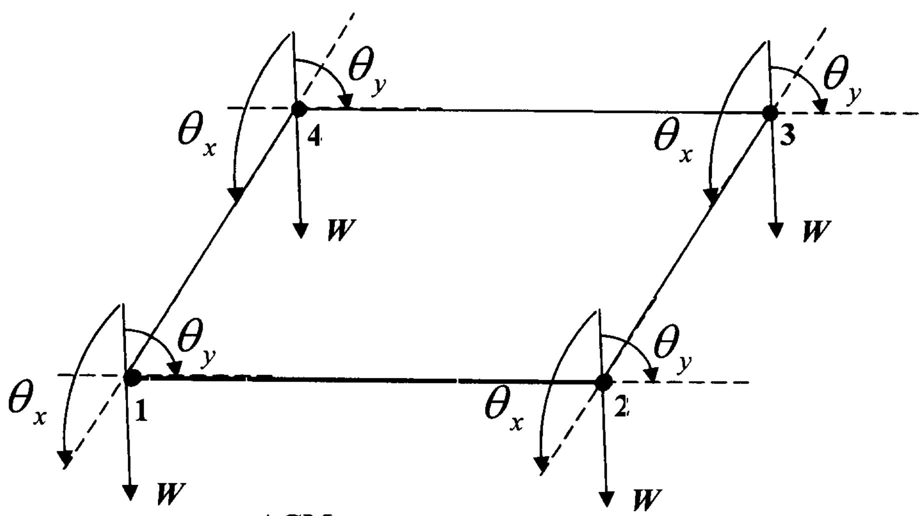

ACM

=

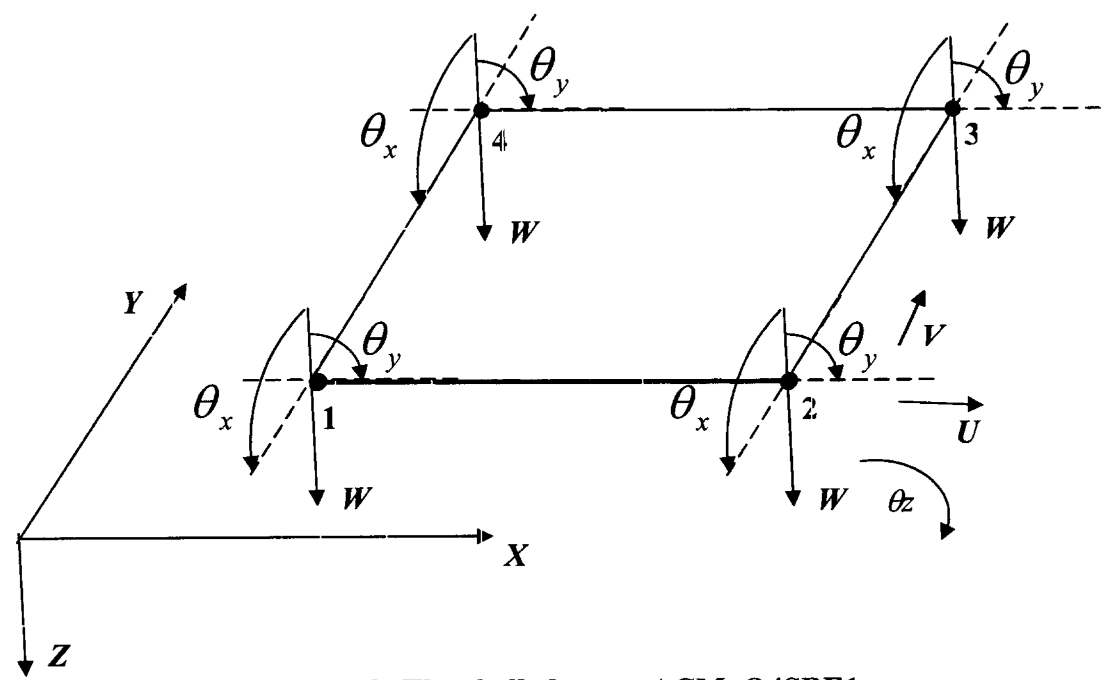

Fig.5.3: The shell element ACM_Q4SBE1

5.2.2. Validation

5.2.2.1. Clamped cylindrical shell

The performance of the developed shell element is evaluated on a standard test problem of a clamped cylindrical shell presented in Fig.5.4 (a). The geometrical dimensions, loading and elastic properties are given in Fig.5.4. Due to symmetry of the cylinder only 1/8 (ABCD) is considered in the finite element idealisations Fig.5.4 (b). The results of this analysis are compared to the exact solution based on the thin shell structures (R/h=100) given by Flugge [FLU 60] and Lindberg *et al* [LIN 69] below:

$W_C = -W_C\ Eh/P = 164{,}24$ deflection under load P in point C only

$V_D = -V_D\ Eh/P = 4{,}11$ deflection in Y direction

This test of thin shells (R/h=100) is considered by some researchers as a sever test. It makes it possible to examine the aptitude of shell element to simulate complicated membrane states problems dominated by bending.

The results obtained for different meshes are given in Table 5.1 as normalised values.

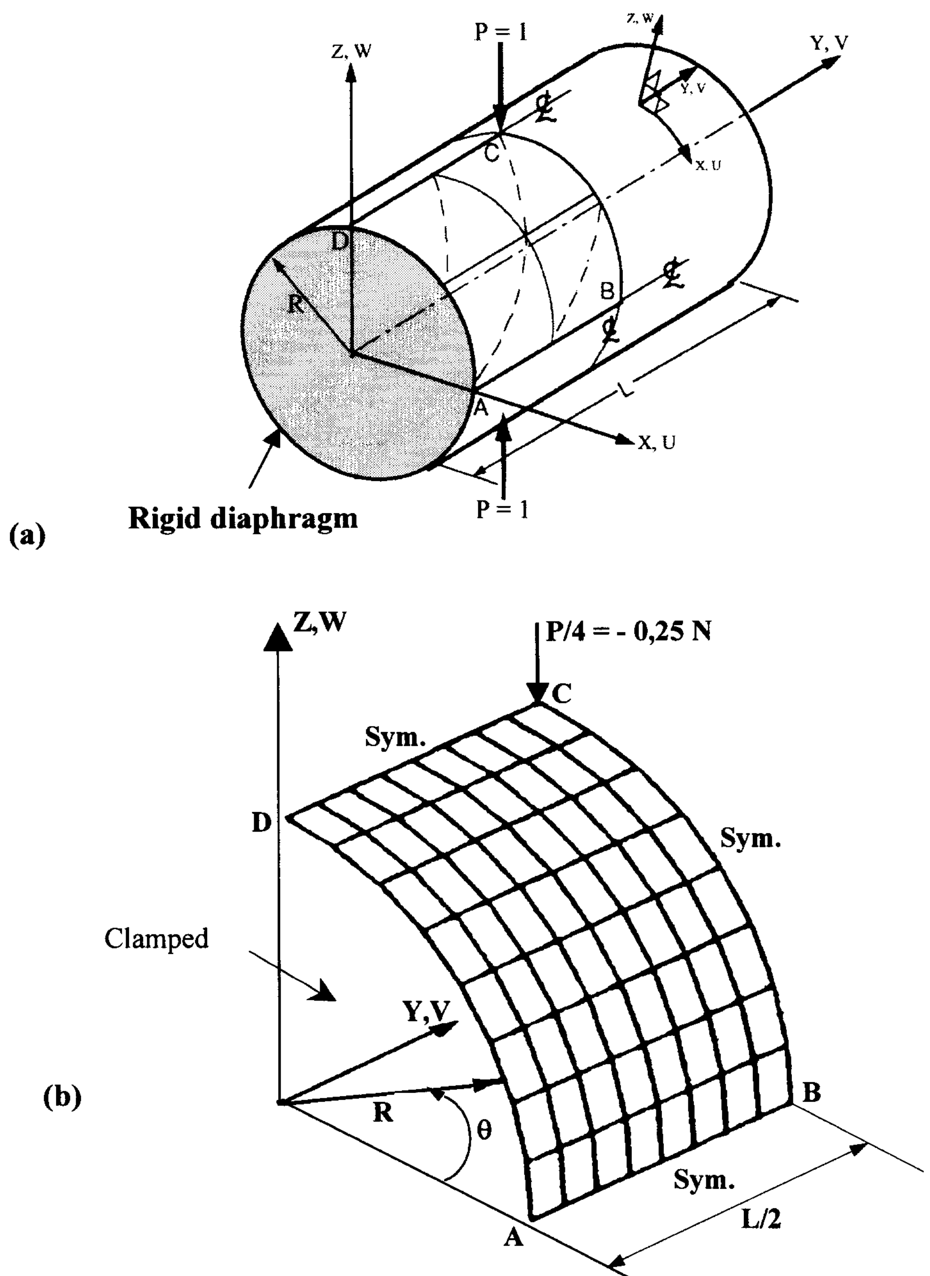

X,U

Data:

L=6 ; R=3m ; h = 0,03m; $E = 3x10^{10}$ Pa ; ν = 0,3

Symmetry conditions:

$W = \theta_Y = \theta_X = 0$ at AB
$V = \theta_X = \theta_Z = 0$ at BC
$U = \theta_Y = \theta_Z = 0$ at CD

Boundary conditions:

$U = W = \theta_Y = 0$ at AD

Fig.5.4: Clamped cylindrical shell

Meshes	Normalised displacements	
	W_C	V_D
4 x 4	0,649	1.510
6 x 6	0,842	1,175
8 x 8	0,955	1,104
20 x 4	0,985	1,013
Exact solution	**(1.00)** **164,24**	**(1.00)** **4,11**

Table 5.1: Clamped cylindrical shell, convergence of W_C and V_D

The results obtained for both deflections W_C and V_D for the refined mesh (20x4) are very good compared to the exact solution. The good convergence of the **ACM_Q4SBE1** element is confirmed.

5.3. Experimental work

Study of the elliptical paraboloid shell (Fig. 5.5)

Denoting the three sets of co-ordinates by *O1, X1, Y1, Z1, O2, X2, Y2, Z2*, and *O3, X3, Y3, Z3*, respectively, the equation for the surface will be written in the following manner [BEL & SOA 75].

$$Z_1 = 4f_x \frac{x^2}{l_x^2} + 4f_y \frac{y^2}{l_y^2} \tag{5.3a}$$

$$Z_2 = 4f_x \frac{x(x-l_x)}{l_x^2} + 4f_y \frac{y(y-l_y)}{l_y^2} \tag{5.3b}$$

$$Z_3 = f_x \left(\frac{2x}{l_x} - 1\right)^2 + 4f_y \frac{y^2}{l_y^2} \tag{5.3c}$$

The corners of the surface occur in the same plane, at a distance $(f_x + f_y)$ from the crown of the paraboloid. If the *OZ* axis points towards the base, the values obtained from equations (5.3a) and (5.3c) will be positive, whilst those obtained from equation (5.3b) will be negative.

* **Note 1:** The mesh size used in numerical analysis is (16 x 8) elements.

Model test

The test model is made of an aluminium alloy in an elliptical shape and has a constant thickness of 2 mm with a plan rectangular projection of 880 mm by 400 mm Fig. 5.6., the material properties have been assumed to be: The modulus of elasticity E=70000 N/mm^2, the Poisson ratio $\upsilon = 0.33$

The model is free along the long edges, fixed at certain points on wooden support along the short edges. Due to the double symmetry in geometry and loading, measuring points are located on one quarter of the area of the model at eight points Fig.5.7. Eight deflections gauges capable of measuring deflections perpendicular to the surface of the shell within 0.01 mm, are located under the shell model, so that the deflections in global co-ordinates can be computed. A further two deflection gauges are mounted to check symmetry Fig.5.7.

Four proving rings are mounted on the four corners of the model to check the distribution of loading, Fig.5.7.

Loading

A uniform normal pressure is applied by covering the shell top surface with a pneumatic pressure bag in close contact with it [HAM 89]. Four different values of loading are applied, 10, 20, 30, and 40 cm of water (in which 1 cm of water =0.0142233 lb/ in^2 equivalent to 2.5x10^{-3} N/mm^2). Each load is applied three times as follows:

The initial readings of the gauges are recorded, then the load is applied, the new readings of the gauges are recorded. The shell is then unloaded and gauge readings are recorded meanwhile to check the initial readings *.

* **Note 2**: Professor J.E. Gibson used this method in his different experimental works [GIB 77].

Numerical and experimental results

The vertical deflections resulting from numerical analysis and experimental work for different loading values are presented in Table 5.2.

	Points	3	4	5	6	7	8
Case a Load $=25x10^{-3}$ N/mm ^{2}	ACM_Q4SBE1	0.24	0.40	2.01	0.16	0.25	0.41
	Exp.Work	0.19	0.31	1.67	0.13	0.18	0.30
Case b Load $=50x10^{-3}$ N/mm ^{2}	ACM_Q4SBE1	0.48	0.80	4.02	0.32	0.50	0.82
	Exp.Work	0.49	0.80	3.10	0.33	0.47	0.85
Case c Load $=75x10^{-3}$ N/mm ^{2}	ACM_Q4SBE1	0.72	1.20	6.03	0.48	0.75	1.23
	Exp.Work	0.66	1.09	5.20	0.43	0.63	1.15
Case d Load $=100x10^{-3}$ N/mm ^{2}	ACM_Q4SBE1	0.96	1.60	8.02	0.65	1.00	1.64
	Exp.Work	1.04	1.70	7.70	0.68	1.00	1.90

Table 5.2: Vertical Displacements W (mm) Under Different Applied Loadings

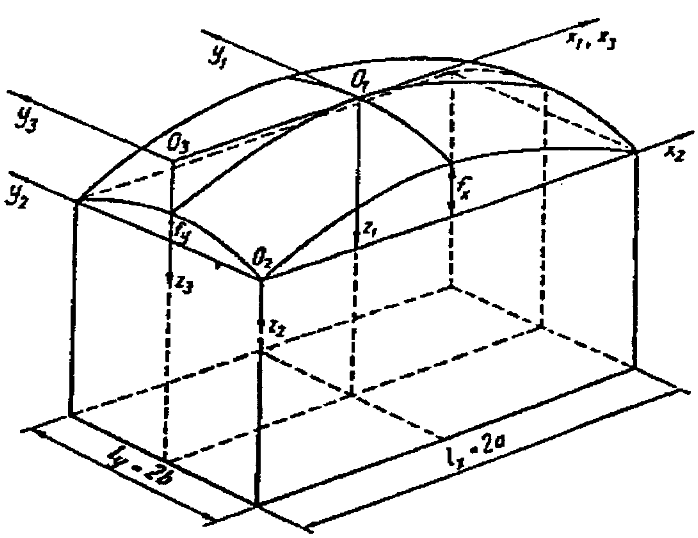

Fig.5.5: Elliptic paraboloid rectangular on plan

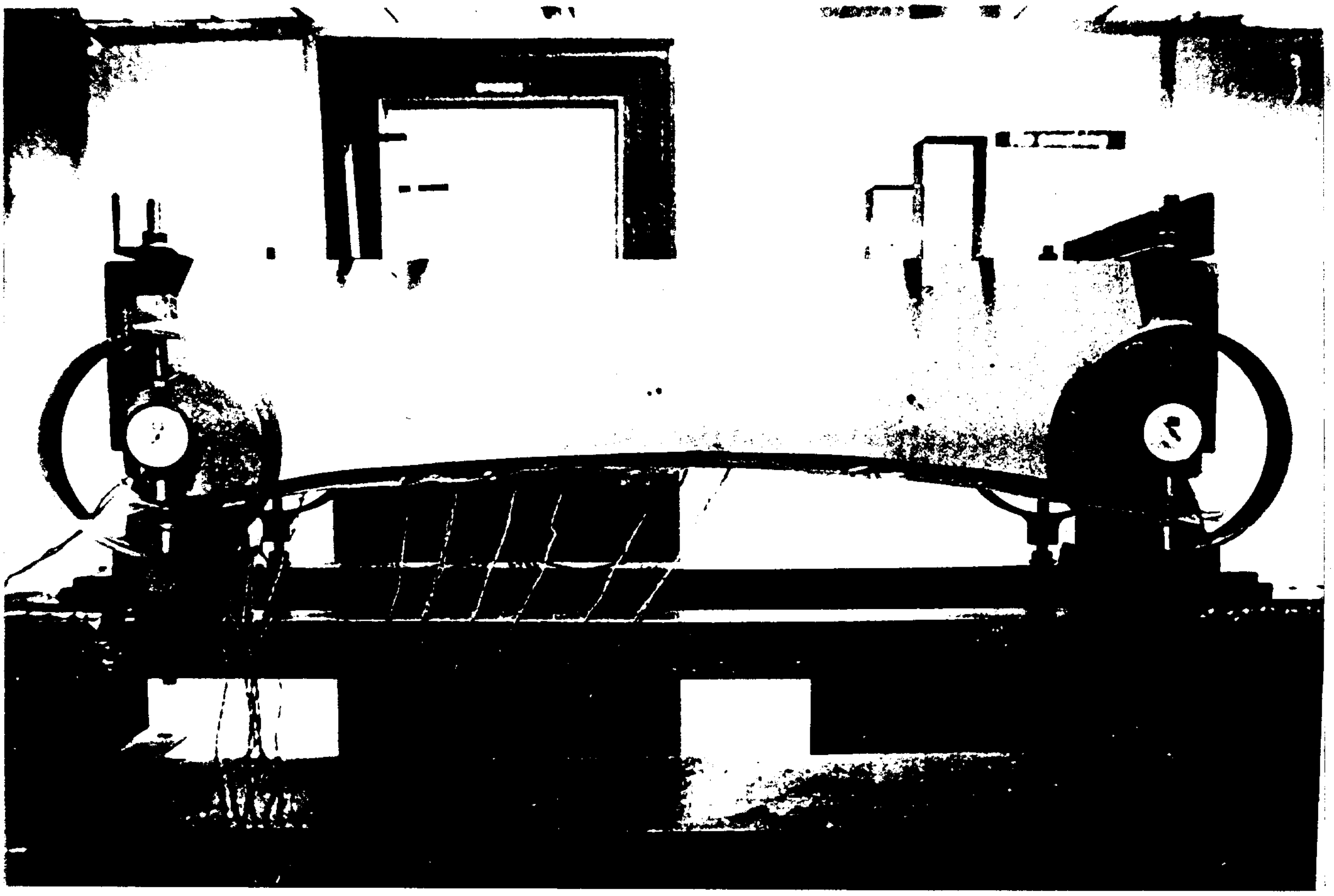

Fig.5.6: The elliptical paraboloid shell undergoing the experimental test.

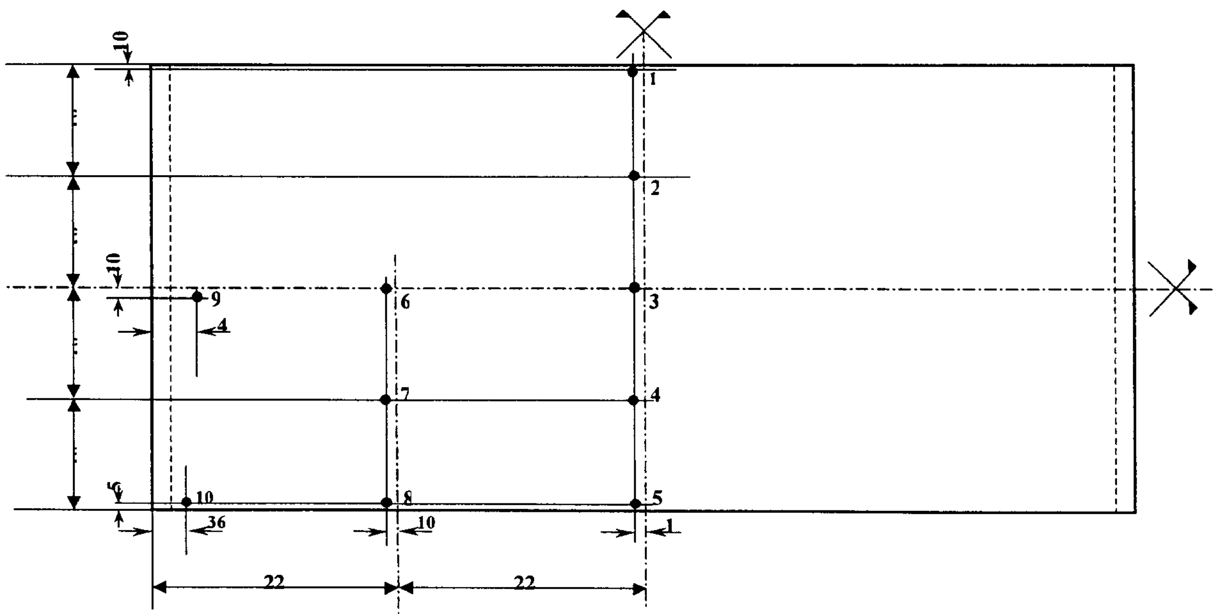

Fig.5.7: Dial gauge positions; (distance in mm)

5.4. Differences between theoretical and experimental results

In elastic analysis as we doubled the loading, the deflections were doubled; this was not the case in this experimental work. This results in a few points which could be explained as follows:

One of the main problems with the experiment was the lack of the uniformity of the distributed load. The air-filled bag did not evenly distribute the pressure because loads measured at the four corners were found to be slightly different.

A further probable cause of inaccuracy was the positioning of the deflection gauges. The problem was to ensure that the gauges were perpendicular to the shell surface. Although this was easy to achieve in the central position (since it is horizontal), this was note so easily achieved near the edges where the shell surface is considerably angled.

In addition to the various experimental inaccuracies, is that in the theoretical analysis non deflecting support conditions are assumed, which is not strictly the case in the experiments

Finally, differences may be results from other considerations.

5.5. Conclusion

From the results obtained from the experimental and the numerical analysis the following conclusion can be drawn:

Fine relatively meshes lead to almost identical results thus proving the efficiency of the strain based element. Excellent agreement between the shell element **ACM_Q4SBE1** results and those from experimental work (in inside points). The presented shell element '**ACM_Q4SBE1**' has been demonstrated to be robust, effective and useful in analysing thin shell structures. It is also exhibits strong convergence, as can be seen in the numerical analysis presented.

CHAPTER 6

AN EFFICIENT PARALLELEPIPED FINITE LEMENT BASED ON THE STRAIN APPROACH "SBP8C"

CHAPTER 6

AN EFFICIENT PARALLELEPIPED FINITE ELEMENT BASED ON THE STRAIN APPROACH «SBP8C"

6.1. Introduction

Calculation by finite elements of structures formed by plates and shells became a real tool with industrial vocation. It is very wide-spread in numerous sectors with high technology, civil or military (aprons of bridges, motor bodies, fuselages and wings planes...). Before 1991 no body imagined that the calculation of the biggest platform in the world: Hibernia (Terre-Neuve, Canada) would be treated in a complete way with thick shell finite elements [AYA 93], with on the whole a number of 420 000 degrees of freedom. Practice shows that the engineers prefer to model their structures with the simplest finite elements of the continuum (nodes in the only summits; the same number of unknowns by node...), such quadrangles with 4 nodes or bricks with 8 nodes.

Numerous studies (theoretical and numerical), were dedicated to the bending plate. Numerically, the calculation of the thick plate with 3D finite elements has been examined by several authors, references [ZIE 77] and [GAL 75] used these elements by maintaining 3D constants, let us quote for example the brick with twenty nodes, B20 and bricks without intermediate nodes following thickness . According to these authors, 3D elements give good results in this last case, but however do not approach known solutions for the thin plates [BELO 2006]. The major inconvenience in the use of these elements of superior order is the high cost because of the large number of points of numeric integration necessary for the exact evaluation of the element stiffness matrix.

The objective of this chapter, is to develop a new parallelepiped finite element, simple and effective baptized **SBP8C** (Strain Based Parallelepiped 8-nodes condensed), contributing to enrich the existing finite elements library. This last one is formulated, by the use of the static condensation, not only for the study of the 3D problems but also and especially for the thin and thick plates bending.

6.2. Description of the SBP8C element

Figure 6.1 shows the geometry of the element **SBP8C** and the correspondent kinematic variables. Each node (i) is attributed the three d.o.f Ui, Vi and Wi.

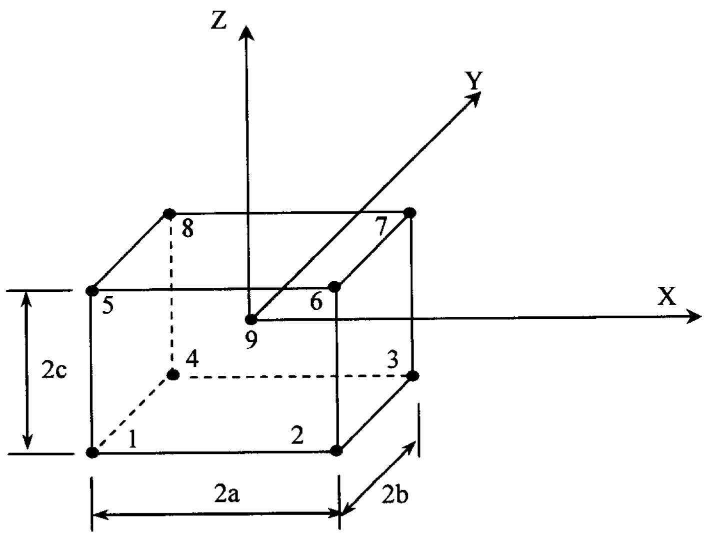

Fig.6.1: Geometry of the element SBP8C

6.3. Analytical formulation of the SBP8C element

6.3. 1. Displacement field

For a linear theory where the unitary strains are small, there are six strain components occurring in completely 3D analysis.

$$\varepsilon_{xx} = U_{,x} \qquad \gamma_{xy} = U_{,y} + V_{,x} \tag{6.1a, b}$$

$$\varepsilon_{yy} = V_{,y} \qquad \gamma_{yz} = V_{,z} + W_{,y} \tag{6.1c,d}$$

$$\varepsilon_{zz} = W_{,z} \qquad \gamma_{xz} = W_{,x} + U_{,z} \tag{6.1e,f}$$

U, V and W: are the displacements in the three directions X, Y and Z respectively.

Equations (6.2) represent the condition of the rigid body modes (RBM). We have:

$$\varepsilon_{ii} = 0 \tag{6.2a}$$

$$\gamma_{ij} = 0 \tag{6.2b}$$

By integrating equations (6.2), we obtain a particular solution:

$$U_R = a_1 + a_4 y + a_6 z \tag{6.3a}$$

$$V_R = a_2 - a_4 x - a_5 z \tag{6.3b}$$

$$W_R = a_3 + a_5 y - a_6 x \tag{6.3c}$$

Equations (6.3) represent the displacement fields corresponding to the rigid body modes (RBM).

The present element is an eight parallelepiped node in addition to the central node, with three degrees of freedom (d.o.f) by node (Fig.6.1). Therefore, the field of displacement has to contain twenty-seven independent constants. Six of them (a_1, a_2 ... a_6) are already used to represent the RBM, it remains so twenty-one (a_7, a_8 ... a_{27}) to represent in a rough way strains in the element, while verifying the six equations of compatibility. The strain field is:

$$\varepsilon_{xx} = a_7 + a_8 y + a_9 z + a_{10} yz + a_{25} x \tag{6.4a}$$

$$\varepsilon_{yy} = a_{11} + a_{12} x + a_{13} z + a_{14} xz + a_{26} y \tag{6.4b}$$

$$\varepsilon_{zz} = a_{15} + a_{16} x + a_{17} y + a_{18} xy + a_{27} z \tag{6.4c}$$

$$\gamma_{yz} = - a_{10} x^2 - a_{19} + a_{20} x + a_{22} x \tag{6.4d}$$

$$\gamma_{xz} = - a_{14} y^2 + a_{21} + a_{22} y + a_{24} y \tag{6.4e}$$

$$\gamma_{xy} = - a_{18} z^2 + a_{20} z + a_{23} + a_{24} z \tag{6.4f}$$

Substituting equations (6.2) and (6.4) into (6.1) and solving the resulting differential equations gives:

$$\begin{aligned} U = {} & a_1 + a_4 y + a_6 z + a_7 x + a_8 xy + a_9 xz + a_{10} xyz - 0.5\, a_{12} y^2 - 0.5\, a_{14} y^2 z \\ & - 0.5\, a_{16} z^2 - 0.5\, a_{18} yz^2 + 0.5\, a_{21} z + 0.5\, a_{23} y + a_{24} yz + 0.5\, a_{25} x^2 \end{aligned} \tag{6.5a}$$

$$\begin{aligned} V = {} & a_2 - a_4 x - a_5 z - 0.5\, a_8 x^2 - 0.5\, a_{10} x^2 z + a_{11} y + a_{12} xy + a_{13} yz + a_{14} xyz \\ & - 0.5\, a_{17} z^2 - 0.5\, a_{18} xz^2 + 0.5\, a_{19} z + a_{20} xz + 0.5\, a_{23} x + 0.5\, a_{26} y^2 \end{aligned} \tag{6.5b}$$

$$\begin{aligned} W = {} & a_3 + a_5 y - a_6 x - 0.5\, a_9 x^2 - 0.5\, a_{10} x^2 y - 0.5\, a_{13} y^2 - 0.5\, a_{14} xy^2 + a_{15} z \\ & + a_{16} xz + a_{17} yz + a_{18} xyz + 0.5\, a_{19} y + 0.5\, a_{21} x + a_{22} xy + 0.5\, a_{27} z^2 \end{aligned} \tag{6.5c}$$

It should be noticed here, that the final displacement functions contain quadratic terms allowing so the change of curvature. The parallelepiped element having the displacement fields given by equations (6.5) is referred to as **SBP8C**. The classic element based on the displacement model will be referred to as DBB8.

6.3.2 Evaluation of the matrix [K_0]

The evaluation of the element stiffness matrix is summarized with the evaluation of the following expression:

$$[K_e] = [A^{-1}]^T \, [K_0] \, [A^{-1}] \tag{6.6}$$

where

$$[K_0] = \iiint_V [Q]^T [D][Q] \, dx.dy.dz \tag{6.7}$$

Since [A] and its inverse can be evaluated numerically, the evaluation of the integral (6.7) becomes the key of the problem. While the shape of the element is regular, numerical integration is reduced to an analytical integration

$$\text{With} \quad \left[\underset{6x27}{Q}\right] = \begin{bmatrix} 0&0&0&0&0&0&1&y&z&yz&0&0&0&0&0&0&0&0&0&0&0&0&0&0&x&0&0 \\ 0&0&0&0&0&0&0&0&0&0&1&x&z&xz&0&0&0&0&0&0&0&0&0&0&0&y&0 \\ 0&0&0&0&0&0&0&0&0&0&0&0&0&0&1&x&y&xy&0&0&0&0&0&0&0&0&z \\ 0&0&0&0&0&0&0&0&0&0&0&0&0&0&0&0&0&-z^2&0&z&0&0&1&z&0&0&0 \\ 0&0&0&0&0&0&0&0&0&-x^2&0&0&0&0&0&0&0&0&1&x&0&x&0&0&0&0&0 \\ 0&0&0&0&0&0&0&0&0&0&0&0&0&-y^2&0&0&0&0&0&0&1&y&0&y&0&0&0 \end{bmatrix} \tag{6.8}$$

[D] is the usual constitutive matrix

For [A] and [K_0] **see the Appendices D.1 and D.2**

6.3.3. Mechanical characteristics of the fictitious material

The matrix (6.9) is a modified form (fictitious material) of the material matrix properties by introducing the plane stress constants and a corrective coefficient of transverse shearing (TS) noted K [AHM 70].

$$[D] = \begin{bmatrix} D1 & D2 & 0 & 0 & 0 & 0 \\ D2 & D3 & 0 & 0 & 0 & 0 \\ 0 & 0 & D4 & 0 & 0 & 0 \\ 0 & 0 & 0 & D5 & 0 & 0 \\ 0 & 0 & 0 & 0 & K\,D6 & 0 \\ 0 & 0 & 0 & 0 & 0 & K\,D7 \end{bmatrix} \tag{6.9}$$

Where:

$$D1 = D3 = \frac{E}{(1-\nu^2)} \;;\quad D2 = \frac{\nu E}{(1-\nu^2)} \;;\quad D4 = \frac{E(1-\nu)}{(1-2\nu)(1+\nu)} \;;\quad D5 = \frac{E}{2(1+\nu)} \;;\quad D6 = D7 = K\frac{E}{2(1+\nu)}$$

K= $\pi^2/12$ in Uflyand-Hencky-Mindlin's theory

K= 5/ 6 in Reissner's theory, ν is the Poisson's ratio

6.4. Numerical examples

The more and more increasing use of structures having an important ratio between the bending stiffness and shearing; this incited the researchers to formulate and to validate an element, which would be reliable for all the types of plates, thin or thick. The precision of the present element **SBP8C** is estimated through a series of standard tests limited to simple but self-important applications to show the interest of the strain model. The peculiarity of these examples lies generally, on one hand, in their geometrical simplicities, and on the other hand, in their very varied behaviour toward the phenomenon of locking in transverse shearing (TS). These two aspects make these examples an ideal tool for the validation of new models of finite elements.

6.4.1. Plate patch tests

In plate problems, the importance of the patch tests is paramount [ZIE 91]. A number of popular numerical problems mainly extracted from the proposed standard set of problems by White and Abel [WHI 89]. All reference solutions are taken from the same paper unless stated otherwise.

6.4.1.1 Constant bending moment patch test for plates

The response of single element cantilever to a constant bending moment applied as shown in Fig.6.2(c) is considered. Vertical deflections at the tip of the plate are calculated. It is seen in Table 6.1 that the **SBP8C** shows the same tip deflection and stresses as theory and gives more accurate results.

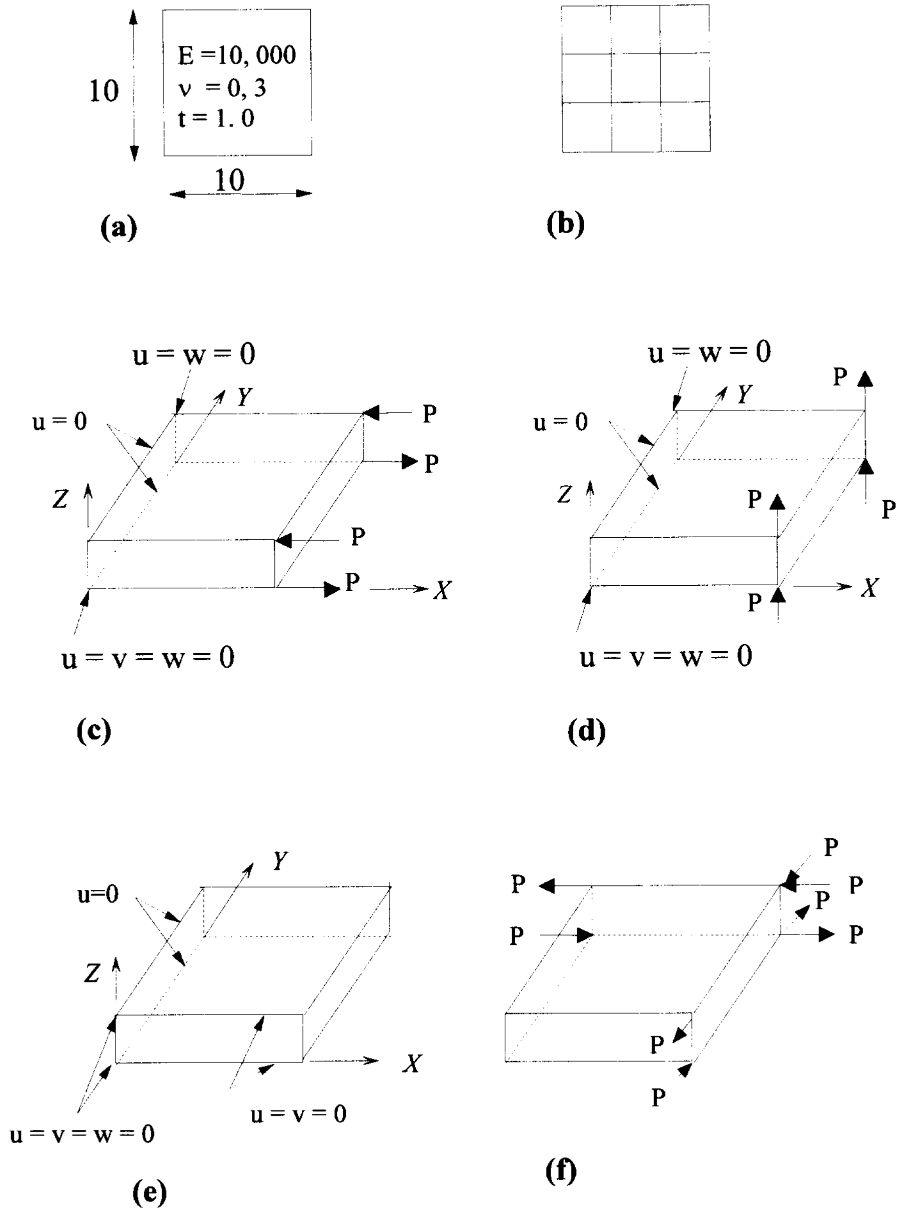

Fig.6.2: Plate patch tests (P = 1.0); Mesh :(a) regular 1x1; (b) regular 3x3.
(c) Constant bending moment test; **(d)** Out-of-plane shear load test;
(e) and **(f)** boundary conditions and loading for twisting moment tests.

Mesh	Tip deflection W (x 10^{-1})			
	Theory	PN30 [VEN 96]	ANSYS	**SBP8C**
1 x 1	0.12	0.1092	0.1092	0.12
3 x 3	0.12	0.1106	0.1092	0.12

Table 6.1: Constant bending moment patch test for plates

6.4.1.2 Out-of-plane patch test for plates

We use the same meshes as in previous section. The boundary conditions and end shear loading used are shown in Fig.6.2 (d). The solutions obtained are shown in Table 6.2. It is seen for the **SBP8C** that the results are satisfactory and convergence to the analytical solution is obtained as the number of elements used is increased.

	Tip deflection W			
Mesh	Theory	PN30 [VEN 96]	ANSYS	**SBP8C**
1 x 1	0.16	0.132	0.121	0.1268
3 x 3	0.16	0.151	0.147	0.1459

Table 6.2: Out-of-plane patch test for plates

6.4.1.3 Constant twisting moment patch test for plates

The boundary conditions and the twisting moment loads are shown in Fig.6.2 (e) and Fig.6.2 (f). Table 6.3 shows the results for the deflection of the tip. It is seen that the strain-based element gives better results.

	Tip deflection $W(10^{-1})$			
Mesh	Theory	PN30 [VEN 96]	ANSYS	**SBP8C**
1 x 1	0.312	0.312	0.312	0.312
3 x 3	0.312	0.314	0.312	0.312

Table 6.3: Constant twisting moment patch test for plates

6.4.2. Cantilever beam under pure bending

A single-element is subjected to a pure bending load applied as portrayed in Fig.6.3. The cantilever is of dimensions 10 x 1 x 1, the material modulus E and Poisson's ratio v are 10^6 and 0.0. The elegance of **SBP8C** can be observed in Table 6.4, in which the vertical deflections are listed.

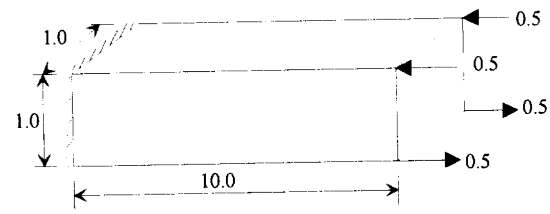

Fig.6.3: Cantilever beam under pure bending

	W
FI [BAS 2000]	$0.11764.\ 10^{-4}$
FCB [BAS 2000]	$0.60000.\ 10^{-3}$
SBP8C	$0.60000.\ 10^{-3}$
Theory	$0.60000.\ 10^{-3}$

Table 6.4: Cantilever beam under pure bending

6.4.3 Simply Supported Square Plate

The test of the simply supported square plate is examined with either a uniform loading (q = 1) or with a concentrated load (P = 1) at the centre (Fig.6.4). The quarter of the plate is divided into a mesh of N x N elements. The convergence tests are carried out on two different L/h ratios of 10 and 100 for thick and thin plates respectively. The results for the central deflection are given in Table 6.5 and Table 6.6. The effect of L/h ratio on the deflection at the centre W_C for a plate is studied. The results presented in Table 6.7 are given for the 12x12 meshes in terms of W_C/W_k where W_k is the reference Kirchhoff solution [ZIE 91] for thin plates.

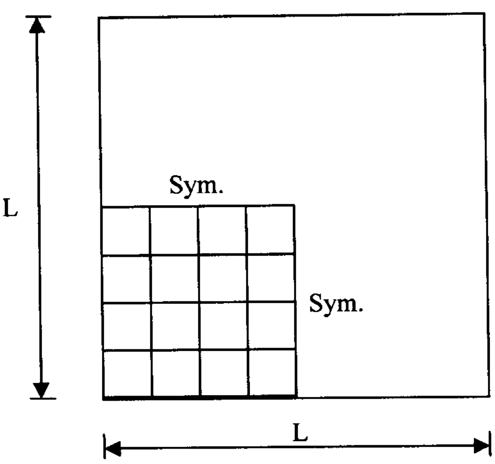

Fig.6.4: Simply supported square plate (L = 10, h = 1. or 0.1, E=10.92, ν = 0.25)

Mesh	$\frac{wD}{qL^4}$x100					
	L/h=10			L/h=100		
	SBP8C	SBH8 [BEL 2000]	DBB8	**SBP8C**	SBH8 [BEL 2000]	DBB8
2x2	0.3812	0.326	0.2283	0.0349	0.0523	0.0045
4x4	0.4218	0.4048	0.351	0.2563	0.3081	0.0171
8x8	0.4229	0.4145	0.3982	0.3856	0.3883	0.0582
12x12	0.4270	0.4249	0.4171	0.4033	0.4029	0.0786
Exact solution [TAY 86]	0.427			0.406		

$D = Eh^3/12(1-v^2)$

Table 6.5: Central deflection of a simply supported plate with a uniform load

Mesh	$\frac{wD}{PL^2}$x100					
	L/h=10			L/h=100		
	SBP8C	SBH8 [BEL 2000]	DBB8	**SBP8C**	SBH8 [BEL 2000]	DBB8
2x2	1.1745	0.9907	0.7269	0.113	0.1452	0.0134
4x4	1.321	1.243	1.097	0.789	0.8387	0.0481
8x8	1.363	1.333	1.289	1.108	1.115	0.1636
12x12	1.372	1.364	1.344	1.152	1.145	0.2269
Kirchhoff solution [TAY 86]				1.16		
Ref. [GAL 75]	1.346					

Table 6.6: Central deflection of a simply supported plate with a concentrated load

L/h	W_c/W_{ref}					
	Uniform load			Concentrated load		
	SBP8C	SBH8 [BEL 2000]	DBB8	**SBP8C**	SBH8 [BEL 2000]	DBB8
5	1.2067	1.2024	1.2016	1.739	1.7317	1.7338
10	1.0522	1.0466	1.0273	1.1866	1.1759	1.1586
20	1.0143	1.0074	0.9206	1.0456	1.0363	0.9473
40	1.0019	0.9975	0.7027	1.0086	1.0008	0.6987
50	1.000	0.996	0.6000	1.0038	0.9959	0.5919
100	0.9931	0.9924	0.1936	0.9895	0.9871	0.1956
W_{ref}	$0.406\text{x}10^{-2}qL^4/D$			$1.16\text{x}10^{-2}PL^2/D$		

Table 6.7: Influence of L/h on the central deflection for simply supported plates

The numerical tests show that:

- The strain based elements **SBP8C** has quite rapid rate of convergence to reference solutions for both thick and thin plates.

- The **SBP8C** elements is free from any shear locking since it converge to the Kirchhoff solution for thin plates, contrarily for the corresponding displacement based element DBB8

- SBH8 and **SBP8C** have similar behaviour, and they have the advantages to be valid for both thin and thick plates.

- The influence of the transverse shear for the strain based elements is much more important for plates with concentrated load than for those with uniform load.

6.5. Conclusion

The present element (**SBP8C**) passes the constant stain patch test and the three plate patch tests. Numerical results obtained using these elements agree well with those from other investigations and theoretical results for both thin and thick plates. The robustness of the present element was demonstrated, the plate bending can be very well simulated with a simple parallelepiped element (**SBP8C**) based on the strain approach.

The performance of this element has been demonstrated in plate bending, and the advantages of using the strain approach are again confirmed.

CONCLUSIONS

In this thesis, a review on the available strain based sector elements for curved structures, led to the development of a new sector finite element **SBMS-BH (Strain Based Mixed Sector Belarbi and Hamadi),** based on the strain approach. This element can be used for the analysis of general plane elasticity in polar coordinates. It has four nodes in addition to the central node, and two degrees of freedom per node, the inclusion of the internal node ameliorates the results obtained. To test the performance of the element, it has been applied to a thick cylinder under internal pressure. The results obtained are shown to converge to the theoretical solution for the problem considered. We should mention here that the convergence is monotone for both deflections and stresses. The good performance of the developed sector element **SBMS-BH** is confirmed. This new sector element "**SBMS-BH**" based on the strain approach is the first element to be developed and requires static condensation.

To overcome the geometrical inconvenience for the structures with irregular forms; a new integration solution routine is formulated. It allows the evaluation of the matrix $[K_0]$ in an automatic way whatever the degree of the polynomial of the kinematics field and the distortion of the element. The interest of this subroutine of integration was shown.

A new quadrilateral strain based element **"Q4SBE1"** that satisfies the equilibrium equations is formulated. This element has two degrees of freedom (d.o.f) at each corner node in addition to the internal node. Through the introduction of additional internal d.o.f, this element proved to be more accurate even though it requires static condensation. The efficiency of this element was established and the convergence of the results for stresses and displacements to a satisfactory degree of accuracy was shown to be faster when compared with the quadrilateral standard element Q4. Furthermore the results obtained are comparable with those obtained when using the robust element Q8.

Applications of the developed element to the analysis of some civil engineering problems have been carried out, and it is shown that satisfactory results can be obtained without the use of large number of elements.

To ameliorate the membrane behaviour of thin shells, the previously developed quadrilateral strain based membrane element **"Q4SBE1"** is combined with the plate bending element **ACM** to obtain a flat shell element called **ACM_ Q4SBE1.** The formulated shell element is applied to various types of shells with different loading and boundary conditions.

Clamped cylindrical shell with a central point load; which is considered by some researchers as a sever test was first analysed. The results obtained for both deflections W_C and V_D for the refined mesh (20 x 4) are very good compared to the exact solution.

The analysis of thin shell structures has generally been purely carried out on a theoretical basis and it is of importance to try to establish the validity of the theories pounded by comparing their correlation with experimental results. It is appreciated that the numerical analysis exposed in this study has assumed that the material from which the shell was constructed is perfectly elastic. In attempting to verify this theory by experimental test it would be natural to use such perfectly elastic material. This would obviously provide the closest correlation between numerical and experimental results. Therefore, the experimental work described in this study is of this type.

The test model is made of an aluminium alloy in an elliptical shape and has a constant thickness of 2 mm with a plan rectangular projection of 880 mm by 400 mm. Due to the double symmetry in geometry and loading, measuring points are located on one quarter of the area of the model at eight points. Eight deflections gauges capable of measuring deflections perpendicular to the surface of the shell within 0.01 mm are located under the shell model, so that the deflections in global co-ordinates can be computed.

From the results obtained from the experimental and the numerical analysis the following conclusions can be drawn:

Fine relatively meshes lead to almost identical results thus proving the efficiency of the strain based element. Excellent agreement observed between the numerical results, and those from experimental work (in inside points).

The presented shell element '**ACM_Q4SBE1**' has been demonstrated to be robust, effective and useful in analysing thin shell structures. It is also exhibits strong convergence, as can be seen in the numerical analysis presented.

Facing the difficulty of achieving C^1 continuity in the formulation of Kirchhoff plate bending finite elements, considerable research works have been oriented to the Reissner/Mindlin plate theory] which can be used for the analysis of both thick and thin plates. Other researchers have used three-dimensional elements (solid elements) for the thick plates in bending. These elements tend to cause undesirable shear locking phenomena when dealing with thin plates.

As alternative for displacement models, a new parallelepiped finite element, simple and effective baptized **SBP8C** (Strain Based Parallelepiped 8-nodes condensed), contributing to enrich the existing finite elements library. This last one is formulated, by the use of the static condensation, not only for the study of the 3D problems but also and especially for the thin and thick plates bending.

To test the performance of the developed element (**SBP8C**) it has been applied to several test problems for which exact solutions and numerical results exist.

Plate patch tests are proposed standard set of problems by White and Abel. The response of single element cantilever to a constant bending moment applied is considered. Vertical deflections at the tip of the plate are calculated. It is shown that the **SBP8C** element shows same tip deflection and stresses as theory.

The test of the simply supported square plate is examined with either a uniform loading or with a concentrated load at the centre of the plate. The convergence tests are carried out on two different L/h ratios of 10 and 100 for thick and thin plates respectively.

The numerical tests show that the performances of the **SBP8C** element are again confirmed by the rapid convergence to the analytical solution for thin plates and to the numerical results given by **DBB8** element for thick plates.

The performance and robustness of the developed elements has been demonstrated, and the advantages of using the strain based approach are again confirmed. The proposed extension of this work is the application of the developed elements in non linear analysis of structures, especially thin shell structures.

REFERENCES

REFERENCES

[ADI 61] Adini A. and Clough R.W., Analysis of plate bending by the finite element method, Report to the Nat. Sci. Found., U.S.A., G 7337, 1961.

[AHM 70] Ahmad S., Irons B.M., Zienkiewicz O.C., Analysis of thick and thin shell structures by curved elements, IJNME, Vol. 2, pp. 419-451, 1970.

[ALL 84] Allman D.J., A compatible triangular element including vertex rotations for plane elasticity, C.S, Vol. 19, pp. 1-8, 1984.

[ALL 88a] Allman D.J., Evaluation of the constant strain triangle with drilling rotations, IJNME, Vol. 26, pp. 2645-2655, 1988.

[ALL 88b] Allman D.J., A quadrilateral finite element including vertex rotations for plane elasticity analysis, IJNME, Vol. 26, pp. 717-730, 1988.

[ARG 60] Argyris J. H., and Kelsey S., Moderne fuselage analysis and the elastic aircraft, Butterworths London, 1960.

[ASH 71a] Ashwell D.G. and Sabir A.B., Limitations of certain curved finite elements when applied to arches, IJMS Vol. 13, pp. 133-139, 1971.

[ASH 71b] Ashwell D.G., Sabir A.B., Roberts T.M., Further studies in the application of curved finite elements to circular arches, IJMS Vol. 13, pp. 507-517, 1971.

[ASH 72] Ashwell D.G. and Sabir A.B., A new cylindrical shell finite element based on simple independent strain functions, IJMS, Vol.14, pp.171-183, 1972.

[ASS 99] Assan A.E., Analysis of multiple stiffened barrel shell structures by strain-based finite elements. Thin-walled structures (35): 233-253, 1999.

[AYA 93] Ayad R., Eléments finis de plaque et coque en formulation mixte avec projection en cisaillement, Thèse de Doctorat, U.T.C, 1993. 217 pages.

[BAB 84] D. Babu and G.F. Pinder "Analytical integration formulae for linear isoparametric element", IJNME, Vol. 20, pp. 1153-1166, 1984.

[BAS 2000] K. Bassayya, K. Bhattacharya and U. Shrinivasa, Eight-node brick, PN340, represents constant stress fields exactly. *Computers and Structures* 74 (2000) 441-460.

[BAT 90b] Batoz J.L. et Dhatt G., Modélisation des structures par éléments finis, Vol. 2 : Poutres et plaques, Eds Hermès, Paris, 1990.

[BATH 76] Bathe K.J. and Wilson E.L., *Numerical Methods in finite element analysis.* Printice Hall, New Jersey (1976).

[BEL & SOA 75] Beles, A. A. Soare, M. V., "Elliptic and Hyperbolic Paraboloidal Shells Used in Construction" , Bucharest, May 1975, pp 145-146.

[BEL 98a] Belarbi M.T. et Charif A., Nouvel élément secteur basé sur le modèle de déformation avec rotation dans le plan, Revue Européenne des Eléments Finis, Vol. 7, N° 4, pp. 439-458, Juin 1998.

[BEL 98b] Belarbi M.T. et Charif A., Nouveau Quadrilatère ''SBQ4'' avec Drilling rotation, Conférence Internationale sur les Mathématiques Appliquées et les Sciences de l'Ingénieur *CIMASI'98* les 27-28 et 29 octobre, Casablanca, Vol. 2, pp. 136-141, 1998.

[BEL 98c] Belarbi M.T. et Charif A., Nouvel hexaèdre simple ''SBH8'' pour l'étude des plaques minces et épaisses, Les Annales Maghrébines de l'Ingénieur, Vol. 12, N° Hors Série, extrait de l'acte du 6ème Colloque Maghrébin sur les Modèles Numériques de l'Ingénieur *C2MNI6*, Tunis les 24-26, Vol. 2, pp. 623-627, Nov. 1998.

[BEL 99] Belarbi M.T. et Charif A., Développement d'un nouvel élément hexaédrique simple basé sur le modèle en déformation pour l'étude des plaques minces et épaisses, Revue Européenne des éléments finis, Vol. 8, N° 2, pp. 135-157, 1999.

[BEL 2000] Belarbi M.T., Développement de nouveaux éléments finis basés sur le modèle en déformation. Application linéaire et non linéaire. *Thèse de Doctorat d'état, Université de Constantine*, Algérie, 2000.

[BEL 2003] Belarbi M.T and Hamadi, D., Amelioration of the Sabir rectangular finite element "SBRIER" based on the strain model. Proc. 1st International Conference of Civil Engineering Science, ICCES1, Vol. 1, pp. 82- 92, Assiut, Egypt 2003.

[BEL 2005a] Belarbi M.T. et Maalem T., On improved rectangular finite element for plane linear elasticity analysis, Revue européenne des éléments finis, Vol. 14, N° 8, 2005.

[BEL 2005b] Belarbi M.T. et Bourezane M., On improved sabir triangular element with drilling rotation, Revue Européenne de génie civil, Vol. 9, N° 9-10, 2005.

[BELO 2004] Belounar L. and Guenfoud M.., A new rectangular finite element based on the Strain approach for plate bending. Thin-Walled Structures 43 (2005) 47- 63.

[BELO 2006] Belounar L. and Hamadi D., Plate bending with a solid strain based element that satisfies the equilibrium equations. 6th European Solid Mechanics Conference. ESMC2006, Budapest 28 August-1 September 2006.

[BER 84] Bergan P.G. and Wang X., (1984). Quadrilateral plate bending elements with shear deformations. Comput Struct, 19: 25-34.

[BER 85] Bergan P.G. & Felippa C.A., A triangular membrane element with rotational degrees of freedom, CMAME, Vol. 50, pp. 25-69, 1985.

[BOU 87] Bouzerira C., Finite element analysis for general plane elasticity, Msc. thesis University of Walles College of Cardiff (G.B), 1987.

[CLO 66] Clough R.W. and Tocher J.L., Finite element stiffness matrices for analysis of plate bending, Proc – Ist Conf. Matrix Meth. Struct. Meth, AFFDL –TR – 66 –80 pp. 515-545, 1966.

[COO 86] Cook R.D., On the Allman triangle and a related quadrilateral element, C.S, Vol. 22, pp. 1065-1067, 1986.

[COO 87] Cook R.D., A plane hybrid element with rotational d.o.f and adjustable stiffness, IJNME, Vol. 24, pp. 1499-1508, 1987.

[DJO 90] Djoudi M.S., Strain based Finite Elements for linear and geometrically nonlinear analysis of structures, PhD thesis University of Walles College of Cardiff (G.B), June 1990.

[DJO 95] Djoudi M.S. & Sabir A.B., Finite element analysis of singly and doubly curved dams of constant or variable thickness. Thin-walled structures (21): 279- 289, 1995.

[DJO 2003] Djoudi M.S. & Bahai H., A shallow shell finite element for the linear and nonlinear analysis of cylindrical shells. Engineering structures (25): 769- 778, 2003.

[DJO 2004a] Djoudi M.S. & Bahai H., A cylindrical strain-based shell element for vibration analysis of shell structures. Finite Elements in Analysis and Design, 40: 1947-1961. 2004.

[DJO 2004b] Djoudi M.S. & Bahai H., Strain- based finite element for the vibration of cylindrical panels with openings. Thin-walled structures (42): 575-588, 2004.

[FEL 66] Felippa C.A., Refined finite element analysis of linear and nonlinear two dimensional structures, Report UCSESM 66-22 Department of Civil Engineering, University of California Berkeley, October 1966.

[FLU 66] Flugge W. and Fosberge K., Point load on shallow elliptic paraboloid, J. Appl. Mech. Vol. 33, pp. 575-585, 1966.

[GAL 75] R.H. Gallagher, *Introduction aux éléments finis* .Printice-Hall, Inc.,Englewood Cliffs, (New Jersey, USA, 1975).

[GIB 77] Gibson, J. E, "Thin Shells Computing and Theory", Pergamon Press Ltd., Headington Hill Hall, Oxford OX3 OBW, England, December 1977, pp 249-251

[GRI 88] D.V. Griffths "Stiffness matrix of the four-node quadrilateral element in closed form ", IJNME, Vol. 37, pp. 1027-1038, 1994.

[HAC 89] W.L. Hacker and H.L. Schreyer "Eigenvalue analysis of compatible and Incompatible rectangular four-node quadrilateral elements", IJNME, Vol. 28, pp. 687- 703, 1989.

[HAM 89] Hamadi, D., "Numerical and Experimental Investigation of an Elliptical Parboloid Thin Shell Structures", Master Thesis, City University London March 1989.

[HAM 2000] Hamadi, D. and Belarbi M.T., "Experimental and numerical analyses of an Elliptical Parboloid thin shell structures." Proc. The Eighth Arab Structural Engineering Conference 21-23 October Vol 1 pp. 109-118. 20003 Cairo

[IBR 90] Ibrahimbegovic A., Taylor R.L. et Wilson E.L., A robust quadrilateral membrane finite element with drilling degrees of freedom, IJNME, Vol. 30, pp. 445-457, 1990.

[IBR 93a] Ibrahimbegovic A., Frey F. et Rebora B., Une approche unifiée de la modélisation des structures complexes : les éléments finis avec degré de liberté de rotation, LSC Rapport Interne 93/10, Ecole polytechnique fédérale de Lausanne (Suisse), Juin 1993.

[IRO 68] Irons B.M. and Zienkiewicz O.C., The isoparametric finite element system, A new concept in finite element analysis, Proc. Conf. On recent advances in stress analysis, Royal Aeronautical Society London , 1968.

[LIN 69] Lindberg G.M., Olson M.D. and Cowper G.R., New development in the finite element analysis of shells, Q. Bull Div. Mech. Eng. and Nat. Aeronautical Establishment, National Research council of Canada, Vol. 4, 1969.

[MAC 88] MacNeal R. H. et Harder R. L., A refined four-noded membrane element with rotational degrees of freedom, C.S., Vol. 28, pp. 75-84, 1988.

[MAC 85] MacNeal R. H. et Harder R. L., A proposed standard set of problems to test finite element accuracy, Finite Element Anal. Des. 1, pp. 3-20, 1985.

[MAC 87] MacNeal R. H., A theorem regarding the locking of tapered four-noded membrane elements, IJNME., Vol. 24, pp. 1793-1799, 1987.

[MAC 89] Mac-Neal R. H. and Harder R. L., A refined four-noded membrane element with rotational degrees, C.S., Vol 28, pp 75-84, 1989

[MEL 62] Melosh R.J., Development of the stiffness method to define bounds on elastic behaviour of structures, PhD thesis University of Washington, 1962.

[MEL 63] Melosh R.J., Basis of derivation of matrices for the direct stiffness method, J.AIAA Vol. 1 N7, pp. 1631-1637, 1963.

[NOB 86] Noboru Kikuchi, Finite element methods in mechanics analysis Cambridge University Press, 1986.

[PIA 84] Pian T.H. and Sumihara K., Rational approach for assumed stress finite elements, IJNME, Vol. 20, pp. 1685-1695, 1984.

[RAJ 69] Raju I.S. and Rao A.K., Stiffness matrices for sector elements, AIAA J. 7, pp. 156-157, 1969.

[RAT 88] H.D. Rathod " Some analytical integration formulae for a four node isoparametric element", Comput. Struct., Vol. 30, pp. 1101-1109, 1988.

[REK 80] Rekatch V., Problèmes de la théorie de l'élasticité, Edition Mir Moscou, 1980.

[SAB 71] Sabir A.B. and Ashwell D.G., A comparaison of curved beam finite elements when used in vibration problems, J. of Sound and Vibration, Vol. 18, pp. 555-563, 1971.

[SAB 75] Sabir A.B., Stiffness matrices for the general deformatioon of curved beam members based on independent strain functions, The Math. F. E. and Appli.IIed J.R. Whiteman, Academic Press, 1975.

[SAB 78] Sabir A.B. and Ashwell D.G., Diffusion of concentrated loads into thin cylindrical shells, The Math. F. E. and Appli.IIIed J.R. Whiteman, Academic Press, 1978.

[SAB 83] Sabir A.B., A new class of Finite Elements for plane elasticity problems, CAFEM 7^{th}, Int. Conf. Struct. Mech. in Reactor Technology, Chicago, 1983.

[SAB 84] Sabir A.B. , Strain based finite element analysis of shear walls. , Pro. 3 rd Int. Conf. on Tall Building, Y.K Cheung and P.K.K. Lee, eds., Hong Kong, 447-453. 1984.

[SAB 85a] Sabir A.B., A rectangular and triangular plane elasticity element with drilling degrees of freedom, Chapter 9 in proceeding of the 2nd international conference on variational methods in engineering, Southampton University, Springer-Verlag, Berlin, pp. 17-25, 1985.

[SAB 85b] Sabir A.B. and Ramadhani F., A shallow shell finite element for general shell analysis, Variational methods in engineering Proceedings of the 2^{nd} international conference, University of Southampton England, 1985.

[SAB 85c] Sabir A.B., A segmental finite element for general plane elasticity problems in polar coordinates. 8th Int. Conf. Struct. Mech. in Reactor Technology, Belgium, 1985.

[SAB 86] Sabir A.B., Salhi H.Y., A strain based finite element for general plane elasticity in polar coordinates, Res. Mechanica 19, pp. 1-16, 1986.

[SAB 95a] Sabir A.B. and Sfendji A., Triangular and Rectangular plane elasticity finite elements. Thin-walled Structures 21.pp 225-232 .1995

[SAB 95b] Sabir A.B. & Moussa A.I., Finite Element Analysis of Cylindrical-Conical Storage Tanks With Girder Stiffeners. *Thin-Walled Structures* 21.pp 269-277.1995

[SAB 96] Sabir A.B. & Moussa A.I., Finite element analysis of cylindrical-conical storage tanks using strain-based elements. Structural Engineering Review (8) 4: 367-374. 1996.

[SAB 97a] Sabir A.B. & Davies G.T., Natural frequencies of plates with square holes when subjected to in-plane uniaxial, biaxial or shear loading. Thin-walled structures (28): 321-335, 1997a.

[SIM 89] Simo J.S., Fox D.D. *et* Rifai M.S., on a stress resultant geometrically exact shell model part II: the linear theory; computational aspects, CMAME., 73, pp. 53-92, 1989.

[SZE 92] Sze K.Y., Chen W. and Cheung Y.K., An efficient quadrilateral plane element with drilling degrees of freedom using orthogonal stress modes, C.S., Vol. 42, N° 5, pp. 695-705, 1992.

[TAY 85] Taylor R.L. and Simo J.C., Bending and membrane elements for analysis of thick and thin shells, in J. Middelton and G.N. Pande (eds.), Proceeding NUMETA 85, pp. 587-591, 1985.

[TAY 86] Taylor R.L., Simo J.C., Zienkiewicz O.C. and Chan A.C., The patch test: A Condition for Assessing Finite Element Convergence, IJNME, Vol. 22, pp. 39-62, 1986.

[TIM 51] Timoshenko S. and Goodier J. N., Theory of Elasticity, Mc Graw-Hill, New York, 1951.

[TIM 70] Timoshenko S. P., and Goodier J. N., Theory of Elasticity, 3rd ed., Mc Graw-Hill, New York, 1970.

[TUR 56] Turner M.J., Clough R.W., Martin H.C. and Topp L.J., Stiffness and deflection analysis of complex structures, J. of Aeron. Sci.,Vol. 23, pp. 805-824, 1956.

[VEN 96] D.N. Venkatesh and U. Shrinivasa, Plate bending with hexahedral P.N. elements. *Computers and Structures* Vol. 60 $n^0$04 (1996) 635-641.

[VIS 65] Visser W., A finite element method for the determination of non-stationary temperature distribution and thermal deformations, Proc.Conf.Math. Methods. Struct..Mech , Air bforce institute of technology Dayton Ohio, 1965 .

[WHI 89] D.W. White and J.F. Abel . Testing of shell finite element accuracy and robustness. *Finite Elem Anal Des* 6 (1989)129-151.

[WILL 84] William W. Jr., and Paul R. J., *Finite elements for structural analysis,* Prentice-Hall,Inc. Englewood Cliffs, 1984.

[YUN 89] Yanus S.M., Saigal S. and Cook R.D., On improved hybrid finite elements with rotational degrees of freedom, IJNME, Vol. 28, pp. 785-800, 1989.

[ZIE 65] Zienkiewicz O.C. and Cheung Y.K., Finite Element in the solution of field problems, the engineer, pp. 507-510, 1965.

[ZIE 77] Zienkiewicz O.C. and Taylor R. L., The Finite Element Method, troisième édition, Mc Graw-Hill, 1977.

[ZIE 88] Zienkiewicz O.C., The finite element method, Mc Graw-Hill, (UK) London,1988.

[ZIE 91] R.H. Gallagher, *Introduction aux éléments finis* .Printice-Hall, Inc.,Englewood Cliffs, (New Jersey, USA, 1975).O.C. Zienkiewicz and R.L. Taylor, *The finite element method in solid and fluid mechanics, dynamics and nonlinearity*, Vol. II,(Mc Graw Hill, New York, 1991).

Appendices

Appendix A.1

The strain matrix [B] for the Sector Element SBMS-BH

$$
[\mathrm{B}] = \begin{bmatrix} 0 & \theta & 0 & 1 & 1 & \theta & r\theta & 0 & \theta & \theta^2 \\ \frac{1}{r} & 0 & -\frac{\theta}{r} & 1 & \frac{\theta}{r} & \theta & \frac{1}{r} & r & r & \left(\theta^2 - r\right) \\ 1 & -\frac{1}{r} & \frac{1}{r} & 0 & \frac{1}{r} & \left(1+\frac{r}{2}\right) & 0 & \frac{\theta}{r} & \frac{2.\theta}{r} & \left(\theta+1\right) \end{bmatrix}
$$

Appendix A.2

a/ Elements of [K₀] matrix (Eq. 2.23c)

$$
[\mathrm{K_0}] = \begin{bmatrix} H_1 & 0 & 0 & H_2 & 0 & 0 & H_3 & H_4 & H_5 & H_6 \\ & H_7 & H_8 & 0 & H_9 & 0 & 0 & H_{10} & 0 & 0 \\ & & H_{13} & 0 & H_{14} & 0 & 0 & 0 & H_{15} & 0 \\ & & & H_{18} & 0 & 0 & H_{19} & H_{20} & H_{21} & H_{22} \\ & & & & H_{23} & 0 & 0 & H_{24} & 0 & 0 \\ & & & & & H_{27} & 0 & 0 & 0 & 0 \\ & & & \text{Symmetry} & & & H_{30} & H_{31} & H_{32} & H_{33} \\ & & & & & & & H_{34} & H_{35} & H_{36} \\ & & & & & & & & H_{37} & H_{38} \\ & & & & & & & & & H_{39} \end{bmatrix}
$$

$D_1 = E(1-\nu)/(1+\nu)(1-2\nu)$; $D_2 = \nu.D_1/(1-\nu)$; $D_3 = E/2(1+\nu)$;

$E_i = (r_2^{\,i} - r_1^{\,i})_{\ i=1,6}$; $AL = ALog(r_2) - Alog(r_1)$;

$A_1 = D_1 - D_2$; $A_2 = D_1 + 2\,D_2$; $A_3 = 2\,D_1 + 2\,D_2$;
$A_4 = D_1 - D_2$; $A_5 = D_2 - D_3 + D_1/2$; $A_6 = D_1 - D_2 + 2\,D_3$;
$A_7 = 5\,D_1 + 4\,D_2$; $A_8 = 8\,D_1 + 16\,D_2 - 24\,D_3$; $A_9 = D_1 + D_2 - D_3/4$;

$H_1 = 2\beta.AL.D^2{}_1$
$H_2 = 2\beta.E_1.A_1$
$H_3 = 2\beta.AL.E1.D_1$
$H_4 = D_1\,\beta^3.AL/3 + 2\beta.E_1$
$H_5 = \beta^2.AL.D_1.E_1$
$H_6 = 2\beta^3.E_1.A_2/3 + \beta.E_2.D_1$
$H_7 = 2\beta.AL.D_4$

$H_{17} = -\,E_1.\beta.E_2.D_2$
$H_{18} = \beta.E_1\,A_1$
$H_{19} = 2\beta.E_1.A_4$
$H_{20} = A_1\,(\beta.E_1 + \beta^2.E_1/2)$
$H_{21} = 3\beta^2.E_1.A_1/2$
$H_{22} = 2\beta^3.E_2.A_1/3 - 2\beta.E_3.A_1/3$
$H_{23} = 2\beta^3.AL.D_2/3 + 2\beta.AL.D_1$

$H_8 = 2\beta.AL.D_3$

$H_9 = 2\beta.AL.D_1$

$H_{10} = -\ 2\beta.D_3\,(E_1 + E_2/2)$

$H_{11} = \beta^3.D_3\,(2.E_3/3 - 3.E_2/2)/3$

$H_{12} = -\ \beta.E_2.D_3$

$H_{13} = 2\beta^3.AL.D_1/3 - 3\beta.AL.D_3$

$H_{14} = -\ 2\beta^3.AL.D_1/3 - 2\beta.AL.D_3$

$H_{15} = -2\beta^3.E_1.A_1/3 + 2\beta.D_3\,(E_1 + E_2/4)$

$H_{16} = -\beta^5.E_2.A_2/5 + 4\beta^3.E_3.A_7/9 - \beta^3.E_2.D_3$

$H_{24} = 2\beta^3.E_1.A_1/3 + 2\beta.D_3\,(E_1 + E_2/4)$

$H_{25} = \beta^3.(\beta^2.E_2.A_2/5 - 4.E_3.A_4/9 + E_2.D_3)$

$H_{26} = \beta.E_2.D_3$

$H_{27} = 2\beta^3.E_2.A_4/3 + \beta.D_3\,(E_2 - 2.E_1/3 + E_4/8)$

$H_{28} = \beta^3(2.A_1\,\beta^2.E_3/5 - A_9.E_4/3 + D_3(2E_2/3 - 2E_5/15))$

$H_{29} = D_2.\beta(E_3/4 - 2.E_1/3)$

$H_{30} = 3AL.2\beta(D_1 - \beta^2.D_3/3)$

$H_{31} = 2\beta.(D_1.(2.E_1 + \beta^2.AL/3) - 2\beta^2.AL.D_3/3)$

$H_{32} = 2\beta^3.AL.(D_1 - 2.D_3)/3$

$H_{33} = (\beta^3/3)(2.E_1.A_1 + D_3.(E_2 - 4.E_1)) - \beta E_2.D_2$

$H_{37} = 3\beta^2.AL(\beta^2.D_4/5) + 4.D_3/3)$

$H_{34} = \beta^2.(D_1.(2.E_1/3 - \beta^2.AL/10) + 2.AL.D_3/3) + \beta.E_2.D_1$

$H_{35} = \beta^3.(D_1.(2.E_1/3 + \beta^2.AL/5) - 4.AL.D_3/3)$

$H_{36} = \beta^3.(A_1.\beta^3(2.E_4/5 + A_5.E_2/3 - 4.E_2.D_3/3) - 2\beta.D_2.E_3/3$

$H_{38} = \beta^2.(2\beta^2.E_1.A_1/5 - E_2.D_1/3 - .D_3.(6.E_1/3 - 2.E_2/3))$

$H_{39} = \beta^3.(2.A_1.\beta^2.E_2/3 - 4.A_6.E_3/4 + D_3.E_4/6 - 4.D_3.E_2/3) + \beta.E_4.D_1/2$

b/ Elements of [A] matrix (Eq. 2.23b)

$$
[A] = \begin{bmatrix}
1 & 0 & -\beta & R_1 & 0 & R_1\beta & 0 & \beta^2/2 & \beta^2 & R_1\beta \\
0 & 1 & R_1 & 0 & R_1 & R_1^{\,2}/2 & \beta & 1 & 0 & -R_1^{\,2}\beta \\
0 & R & 2 & 0 & R & 0 & 0 & 0 & 2\beta & -4\beta \\
1 & 0 & 1 & R_2 & R & R_2\beta & 0 & 0 & \beta^2 & R_2\beta^2 \\
0 & 1 & \beta & 0 & R_2 & R_2\,/2 & R & 0 & 0 & -R_2^{\,2}\beta \\
R & 0 & 2 & 0 & 0 & 0 & 0 & 0 & -2\beta & 1 \\
1 & 0 & \beta & R_2 & R & -R_2\beta & 0 & \beta^2/2 & \beta^2 & R_2\beta^2 \\
0 & 1 & R_2 & 0 & R_2 & R_2/2 & R & R_2\beta & 0 & R_2^{\,2}\beta \\
0 & R & 2 & 0 & \beta & 0 & \beta^2 & 0 & 2\beta & 2R_2\beta \\
1 & 0 & \beta & R_1 & -\beta & -R_1\beta & 0 & \beta^2/2 & 1 & R_1\beta^2
\end{bmatrix}
$$

Appendix B.1

Integration Subroutine

```
******************************************************************
      SUBROUTINE INTEGRATION(TI,X,Y)
      IMPLICIT REAL*8(A-H,O-Z)
      PARAMETER (SMALL=1.0D-15)
      COMMON /COEFFICIENT/ A1,B1,A2,B2,A3,B3,A4,B4
     DIMENSION TI(49),X(4),Y(4),T(2),ICORD(4),dx(4),dy(4)
     DIMENSION TI1(49),TI2(49),TI3(49)
      do 87 iu=1,49
      ti1(iu)=0.
      ti2(iu)=0.
      ti3(iu)=0.
87   continue
     CALL FORM _ICORD(X,ICORD)
     CALL COEFF(ICORD,XY,DX,DY)
c***************   INTEGRAL No.1   ***************
     if(abs(dx(1)).GT.small.AND.abs(dx(4)).GT.small)then
     CALL EXPRES(x(Icord(1)),x(Icord(2)),a1,b1,a4,b4,1,ti1)
     endif
c***************   INTEGRAL No.2   *****************
     if(abs(dx(2)).GT.small.AND.abs(dx(4)).GT.small)then
     ICO1=ICORD(1)+1
     IF(ICO1 .EQ. 5) ICO1=1
     CALL EXPRES(x(Icord(2)),x(Icord(3)),a2,b2,a4,b4,2,ti2)
     if(abs(dx(1)).GT.small.AND.abs(dx(3)).GT.small)then
    ICO1=ICORD(1)-1
     IF(ICO1 .EQ. 0) ICO1=4
     if(Icord(2).EQ.ICO1)then
     CALL EXPRES(x(Icord(2)),x(Icord(3)),a1,b1,a3,b3,2,ti2)
     endif
     endif
c***************   INTEGRAL No3   **************************
     if(abs(dx(3)).GT.small.AND.abs(dx(4)).GT.small)then
     ICO1=ICORD(1)-1
         CALL EXPRES(x(Icord(3)),x(Icord(4)),a3,b3,a4)
     endif
     endif
     if(abs(dx(2)).GT.small.AND.abs(dx(3)).GT.small)then
    ICO1=ICORD(1)+2
     IF(ICO1.EQ. 5) ICO1=1
     IF(ICO1 .EQ. 6) ICO1=2
     if(Icord(4).EQ.ICO1)then
     CALL EXPRES(x(Icord(3)),x(Icord(4)),a2,b2,a3,b3,3,ti3)
     endif
     endif
      if(Icord(4).EQ.ICO1)then
     CALL EXPRES(x (Icord(3)),x(Icord(4)),a1,b1,a2,b2,3,ti3)
     endif
     CALL TII(ti1,ti2,ti3,ti)
     RETURN
     END
******************************************************************

      SUBROUTINE EXPRES(XZ,XXZ,A,B,C,D,IY,TI)
       IMPLICIT REAL*8(A-H,O-Z)
       PARAMETER (SMALL=1.0D-15)
      COMMON /COEFFICIENT/ A1,B1,A2,B2,A3,B3,A4,B4
```

```
      DIMENSION TI(49),T(3),ICORD(4),
      INTEGER IC(8)
      I=1
      DO 160 kK=1,49
160   TI(kK)=0.
      DO 1 IB=0,6
      GO TO (10,11,12,13,14,15,16),II
10    IC(1)=1
      IC(2)=1
      GO TO 100
12    IC(1)=1
13    IC(1)=1
      GO TO 100
14    IC(1)=1
      IC(2)=5
      IC(6)=1
      GO TO 100
15    IC(1)=1
       GO TO 100
16    IC(1)=1
      IC(2)=21
      IC(3)=7
      IC(4)=34
      IC(5)=35
100   CONTINUE
      DO 2 IA=0,6
      T(iy)=0.
       DO 3 K=1,IB+2
       AX1(K)=C**(K-1)*D3
       BX1(K)=A**(K-1)*B2
       AA1=(IC(K)*(AX1(k)-BX1(k))*(XXZ
       T(IY)=T(IY)-AA2
3      CONTINUE
      RETURN
      END
```

SUBROUTINE FORM_ICORD(X,ICORD)

```
      IMPLICIT REAL*8(A-H,O-Z)
      DIMENSION XY(2,4), X(4)
      XY(1,1)=X(1)
      XY(1,2)=X(2)
      XY(1,4)=X(4)
      ICORD(1)=1
     DO 100 i=1,4
      DO 200 j=1,i
      IF(xy(1,i) .LT. xy(1,j)) then
     XY(1,2)=X(2)
      XY(1,4)=X(4)
      ti=xy(1,i)
      xy(1,i)=xy(1,j)
      xy(1,j)=ti
      endif
     XY(1,2)=X(2)
      XY(1,4)=X(4)
200   continue
      return
      End
```

```
SUBROUTINE COEFF(ICORD,X,Y,DX,DY)
 IMPLICIT REAL*8(A-H,O-Z)
 DIMENSION ICORD(4),x(4), y(4),dx(4),dy(4)
  PARAMETER (SMALL=1.0D-15)
 COMMON /COEFFICIENT/ A1,B2,A3,B1,A2,
C  CALCUL Y1
 ICO1=ICORD(1)+1
 IF(ICO1 .EQ. 5) ICO1=1
 dx(1)=x(Icord(1))-x(ICO1)
 a1=dy(1)/dx(1)
 b1=y(Icord(2))-a1*x(Icord(1))
 ELSE
 a1=0
 b1=0
 ENDIF
C  CALCUL Y2
 ICO2=ICORD(1)-1
 IF(ICO2.EQ. 5) ICO2=1
 IF(ICO2 .EQ. 6) ICO2=2
 dx(2)=x(ICO1)-x(ICO2)
 IF(abs(dx(2)) .EQ. SMALL) THEN
 a2=dy(2)/dx(2)
 b2=y(ICOl)-a1
 ELSE
 b2=0
 a2=0
 ENDIF
C  CALCUL Y3
 ICO1=ICORD(1)-1
 dx(3)=x(ICO1)+(ICO2)
 dy(3)=y(ICO1)+y(ICO2)
 IF(abs(dx(3)) .GT. SMALL) THEN
 ENDIF
C  CALCUL Y4
 dx(4)=x(Icord(1))-x(ICO1)
 dy(4)=y(Icord(1))-y(ICO1)
 IF(abs(dx(4)) .GT. SMALL) THEN
 a4=dy(4)/dx(4)
 b4=y(Icord(1))-a4*x(Icord(1))
 ELSE
 a3=dy(3)/dx(3)
 b3=y(ICO1)-a3*x(ICO1)
 ELSE
 a4=0
 b4=0
 ENDIF
 RETURN
 END
 SUBROUTINE TII(TI1,TI2,TI3,TI)
 IMPLICIT REAL*8(A-H,O-Z)
 dimension ti(49),ti1(49),ti2(49),ti3(49)
 do 17 j=1,49
17   ti(j)=0.
 do 10 i=1,49
10  ti(i)=ti1(i)+ti2(i)+ti3(i)
 return
 End
```

Appendix B.2

Calculation of the element stiffness matrix [K_0],

```
      SUBROUTINE FORM_ K0(TI, E, V, th,ELKO)
      IMPLICIT DOUBLE PRECISION(A-H,O-Z)
      DIMENSION ELKO(12,12),TI(49)
      DO 51 I=1,12
      DO 51 J=1,12
      ELKO(I,J)=0.D0
51    CONTINUE
      D11=E/(1.D0-V**2)
      D12=E*V/(1.D0-V**2)
      D22=D11
      D33=E/(2*(1.D0+V))
      ELKO(4,4)=D11*TI(1)
      ELKO(4,7)=D12*TI(1)
      ELKO(4,8)=D12*TI(2)
      ELKO(4,10)=D11*TI(15)-D12*TI(3)
      ELKO(4,11)=2.D0*D11*TI(23)-
      ELKO(5,5)=4.D0*D33*TI(1)
      ELKO(5,6)=4.D0*D33*TI(2)
      ELKO(5,9)=4.D0*D33*TI(8)
      ELKO(5,12)=ELKO(5,6)
      ELKO(6,6)=D11*TI(15)-4.D0*D33*TI(3)
      ELKO(6,8)=(D12+4.D0*D33)*TI(9)
      ELKO(6,9)=4.D0*D33*TI(9)
      ELKO(7,7)=D22*TI(1)
      ELKO(7,8)=D22*TI(2)
      ELKO(7,10)=D12*TI(15
      ELKO(7,11)=2.D0*D12*TI(23)
      ELKO(8,8)=D22*TI(3)+4.D0*D33*TI(15)
      ELKO(8,9)=4.D0*D33*TI(15)
      ELKO(8,10)=D12*TI(16)-D22*TI(4)
      ELKO(8,11)=2.d0*D12*TI(24)-2.D0*D22*TI(12)
      ELKO(8,12)=4.D0*D33*TI(9)
      ELKO(9,9)=4.D0*D33*TI(15)
      ELKO(9,12)=4.D0*D33*TI(9)
      ELKO(10,10)=D11*TI(29)+2.D0*D12*TI(17)+D22*TI(5)
      ELKO(11,11)=4.D0*D11*TI(45
      DO 15 I=1,12
      DO 15 J=1,12
      ELKO(J,I)=ELKO(I,J)
15    CONTINUE
      RETURN
      END
```

Appendix C.1

Matrices [A] and [k$_0$] for Q4SBE1 element:

$$[A]=\begin{bmatrix}
1 & 0 & 0 & 0 & 0 & 0 & 0 & 0 & 0 & 0\\
0 & 1 & 0 & 0 & 0 & 0 & 0 & 0 & 0 & 0\\
1 & 0 & 0 & a & 0 & 0 & 0 & 0 & \frac{a^2}{2} & 0\\
0 & 1 & a & 0 & \frac{-a^2(R+1)}{2} & 0 & 0 & \frac{a}{2} & 0 & \frac{-Ha^2}{2}\\
1 & 0 & -b & a & ab & 0 & \frac{-b^2(R+1)}{2} & \frac{b}{2} & \frac{a^2-Hb^2}{2} & 0\\
0 & 1 & a & 0 & \frac{-a^2(R+1)}{2} & b & ab & \frac{a}{2} & 0 & \frac{b^2-Ha^2}{2}\\
1 & 0 & -b & 0 & 0 & 0 & \frac{-b^2(R+1)}{2} & \frac{b}{2} & \frac{-Hb^2}{2} & 0\\
0 & 1 & 0 & 0 & 0 & b & 0 & 0 & 0 & \frac{b^2}{2}\\
1 & 0 & -\frac{b}{2} & \frac{a}{2} & \frac{ab}{4} & 0 & -\frac{b^2}{8}(R+1) & \frac{b}{4} & \frac{a^2-Hb^2}{8} & 0\\
0 & 1 & \frac{a}{2} & 0 & -\frac{a^2}{8}(R+1) & \frac{b}{2} & \frac{ab}{4} & \frac{a}{4} & 0 & \frac{b^2-Ha^2}{8}
\end{bmatrix}$$

$$[K_0]=\begin{bmatrix}
H_1 & 0 & 0 & H_2 & 0 & 0 & H_3 & H_4 & H_5 & H_6\\
 & H_7 & H_8 & 0 & H_9 & 0 & 0 & H_{10} & 0 & 0\\
 & & H_{13} & 0 & H_{14} & 0 & 0 & 0 & H_{15} & 0\\
 & & & H_{18} & 0 & 0 & H_{19} & H_{20} & H_{21} & H_{22}\\
 & & & & H_{23} & 0 & 0 & H_{24} & 0 & 0\\
 & & & & & H_{27} & 0 & 0 & 0 & 0\\
 & & & & & & H_{30} & H_{31} & H_{32} & H_{33}\\
 & & & & & & & H_{34} & H_{35} & H_{36}\\
 & & & & & & & & H_{37} & H_{38}\\
 & & & & & & & & & H_{39}
\end{bmatrix}$$

$$H_1 = abD_{11}$$

$$H_2 = \frac{1}{2}ab^2D_{11}$$

$$H_3 = abD_{12}$$

$$H_4 = \frac{1}{2}ba^2D_{12}$$

$$H_5 = \frac{1}{2}ba^2D_{11}$$

$$H_6 = \frac{1}{2}ab^2D_{12}$$

$$H_7 = \frac{1}{3}\left(ab^3D_{11} + ba^3R^2D_{33}\right)$$

$$H_8 = \frac{1}{2}ab^2D_{12}$$

$$H_9 = \frac{a^2b^2}{4}\left(R^2D_{33} + D_{12}\right)$$

$$H_{10} = -\frac{1}{2}Rba^2D_{33}$$

$$H_{11} = \frac{a^2b^2}{4}\left(RHD_{33} + D_{11}\right)$$

$$H_{12} = \frac{1}{3}\left(ab^3D_{12} + ba^3RHD_{33}\right)$$

$$H_{13} = abD_{22}$$

$$H_{14} = \frac{1}{2}ba^2D_{22}$$

$$H_{15} = \frac{1}{2}ba^2D_{12}$$

$$H_{16} = \frac{1}{2}ab^2D_{22}$$

$$H_{17} = \frac{1}{3}\left(ba^3D_{22} + ab^3R^2D_{33}\right)$$

$$H_{18} = -\frac{1}{2}ab^2RD_{33}$$

$$H_{19} = \frac{1}{3}\left(ba^3D_{12} + ab^3RHD_{33}\right)$$

$$H_{20} = \frac{a^2b^2}{4}\left(RHD_{33} + D_{22}\right)$$

$$H_{21} = abD_{33}$$

$$H_{22} = -\frac{1}{2}ab^2HD_{33}$$

$$H_{23} = -\frac{1}{2}ba^2HD_{33}$$

$$H_{24} = \frac{1}{3}\left(ab^3H^2D_{33} + ba^3D_{11}\right)$$

$$H_{25} = \frac{a^2b^2}{4}\left(H^2D_{33} + D_{12}\right)$$

$$H_{26} = \frac{1}{3}\left(ba^3H^2D_{33} + ab^3D_{22}\right)$$

$H_{27} = ab\ D_{11}$ $H_{28} = RH_{17}$ $H_{29} = 3ab\ DR_{11}$ $H_{30} = 1/2\ ab\ D_{11}$

$H_{31} = 4\ abH\ D_{11}\ D_{22}$ $H_{32} = abH\ D_{33}$ $H_{33} = \left(ab\ D_{11} + 3ab\ DR_{11}\right)$ $H_{34} = 5H\ ab^3$

$H_{35} = abR^2\ D_{12}$ $H_{36} = ab\ HD_{11}$ $H_{37} = 3a^3b\ D_{11}$ $H_{38} = ab\ D_{33}$

$H_{39} = ab\ D_{22}\left(ab\ D_{33} + 2ab\ DR_{22}\right)$

Where: $D11 = D22 = \dfrac{E}{\left(1-\nu^2\right)}$; $D12 = \dfrac{\nu.E}{\left(1-\nu^2\right)}$; $D33 = \dfrac{E}{2\left(1+\nu\right)}$; $H = \dfrac{2}{\left(1-\nu\right)}$; $R = \dfrac{2\nu}{\left(1-\nu\right)}$

Appendix C.2.

In general, the multiplication [Q]T[D][Q] can be done manually, we will end up by calculating the double integrals of the form (see equation [14]):

$$I = [K_0] = \iint_S C.x^{\alpha} y^{\beta}\, dx.dy$$

The calculation of integral I is the principal problem of the calculation of the element stiffness matrix [Ke].

To illustrate the step of calculation of the integral in detail, let us take the case of an arbitrary element as shown below. The integral is composed of three parts symbolized on the figure by Roman numerals I1 II2 and III3 , each integral must be calculated separately.

The integral will be solved easily if one can determine the limits of the integral with precaution, which is far from being obvious. The fact that the limits can change with the geometry of the element raises difficulties, which make the programming enormously complex.

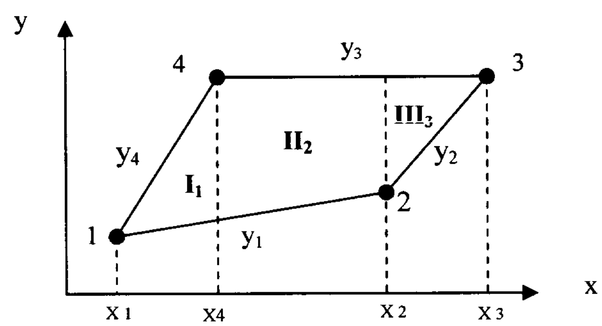

$$I = I_1 + II_2 + III_3$$

Where: $I_1 = C.\int_{x_1}^{x_4}\int_{y_1}^{y_4} x^{\alpha}y^{\beta}dxdy$; $I_2 = C.\int_{x_4}^{x_2}\int_{y_1}^{y_3} x^{\alpha}y^{\beta}dxdy$; $I_3 = C.\int_{x_2}^{x_3}\int_{y_2}^{y_3} x^{\alpha}y^{\beta}dxdy$

This means calculating the double integrals of the following form:

$$I = \iint_S C.x^{\alpha} y^{\beta}\, dx.dy \qquad [a]$$

Where:

C: constant

y: the ordinate of the segment of equation $y = ax + b$ [b]

$y^2 = (ax + b)^2 = \mathbf{1}a^2x^2 + \mathbf{2}abx + \mathbf{1}b^2$ [c]

$y^3 = (ax + b)(ax + b)^2 = \mathbf{1}\, a^3x^3 + \mathbf{3}a^2\, bx^2 + \mathbf{3}ab^2x + \mathbf{1}b^3$ [d]

We will end up with the general form of y^{β}:

$$y^{\beta} = \sum_{k=1}^{\beta+1} C(k).a^{\beta+1-k}.b^{k-1}.x^{\beta+1-k} = \sum_{k=1}^{\beta+1} C(k).a^{k-1}.b^{\beta+1-k}.x^{k-1} \qquad [e]$$

Where

C(k): Coefficients function of β (see Table 1), is for example:
If $\beta=1$ we will have 2 coefficients (see [b]).
If $\beta=2$ we will have 3 coefficients (see [c]).
If $\beta=3$ we will have 4 coefficients (see [d]).

β	$C(k)_{K=1,6}$					
	C(1)	C(2)	C(3)	C(4)	C(5)	C(6)
0	1	-	-	-	-	-
1	1	1	-	-	-	-
2	1	2	1	-	-	-
3	1	3	3	1	-	-
4	1	4	6	4	1	-
5	1	5	10	10	5	1

Table 1. ***C(k) coefficients relating to the relation (e)***

In which

$$\int y^{\beta} dy = \frac{1}{\beta+1} y^{\beta+1} = \frac{1}{\beta+1}(ax+b)^{\beta+1} = \frac{1}{\beta+1}\sum_{k=1}^{\beta+2} C(k).a^{k-1}.b^{\beta+2-k}.x^{k-1}$$

Therefore:

$$\int_{y_i}^{y_j} y^{\beta} dy = \frac{1}{\beta+1}\sum_{k=1}^{\beta+2} C(k)\left(a_j^{k-1}.b_j^{\beta+2-k} - a_i^{k-1}.b_i^{\beta+2-k}\right)x^{k-1}$$

$$\iint x^{\alpha} y^{\beta} dx.dy = \int_m^n \frac{1}{\beta+1}\sum_{k=1}^{\beta+2} C(k).\left(a_j^{k-1}.b_j^{\beta+2-k} - a_i^{k-1}.b_i^{\beta+2-k}\right).x^{k+\alpha-1}.dx$$

$$\iint x^{\alpha} y^{\beta} dx.dy = \frac{1}{\beta+1}\sum_{k=1}^{\beta+2} \frac{1}{k+\alpha} C(k).\left(a_j^{k-1}.b_j^{\beta+2-k} - a_i^{k-1}.b_i^{\beta+2-k}\right)\left(x_n^{k+\alpha} - x_m^{k+\alpha}\right)$$

In our case:

$$I = \sum_{P=1}^{3} I_P$$

The general expression of I_P for a quadrilateral would be:

$$I_P = \frac{C}{\beta+1}\sum_{k=1}^{\beta+2} \frac{1}{k+\alpha}.C(k)\left(a_j^{k-1}.b_j^{\beta+2-k} - a_i^{k-1}.b_i^{\beta+2-k}\right)\left(x_n^{k+\alpha} - x_m^{k+\alpha}\right)$$

In a very simple and effective manner, the integral is solved by the subroutine "INTEGRATION"

Appendix D.1

Elements of matrix [A $_{27x27}$]

$$[A_i]=\begin{matrix} 1 & 0 & 0 & y & 0 & z & x & xy & xz & xyz & 0 & -0.5\cdot y^2 & 0 & -0.5\cdot y\cdot z & 0 & -0.5\cdot z^2 & 0 & -0.5\cdot y\cdot z^2 & 0 & 0 & 0.5\cdot z & 0 & 0.5\cdot y & y\cdot z & 0.5\cdot x^2 & 0 & 0 \\ 0 & 1 & 0 & -x & -z & 0 & 0 & -0.5\cdot x^2 & 0 & -0.5\cdot x^2\cdot z & y & x\cdot y & y\cdot z & x\cdot y\cdot z & 0 & 0 & -0.5\cdot z^2 & -0.5\cdot x\cdot z^2 & 0.5\cdot z & x\cdot z & 0 & 0 & 0.5\cdot x & 0 & 0 & 0.5\cdot y^2 & 0 \\ 0 & 0 & 1 & 0 & y & -x & 0 & 0 & -0.5\cdot x^2 & -0.5\cdot x^2\cdot y & 0 & 0 & 0.5\cdot y^2 & -0.5\cdot x\cdot y^2 & z & x\cdot z & y\cdot z & x\cdot y\cdot z & 0.5\cdot y & 0 & 0.5\cdot x & x\cdot y & 0 & 0 & 0 & 0 & 0.5\cdot z^2 \end{matrix}$$

$$[A]=[[A_1][A_2][A_3][A_4][A_5][A_6][A_7][A_8][A_9]]^T$$

Where:

$[A_1]=\begin{bmatrix}U_1\\V_1\\W_1\end{bmatrix}$, at node **1** $x_1=-a$, $y_1=-b$, $z_1=-c$ $[A_2]=\begin{bmatrix}U_2\\V_2\\W_2\end{bmatrix}$, at node **2** $x_2=a$, $y_2=-b$, $z_2=-c$ $[A_3]=\begin{bmatrix}U_3\\V_3\\W_3\end{bmatrix}$, at node **3** $x_3=a$, $y_3=b$, $z_3=-c$

$[A_4]=\begin{bmatrix}U_4\\V_4\\W_4\end{bmatrix}$, at node **4** $x_4=-a$, $y_4=b$, $z_4=-c$ $[A_5]=\begin{bmatrix}U_5\\V_5\\W_5\end{bmatrix}$, at node **5** $x_5=-a$, $y_5=-b$, $z_5=c$ $[A_6]=\begin{bmatrix}U_6\\V_6\\W_6\end{bmatrix}$, at node **6** $x_6=a$, $y_6=-b$, $z_6=c$

$[A_7]=\begin{bmatrix}U_7\\V_7\\W_7\end{bmatrix}$, at node **7** $x_7=a$, $y_7=b$, $z_7=c$ $[A_8]=\begin{bmatrix}U_8\\V_8\\W_8\end{bmatrix}$, at node **8** $x_8=-a$, $y_8=b$, $z_8=c$ $[A_9]=\begin{bmatrix}U_9\\V_9\\W_9\end{bmatrix}$, at node **9** $x_9=0$, $y_9=0$, $z_9=0$

Appendix D.2

Elements of matrix $[K_{0\ 27x27}]$

$$
\left[\underset{24x24}{Ko}\right]=
\begin{bmatrix}
0&0&0&0&0&0&0&0&0&0&0&0&0&0&0&0&0&0&0&0&0&0&0&0\\
&0&0&0&0&0&0&0&0&0&0&0&0&0&0&0&0&0&0&0&0&0&0&0\\
&&0&0&0&0&0&0&0&0&0&0&0&0&0&0&0&0&0&0&0&0&0&0\\
&&&0&0&0&0&0&0&0&0&0&0&0&0&0&0&0&0&0&0&0&0&0\\
&&&&0&0&0&0&0&0&0&0&0&0&0&0&0&0&0&0&0&0&0&0\\
&&&&&0&0&0&0&0&0&0&0&0&0&0&0&0&0&0&0&0&0&0\\
&&&&&&H1&H2&H3&H4&H5&H6&H7&H8&0&0&0&0&0&0&0&0&0&0\\
&&&&&&&H9&H10&H11&H12&H13&H14&H15&0&0&0&0&0&0&0&0&0&0\\
&&&&&&&&H16&H17&H18&H19&H20&H21&0&0&0&0&0&0&0&0&0&0\\
&&&&&&&&&H22&H23&H24&H25&H26&0&0&0&0&H27&H28&0&H29&0&0\\
&&&&&&&&&&H30&H31&H32&H33&0&0&0&0&0&0&0&0&0&0\\
&&&&&&&&&&&H34&H35&H36&0&0&0&0&0&0&0&0&0&0\\
&&&&&&&&&&&&H37&H38&0&0&0&0&0&0&0&0&0&0\\
&&&&&&&&&&&&&H39&0&0&0&0&0&0&H40&H41&0&H42\\
&&&&&&&&&&&&&&H43&H44&H45&H46&0&0&0&0&0&0\\
&&&&&&&\text{Sym}&&&&&&&&H47&H48&H49&0&0&0&0&0&0\\
&&&&&&&&&&&&&&&&H50&H51&0&0&0&0&0&0\\
&&&&&&&&&&&&&&&&&H52&0&H53&0&0&H54&H55\\
&&&&&&&&&&&&&&&&&&H56&H57&0&H58&0&0\\
&&&&&&&&&&&&&&&&&&&H59&0&H60&H61&H62\\
&&&&&&&&&&&&&&&&&&&&H63&H64&0&H65\\
&&&&&&&&&&&&&&&&&&&&&H66&0&H67\\
&&&&&&&&&&&&&&&&&&&&&&H68&H69\\
&&&&&&&&&&&&&&&&&&&&&&&H70
\end{bmatrix}
$$

Where:

$H1 = a\,b\,c\,D1$

$H2 = \frac{a\,b^2\,c\,D1}{2}$

$H3 = \frac{D1\,b\,a\,c^2}{2}$

$H4 = \frac{D1\,a\,c^2\,b^2}{4}$

$H5 = a\,b\,c\,D2$

$H6 = \frac{D2\,c\,b\,a^2}{2}$

$H7 = \frac{D2\,a\,b\,c^2}{2}$

$H8 = \frac{D2\,c^2\,b\,a^2}{4}$

$H9 = \frac{D1\,a\,b^3\,c}{3}$

$H10 = \frac{D1\,a\,c^2\,b^2}{4}$

$H11 = \frac{D1\,a\,b^3\,c^2}{6}$

$H12 = \frac{D2\,b^2\,c\,a}{2}$

$H15 = \frac{D2\,a^2\,b^2\,c^2}{8}$

$H16 = \frac{D1\,a\,b\,c^3}{3}$

$H17 = \frac{D1\,a\,b^2\,c^3}{6}$

$H18 = \frac{D2\,a\,b\,c^2}{2}$

$H19 = \frac{D2\,c^2\,b\,a^2}{4}$

$H20 = \frac{D2\,a\,b\,c^3}{3}$

$H21 = \frac{D2\,b\,a^2\,c^3}{6}$

$H22 = \frac{D1\,c^3\,a\,b^3}{9} + \frac{D6\,c\,b\,a^5}{5}$

$H23 = \frac{D2\,a\,b^2\,c^2}{4}$

$H24 = \frac{D2\,a^2\,b^2\,c^2}{8}$

$H25 = \frac{D2\,b^2\,a\,c^3}{6}$

$H26 = \frac{D2\,c^3\,b^2\,a^2}{12}$

$H29 = -\frac{D6\,c\,b\,a^4}{4}$

$H30 = D3\,c\,b\,a$

$H31 = \frac{D3\,c\,b\,a^2}{2}$

$H32 = \frac{D3\,a\,b\,c^2}{2}$

$H33 = \frac{D3\,b\,c^2\,a^2}{4}$

$H34 = \frac{D3\,a^3\,b\,c}{3}$

$H35 = \frac{D3\,b\,c^2\,a^2}{4}$

$H36 = \frac{D3\,c^2\,b\,a^3}{6}$

$H37 = \frac{D3\,a\,b\,c^3}{3}$

$H38 = \frac{D3\,b\,c^3\,a^2}{6}$

$H39 = \frac{D3\,b\,c^3\,a^3}{9} + \frac{D7\,a\,b^5\,c}{5}$

$H40 = -\frac{D7\,a\,c\,b^3}{3}$

$H43 = D4\,a\,b\,c$

$H44 = \frac{D4\,b\,a^2\,c}{2}$

$H45 = \frac{D4\,c\,b^2\,a}{2}$

$H46 = \frac{D4\,c\,b^2\,a^2}{4}$

$H47 = \frac{D4\,c\,b\,a^3}{3}$

$H48 = \frac{D4\,c\,b^2\,a^2}{4}$

$H49 = \frac{D4\,c\,b^2\,a^3}{6}$

$H50 = \frac{D4\,c\,b^3\,a}{3}$

$H51 = \frac{D4\,c\,b^3\,a^2}{6}$

$H52 = \frac{D4\,c\,b^3\,a^3}{9} + \frac{D5\,a\,b\,c^5}{5}$

$H53 = -\frac{D5\,a\,b\,c^4}{4}$

$H54 = -\frac{D5\,a\,b\,c^3}{3}$

$H57 = \frac{D6\,c\,b\,a^2}{2}$

$H58 = \frac{D6\,c\,b\,a^2}{2}$

$H59 = \frac{D5\,a\,b\,c^3}{3} + \frac{D6\,c\,b\,a^3}{3}$

$H60 = \frac{D6\,c\,b\,a^3}{3}$

$H61 = \frac{D5\,b\,c^2\,a}{2}$

$H62 = \frac{D5\,a\,b\,c^3}{3}$

$H63 = D7\,c\,b\,a$

$H64 = \frac{D7\,c\,a\,b^2}{2}$

$H65 = \frac{D7\,c\,a\,b^2}{2}$

$H66 = \frac{D6\,c\,b\,a^3}{3} + \frac{D7\,a\,c\,b^3}{3}$

$H67 = \frac{D7\,a\,c\,b^3}{3}$

$H68 = a\,b\,c\,D5$

ABSTRACT

The general purpose of this thesis is to develop new finite elements based on the strain approach. In order to ameliorate the accuracy of the results, the static condensation technique has been used. Most of the finite elements developed by Sabir are characterized by a regular form and appropriate coordinates with the form of the element. To overcome this geometrical inconvenience; a new analytical integration is developed to evaluate the element stiffness matrix for the finite elements with distorted shapes. This will help to know how the elements will behave when they have irregular form, and to extend their applications domain for the curved structures no matter what the geometrical shape of the element might be.